ISSN 8755-6839

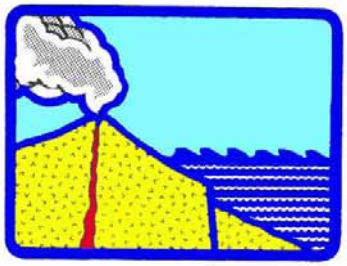

SCIENCE OF TSUNAMI HAZARDS

The International Journal of The Tsunami Society

Volume 25 Number 3 Published Electronically 2006

OBJECTIVE: **The Tsunami Society** publishes this journal to increase and disseminate knowledge about tsunamis and their hazards.

DISCLAIMER: Although these articles have been technically reviewed by peers, **The Tsunami Society** is not responsible for the veracity of any statement, opinion or consequences.

Submit manuscripts of articles, notes or letters to the Editor. If an article is accepted for publication the author(s) must submit a scan ready manuscript, a Doc, TeX or a PDF file in the journal format. Issues of the journal are published electronically in PDF format. Recent journal issues are available at

http://www.sthjournal.org.

Tsunami Society members will be advised by e-mail when a new issue is available. There are no page charges or reprints for authors.

Issues of the journal from 1982 thru 2005 are available in PDF format at

http://epubs.lanl.gov/tsunami/

and on a CD-ROM from the Society to Tsunami Society members.

ISSN 8755-6839 **http://www.sthjournal.org**

Published Electronically by The Tsunami Society in Honolulu, Hawaii, USA

A CATALOG OF TSUNAMIS IN THE INDIAN OCEAN

B. K. Rastogi and R. K. Jaiswal
National Geophysical Research Institute,
Hyderabad, India

SUMMARY

A catalog of about ninety tsunamis in the Indian Ocean has been prepared from 326 BC to 2005 AD. In the nineteenth and twentieth centuries tsunamis have occurred once in three years or so. Sunda Arc is the most active region that has produced about seventy tsunamis. The source zones of the remaining tsunamis are Andaman-Nicobar islands, Burma-Bangladesh region in the eastern side, while Makran accretion zone and Kutch-Saurashtra region are in the west. These zones are subduction zones or zones of compression.

Science of Tsunami Hazards, Vol. 25, No. 3, page 128 (2006)

GENERAL DESCRIPTION

Tsunamis are not as common in the Indian Ocean as in the Pacific. As compared to average eight tsunamis per year in the Pacific, Indian Ocean has one in three years or so. A catalog of tsunamis presented here includes about ninety tsunamis in the Indian Ocean out of which over 70 tsunamis are from Sunda. Some 20 tsunamis are reported from rest of the Indian Ocean, though source region of five of them may be in Sunda arc. Hence, eighty percent of the tsunamis of the Indian Ocean originate in Sunda arc covering Java and Sumatra. Figure 1 shows the locations of significant tsunamis and Figure 2 shows the annual number. Table 1 gives the list of tsunamis from Sunda arc and Table 2 from rest of the Indian Ocean.

The Sunda belt extends northward to Andaman-Nicobar Islands where a few tsunamis have originated. Further north, Bangladesh-Myanmar coast has produced some well-documented tsunamis. Makran coast in the northwest is known to have generated at least one major tsunami. Karachi-Kutch coast region has also produced some possible tsunamis. Cause of tsunamis is mostly thrust-type earthquakes with vertical uplift in subduction zones and zones of compression. The seismic gap areas along the subduction zones are possible sites of future great earthquakes. Along the Sunda arc, great earthquakes of magnitude 8.5 or greater can repeat every two centuries at a site but smaller tsunamigenic earthquakes can repeat every few decades. Along Sunda Arc volcanic eruptions have also given rise to large tsunamis. There appears to have been a hiatus in tsunami generation in this region, with a significant gap in events occurring from around 1909 through 1967 (Tsunami Laboratory, Novosibirsk, Russia). The Carlsberg spreading ridge or old oceanic ridges like Chagos Ridge and Ninetyeast Ridge with normal faulting can give rise to local tsunamis. Many of the tsunamis and their effects are described in some details. However, tsunamis from Java region are not described in detail as they did not affect the countries other than Indonesia.

TSUNAMIS FROM SUNDA ARC REGION

Newcomb and McCann (1987) compiled historical records of earthquakes and tsunamis from Sunda arc region. Heck (1947), Berninghausen (1966), Litzin (1974) and USGS catalogs list some more. Updated list is given in **Table 1**. The Sumatra part of the Sunda arc had been much more active than Java part. Detailed description of some of the significant earthquakes and the tsunamis caused by them are given below:

Earthquakes/Tsunamis in Sumatra

11 Dec 1681. “Strong earthquake” shook the Sumatra mountains near Mentawai Archipelago and a seaquake was observed.

3 Nov 1756. Many houses collapsed in several towns of Sumatra near to Enganno Is. No tsunami was reported.

No date, 1770. Severe damage in the same general area as the 1756 event, but a tsunami was reported.

10-11 Feb 1797, Mw 8.2. A large earthquake and tsunami was observed in ports on the coast of the mainland and on the Batu Is. Waves of great force near Padang (0.99S 100.37E) The town was inundated and more than 300 fatalities occurred (Heck, 1947).

18 Mar 1818. A very strong shock associated with both tsunami and seaquake near to Enganno Is.

24 Nov 1833. The great earthquake of magnitude > 8.7 had maximum intensities and generated a tsunami over 550km along the south central coast of Sumatra that also caused

much damage to the coast. Numerous deaths occurred in W. Sumatra. This earthquake ruptured the plate margin from the southern island of Enggano to Batu.

5-6 Jan 1843, Mw 7.2. The earthquake caused severe damage, liquefaction and many fatalities in Nias Is. A tremendous tsunami wiped out towns on the east coast of Nias and mainland. The damage and associated tsunami were very localized. The village of Barus (2N 98.38E) and Palan Nias (Nias Is. 1.1N 97.55E) reported large waves on two days.

11 Nov 1852. Earthquake near Nias generated seaquake.

16 Feb 1861. A great earthquake of magnitude 8.5 ruptured a major segment of the plate boundary in northern Sumatra. The tsunami that was generated extended over 500km along the arc. Tsunami destroyed southern towns of Batu Is., and a town on the southwest side of Nias experienced a tsunami height of 7m. The earthquake and tsunami caused 1000s of fatalities at west coast of Sumatra. Two aftershocks on March 9 and April 26, 1861 also caused tsunamis. There was no major shock for almost 50years.

The historic record shows that the strongest tsunami was associated with the volcanic eruption of Krakatau in Indonesia on 27 Aug. 1883. The 35m-high tsunami took a toll of 36,000 lives in western Java and southern Sumatra. Tsunami waves were observed throughout the Indian Ocean, the Pacific Ocean, the American West Coast, South America, and even as far away as the English Channel. On the facing coasts of Java and Sumatra the sea flood went many kilometers inland and caused such vast loss of life that one area was never resettled and is now the Ujung Kulon nature reserve.

Subsequent local tsunamis in the Sunda Strait were generated by the 1927 and 1928 eruptions of the new volcano of Anak Krakatau (Child of Krakatau) that formed in the area. Although large tsunamis were generated from these recent events, the heights of the waves attenuated rapidly away from the source region, because their periods and wavelengths were very short. There was no report of damage from these more recent tsunamis in the Sunda Strait (George, 2003).

According to ancient Japanese scriptures, the first known supercolossal eruption of Krakatau occurred in the year 416 A. D. – Some have reported it to occur in 535 A.D. The energy of this eruption is estimated to have been about 400 megatons of TNT, or the equivalent of 20,000 Hiroshima bombs. This violent early eruption destroyed the volcano, which collapsed and created a 7 km wide submarine caldera. The remnants of this earlier violent volcanic explosion were the three islands of Krakatau, Verlaten and Lang (Rakata, Panjang, and Sertung). Undoubtedly the 416 A.D. eruption/explosion/collapse generated a series of catastrophic tsunamis, which must have been much greater than those generated in 1883. The time of tsunami with wave height of several meters that affected Tamilnadu in India matches with this early Krakatau eruption. However, there are no other records to document the size of these early tsunamis or the destruction they caused. Subsequent to the 416 A.D. eruption and prior to 1883, three volcanic cones of Krakatau and at least one older caldera had combined again to form the island of Rakata.

4 Jan 1907, Ms 7.6. This event caused tsunamis that devastated Simeuleu, Nias and Batu Islands of Sumatra and extended over 950km as measured by tide gauges.

25 June 1914. M7.6 earthquake destroyed buildings in southern Sumatra. No tsunami was reported.

1935: Mw 7.7. Tsunami in SW Sumatra.

The 2004 Sumatra-Andaman earthquake of magnitude 9.3 generated 30m-high tsunami when upward slip of the ocean floor was up to 15m along a 1300 km long and 160 to 240km wide rupture. It was the deadliest tsunami killing about 300.000 people in 13 countries situated all around the Indian Ocean. The earthquake had created large thrust ridges, about 1500m high, which collapsed in places to produce large landslides, several kilometers across. The force of displaced water was such that blocks of rocks, massing

millions of tons apiece, were dragged as much as 10km. An oceanic trench several kilometers wide was also formed. The run up in the India was 5m or less.

Magnitude 8.7 great Sumatra Earthquake of 28 Mar. 2005 with an upward movement of 2m of seafloor in an area of 400kmx100km generated locally damaging 4m-high tsunami that struck nearby islands and coastal Sumatra and was recorded by tidal stations in the Indian Ocean (asc.India.org). The earthquake and tsunami killed 665 people. The tsunami struck Nias Island with wave heights of 4-5 m. A 3-4m wave struck the islands of Banyak and Simeulue and the Singkil district of Sumatra. According to the Pacific Tsunami Warning Center (PTWC) tide gauges in the Indian Ocean recorded minor wave activity in the Australian Cocos Island (10-22cm), the Maldives (10cm), and Sri Lanka (25-30cm).

TSUNAMIS THAT AFFECTED THE INDIAN REGION AND VICINITY

Though rare, tsunamis have hit India earlier. The tsunamis in the Indian region and vicinity are listed in Table 2. The oldest record of tsunami is available from November 326 BC earthquake near the Indus delta /Kutch region that set off massive sea waves in the Arabian Sea. Alexander the Great was returning to Greece after his conquest and wanted to go back by a sea route. But a tsunami due to an earthquake of large magnitude destroyed the mighty Macedonian fleet (Lisitzin, 1974).

Poompuhar is a town in the southern part of India in the state of Tamil Nadu. It was a flourishing ancient town known as Kaveripattinam that was washed away in what is now recognized as an ancient Tsunami in about 500 AD This time matches with the Krakatoa explosion

There is mention of tsunami effect in scriptures at Nagapattinam in 900AD that destroyed a Budhist monastery. According to literature available in the library of Thondaiman kingdom in Puduckottai, Tamilnadu, it was during the reign of Raja Raja Chola that waves had washed away the monastery and several temples and killed hundreds of people. There is evidence of this in Kalaki Krishnamurty's book "Ponniyin Selvan- The Pinacle of Sacrifice". In the chapter "The Sea Rises", the author explains how the sea had risen very high and the black mountain of water moved forward. The sea inundated warehouses and sheds and began to flow into the streets. Ships and boats seemed suspended in mid-air, precariously poised on the water peaks. The book also describes how an elephant was swallowed by the gushing water.

Tsunami has been observed in the North Indian Ocean on the Iranian coast from a local earthquake between 1st April and 9th May 1008 (Murty et al., 1999).

An earthquake occurred during 1524 A.D. off the coast of Dabhol, Maharashtra and. a resulting large tsunami caused considerable alarm to the Portuguese fleet that was assembled in the area (Bendick and Bilham, 1999).

A tsunami is known to have occurred in the Bay of Bengal on April 2, 1762, caused by an earthquake in Bangladesh – Myanmar border region. The epicenter is believed to be 40 km SE of Chittagong, or 61 km N of Cox's Bazaar, or 257 km SE of Dhaka, Bangladesh. The shock caused severe damage at Chittagong and other areas on the eastern seaboard of the Bay of Bengal. The Arakan coast was elevated for more than 160 km. The quake also caused a tsunami in the Bay of Bengal. The water in the Hoogly River in Kolkata rose by two meters. The rise in the water level at Dhaka was so sudden that hundreds of boats capsized and many people were drowned. This is the earliest well-documented tsunami in the Bay of Bengal (Mathur, 1998).

1819 June 16, India, Kutch, Mw 7.8. Severe earthquake with large changes in the elevation of the land. The town of Sindri (26.6N 71.9E) and adjoining country were

inundated by a tremendous rush from the ocean, and all submerged, the ground sinking apparently by about 5m (Macmurdo,1821)

An earthquake on 11th November 1842 near the northern end of Bay of Bengal caused a tsunami by which waters of the distributaries of the Ganges Delta were agitated. Boats were tossed about as if by waves in a squall of wind.

1845 June 19, India, Kutch. "The sea rolled up the Koree (Kori creek, 23.6N 68.37E) (the east) mouth of the Indus overflowing the country as far westward as the Goongra river, northward to the vicinity of Veyre, and eastward to the Sindree Lake," (Nelson,1846)

On October 31, 1847 the small island of Kondul (7°13'N 93°42'E) near Little Nicobar was inundated (Heck, 1947; Berninghausen, 1966) by an earthquake whose Mw, magnitude could have been >7.5 (Bilham et al. 2005).

Mihir Guha (http://www.freejournal.net), former Director General of the India Meteorological Department, informed that a tsunami struck Sunderbans (Bangladesh) in May 1874, killing several hundred thousand people. It was result of an earthquake in Bhola district. Earthquake and tsunami both played havoc in vast areas of Sunderbans, 24-Prganas, Midnapore, Barishal, Khulna and Bhola. Even Kolkata felt its impact. It was the same year that the meteorological center in Alipore was set up. However, no written record of such an earthquake or tsunami is available.

Other minor tsunamis of height up to 2m hit the east coast of India in 1842 and 1861 (from Sumatra), 1881 (from Car Nicobar), 1883 (Krakatau), 1907 (Sumatra) and 1941 (Andaman). The 1881 Andaman earthquake of Mw7.9 caused 1.2-m high tsunami. Indonesian earthquake of 1907 registered about a meter high tsunami in India. Madras Port Trust recorded a 2m high tsunami due to the eruption of the Krakatau volcano in Indonesia on 27 Aug 1883. Andaman earthquake of Mw7.7 in 1941 registered a 1.5m high tsunami. Some of these tsunamis are described below:

An earthquake of magnitude Mw 7.9 occurred at Car Nicobar Island on 31 Dec. 1881. A tsunami was generated by this earthquake in the Bay of Bengal. Though the run-ups and waves heights were not large, its effects were observed in the Andaman & Nicobar Islands and were recorded on the east coast of India. A meter high wave was recorded at Port Blair on South Andaman Island (Berninghausen, 1966). In the Nicobar Islands, the waves were less than 75 cm high. On the east coast of India, the tsunami first arrived at Nagapatinam at around 10:15 am local time (LT) with a 1.2m high waves. Tidal gauges at other locations recorded minor variations from normal tidal changes. The tsunami then struck the rest of the Tamil Nadu coast, first hitting Chennai and then progressing north toward Vishakhapatnam in Andhra Pradesh at 10:43 LT. Waves arrived at False Point on the Mahanadi delta in Orissa at 11:15 LT and at Pamban in the Gulf of Mannar at 11:32 LT. Waves less than 0.3 metres high were recorded later in the day in West Bengal by tidal gauges at Dublat at the mouth of the Hoogly river at 13:00 LT and then in Diamond Harbour at 15:10 LT (Ortiz and Bilham, 2003). Waves attributed to this tsunami were also observed at Batticaloa and Trincomalee on the east coast of Sri Lanka (Berninghausen, 1966). No tsunami was reported from tidal gauges in Myanmar (Ortiz and Bilham, 2003).

A tsunami was noticed at Dublet (mouth of Hoogly River) near Kolkata due to earthquake in the western part of the Bay of Bengal in 1884 (Murty et al. 1999) that reached up to Port Blair.

June 26, 1941 Andaman earthquake had a moment magnitude Mw 7.7 and was located at 12.1^{o} N and 92.5^{o} E (Bilham et al., 2005). A tsunami was triggered by this earthquake in the Bay of Bengal. Height of the tsunami was reported to be of the order of 0.75 to 1.25 meters. At the time no tidal gauge was in operation. Mathematical calculations suggest that the height could be of the order of 1m. This tsunami was witnessed along the eastern coast of India. It is believed that nearly 5,000 people were killed by the tsunami on the east coast

of India. Local newspapers are believed to have mistaken the deaths and damage to a storm surge, however, a search of meteorological records does not show any storm surge on that day on the Coromandel Coast (Murty, 1984). National dailies like the Times of India, which reported the quake's shaking effects, did not mention any deaths, either as a result of a storm surge or a tsunami.

The deadliest tsunami prior to 2004 in South Asia was in November 1945, which originated off the Makran coast of Pakistan in the Arabian Sea and caused deaths as far as Mumbai. More than 4000 people were killed on the Makran Coast by both the earthquake and the tsunami. The earthquake was also characterized by the eruption of a mud volcano, a few kilometers off the Makran Coast, which are common features in Western Pakistan and Myanmar. It led to the formation of a four small islands. A large volume of gas that erupted from one of the islands, sent flames leaping "hundreds of meters" into the sky (Mathur, 1988). The most significant aspect of this earthquake was the tsunamis that it triggered. The tsunami reached a height of 17m in some Makran ports and caused great damage to the entire coastal region. A good number of people were washed away. The tsunami was also recorded at Muscat and Gwadar. The tsunami had a height of 11.0 - 11.5 m in Kutch, Gujarat (Pendse, 1945). At 8:15am, it was observed on Salsette Island i.e Mumbai (Newspaper archives, Mumbai). It was recorded in Bombay Harbour, Versova (Andheri), Haji Ali (Mahalaxmi), Juhu (Ville Parle) and Danda (Khar). At Versova (Andheri, Mumbai), 5 persons who were fishing were washed away. At Haji Ali (Mahalaxmi, Mumbai), 6 persons were swept into the sea. At Danda and Juhu, several fishing boats were torn off their moorings. The tsunami did not do any damage to Bombay Harbour. Most persons who witnessed the tsunami said that it rose like the tide coming in, but much more rapidly. The height of the tsunami in Mumbai was 2m. A total of 15 persons were washed away in Mumbai.

Mw 7.7, 1983 earthquake in Chagos Archipelago, was one of the strongest earthquakes ever recorded in the Indian Ocean. It occurred at 17:46pm UTC. The earthquake caused some damage (NEIC) to buildings and piers on Diego Garcia. Diego Garcia is part of the Chagos Archipelago. The 1983 earthquake spawned a tsunami in the region. In the lagoon, on Diego Garcia, there was a 1.5-meter rise in wave height and there was some significant wave damage near the southeastern tip of the island. A 40 cm wave was also recorded at Victoria, Seychelles. There was a large zone of discolored seawater observed 60 - 70 km NNW of Diego Garcia. Moment-tensor solution indicated normal faulting along an E-W plane at a depth of 10km with source duration of 34 sec.

CONCLUSIONS

The catalog prepared for tsunamis in the Indian Ocean includes about ninety tsunamis. Eighty percent of the tsunamis in the Indian Ocean are from Sunda arc region where on an average tsunamis are generated once in three years. In rest of the Indian Ocean tsunamis can be generated once in ten years or so. The Makran accretion zone of southern Pakistan has produced some tsunamis. The 28 Nov. 1945 (Mw 8.0) earthquake generated the last major tsunami in the Arabian Sea. Indus Delta and may be the Coasts of Kutch and Saurashtra are also potential zones for great earthquakes and tsunami. Tsunami was generated by an earthquake in 1762 in Myanmar and in 1874 by an earthquake near Bangladesh. The Chagos ridge has given rise to a local tsunami due to a normal earthquake of Mw 7.7 on 30 Nov. 1983 near Diego Garcia.

This work was carried out under CSIR Emeritus Scientist Scheme.

REFERENCES

Bendick, R, and R. Bilham, (1999). A Search for Buckling of the SW Indian Coast related to Himalayan Collision, in Macfarlane, A., Sorkhabi, R. B., and Quade, J., eds., Himalaya and Tibet: Mountain Roots to Mountain Tops: Geol Soc Amer. Special paper 328. 313-322.

Berninghausen, W. H., (1966). Tsunamis and Seismic Seiches reported from regions adjacent to the Indian Ocean, Bull. Seism. Soc. Am., 56 (1), 69-74.

Bilham, R, R. Engdahl, N.Feld, and S.P. Sayabala (2005). Partial and complete rupture of the Indo-Andaman plate boundary 1847-2004, Seism. Res. Lett., 76 (3), 299-311.

George Pararas-Carayannis (2003). Near and Far-Field Effects of Tsunamis Generated By the Paroxysmal Eruptions, Explosions, Caldera Collapses and Massive Slope Failures of The Krakatau Volcano in Indonesia on August 26-27, 1883, Science of Tsunami Hazards, 21 (4), 191-222.

Heck, N.H. (1947). List of seismic sea waves, Bull.Seism. Soc. Am., 37, 269-286.

Lisitzin, E. (1974). Sea Level Changes, Elsevier Oceanographic Series, No.8, New York, 273pp.

Macmurdo, Captain (1821). Account of the earthquake which occurred in India in June 1819, Edinburgh Phil.J. 4, 106-109.

Mathur, S.M., (1998). "Physical Geology of India", National Book Trust of India, New Delhi.

Murty, T. S., A. Bapat & Vinayak Prasad (1999). Tsunamis on the coastlines of India, Science of Tsunami Hazards, 17 (3), 167-172.

Murty, T.S. (1984). Storm surges- meteorological ocean tides, Bull. Fisheries Research Board of Canada, Ottawa.

Nelson, Captain (1846). Notice of an earthquake and a probable subsidence of the land in the district of Cutch, near the mouth of Koree, or the eastern branch of the Indus in June 1845, Geol.Soc. London, Quart. J.,2, 103.

Newcomb, K.R. and McCann, W.R. (1987). Seismic history and tectonics of the Sunda Arc, JGR, 92 (B1), 421-439.

Ortiz, M., and Bilham, R. (2003). Source Area and Rupture Parametres of the 31 December 1881 Mw=7.9 Car Nicobar Earthquake estimated from tsunamis recorded in the Bay of Bengal, J. Geophys. Res- Solid Earth, 108(4), ESE 11, 1-16.

Pendse, C. G. (1945). The Mekran earthquake of the 28th November 1945, India Met. Deptt. Scientific Notes, 10, 141-145.

Table 1

List of Tsunamis in Sumatra-Java region

N	Year	Location	Long.	Lat.	Mag	Ca	Pro	I	Max Run up (run ups)	Ref.
1	416.09.10	Java-S	120	-10		6	2			NOAA/NESDIS
2	1681.12.11	Sumatra				1	4			Newcomb& Mccann
3	1768.06.22	Bali Sea	115	-7	Ms 7.5	1	4			NOAA/NESDIS
3	1770	Sw. Sumatra	102	-5	Ms 7	1	3	0.5	(1)	NGDC/NOAA
4	1797.02.10	Sw. Sumatra	99	-1	Ms 8	1	4	3.0	(1)	Berninghausen
5	1799	Se. Sumatra	104.75	-2.983		1	2			Berninghausen
6	1815.04.10	Java-Flores Sea	118	-8.2		6	4			NOAA/NESDIS
7	1815.11.22	Bali Sea	115.2	-8	Ms 7	3	3			NOAA/NESDIS
8	1816.04.29	Penang Island	100.25	5.383		1	2		(1)	NGDC/NOAA
9	1818.03.18	Bengkulu, Sumatra	102.267	-3.77	Ms 7	3	3	1.5	(1)	Berninghausen
10	1818.11.08	Bali Sea	117	-7	Ms 8.5	1	2			NOAA/NESDIS
11	1820.12.29	Flores Sea	119	-7	Ms 7.5	1	4			NOAA/NESDIS
12	1823.09.09	Java	108.5	-6.5	Ms 6.8	1	2			NOAA/NESDIS
13	1833.01.29	Bengkulu, Sumatra								Berninghausen (1966)
14	1833.11.24	Sw. Sumatra	102.2	-3.5	Mw 8.7	1	4	2.5	(3)	NGDC/NOAA, Newcomb & McCann (1987)
15	Sep. 1837	Banda Ache	96	5.5	Ms 7.2	4	2	0.5	(1)	NGDC/NOAA
16	1843.01.05	Sw. Sumatra	98	1.5	Ms 7.2	1	4	3.0	(3)	Berninghausen (1966), Heck1947
17	1843.01.06	Sw. Sumatra	97.33	1.05						Berninghausen (1966)m Heck1947
18	1852.11.11	Sibolga, Sumatra	98.8	1.7	Ms 6.8	1	1		(1)	NGDC/NOAA
19	1856.07.25	Java-Flores Sea	116	-8.5		1	2			NOAA/NESDIS
20	1857.05.13	Bali Sea	115.5	-8	Ms 7	1	4		(2)	NOAA/NESDIS
21	1859.10.20	S. Java Sea	111	-9		1	2		(1)	Berninghausen (1966)
22	1861.02.16	Sw. Sumatra	97.5	-1	Ms 8.5	1	4	3.0	(9)	Berninghausen (1966)
23	1861.03.09	Sw. Sumatra	99.37	0.3	Ms 7	1	4	2.0	(4)	NGDC/NOAA
24	1861.04.26	Sw. Sumatra	97.5	1	Ms 7	1	4	1.5	(1)	NGDC/NOAA
25	1861.06.05	Java,	107.3	-6.3			2			NOAA/NESDIS
26	1861.06.17	Sw. Sumatra	97.5	1	Ms 6.8	1	3			NOAA/NESDIS

27	1861.09.25	Sw. Sumatra	100	-1.5	Ms 6.5	1	3	1.5	(1)	Berninghausen (1966)
28	1864	Sumatra								Berninghausen
29	1883.08.26	Krakatau	105.423	-6.10		6	3	1.0	(8)	Berninghausen
30	1883.08.27	Krakatau (Volcano)	105.25	-6.06		6	4	4.5	35 (67)	Berninghausen
31	Feb. 1884	Krakatau	105.423	-6.10		1	2			Murty et al. (1999)
32	1885.07.29	Ajerbangis	99.383	0.2	Ms 6.8	1	2			NGDC/NOAA
33	1889.08.16	Java, Indones.	106	-6	Ms 6	1	3	1.0		NGDC/NOAA
34	1892.05.17	Malay Peninsula	99.5	2.5	Ms 7.5	1	3		4 (4)	NGDC/NOAA
35	1896.10.10	Sw. Sumatra	102.5	-3.5	Ms 6.8	1	2		1 (1)	NGDC/NOAA
36	1904.07.04	Sumatra								
37	1907.01.04	Sw. Sumatra	94.5	2	Ms 7.6	1	4	2.0	2.8 (7)	NGDC/NOAA / Newcomb &McCann
38	1908.02.06	Sw. Sumatra	100	-5	Ms 7.5	1	4	1.0	1.4 (1)	NGDC/NOAA
39	1909.06.03	Sumatra	101	-2	Ms 7.7	1	2	1.0	1.4	NGDC/NOAA
40	1914.06.25	W. Coast Of S. Sumatra	102.5	-4.5	Ms 8.1	1	0			NGDC/NOAA
41	1917.01.21	Bali Sea	115.4	-8	Ms 6.5	1	3		2	NGDC/NOAA
42	1921.09.11	S. Java Sea	111	-11	Ms 7.5	1	4		0.2	NGDC/NOAA / Newcomb &McCann
43	1922.07.08	Lhoknga, Ache	95.233	5.467		1	1			NGDC/NOAA
44	1926.06.28	Sw. Sumatra	99.5	-1.5	Ms 6.7	1	0			NGDC/NOAA
45	1928.03.26	Krakatau	105.423	-6.102		6	1			NGDC/NOAA
46	1930.03.17	Java-S.	105.4	-6.1		6	1			NGDC/NOAA
47	1930.06.19	Java-S.	105.3	-5.6	Ms 6	1	3		0.7	NGDC/NOAA
48	1930.07.19	S. Java Sea	114.3	-9.3	Ms 6.5	1	2		0.1	NGDC/NOAA
49	1931.09.25	Sw. Sumatra	102.7	-5	Ms 7.5	1	3		31.4	NGDC/NOAA
50	1935.12.28	Sw. Sumatra	98.25	.001	Ms 8.1	1	1			NGDC/NOAA
51	1936.08.23	Malay Peninsula	95	6	Ms 7.3	1	2			NGDC/NOAA
52	1948.06.02	Malay Peninsula	94	5.5	Ms 6.5	1	2		0.7	NGDC/NOAA
53	1949.05.09	Malay Peninsula	95	5	Ms 6.7	1	2			NGDC/NOAA
54	1955.05.17	Malay Peninsula	94	6.5	Ms 7.2	1	2			NGDC/NOAA
55	1957.09.26	S. Java Sea	107.3	-8.2	Ms 5.5	1	3		0.7	NGDC/NOAA
56	1958.04.22	Sw. Sumatra	104	-4.5	Ms 6.5	1	2		1	NGDC/NOAA
57	1963.12.16	Java	105.4	-6.2	6.5	1	2		0.7	NGDC/NOAA
58	1964.04.02	Off Nw Coast Of Indon.	95.7	5.9	Ms 7.0	8	3		0.7	NOAA/NESDIS
59	1964.04.02	Malay	95.7	5.9	Ms 7.0	1	3		**2**	NOAA/NESDIS

		Peninsula								
60	1967.04.12	Malay Peninsula	97.3	5.5	Ms 7.5	1	3	**1.5**		NGDC/NOAA
61	1977.08.19	Sunda Islands	118.4	-11	Ms 8	1	4			NOAA/NESDIS
62	1982.02.24	Java Trench	97.7	4.37	Ms 5.4	1	4			NGDC/NOAA
63	1984	Off West Coast Of Sumatra	97.955	0.18	7.2					Engdahl et al. (1998)
64	1985.04.13	Bali Island, Indonesia	114.2	-9.2	Ms 6.2	1	2			NGDC/NOAA
65	1994.02.15	Southern Sumatra	104.3	-5	Ms 7.0	1				NGDC/NOAA
66	1994.06.02	Java, Indonesia	112.8	-10.5	Ms 7.2	1	4		**13** (15)	NGDC/NOAA
67	2000.06.04	Off West Coast of Sumatra	102.09	-4.72	Ms 7.8				(1)	USGS/NEIC(PDE)
68	2000.06.18	South Indian Ocean	97.45	-13.8	Ms 7.8	1	4		**0.3**	NOAA/NESDIS
69	2004.12.26	Off West Coast Of Sumatra	95.947	3.307	Mw 9.3	1	4	**3.0**	**24** (302)	NGDC/NOAA
70	2005.03.28	Off West Coast Of Sumatra	97.013	2.074	Mw 8.7	1	4		**4** (2)	NOAA/NESDIS
71	2005.04.10	Kepulauanmentavia	99.607	-1.64	Ms 6.7	1	4		**1** (1)	NOAA/NESDIS

I is tsunami intensity, max. run up is in meters, reported number of runups are given within brackets. The data are taken from National Geophysical Data Center (NGDC); National Oceanic and Atmospheric Administration (NOAA) and National Environmental Satellite, Data, and Information Service (NESDIS). A "-1" is used as a flag (missing) value in some fields. The cause and probability of the tsunamis are shown by “Ca.” and “Pro.” respectively. The cause and probability of the tsunamis are given by following codes.

Cause Code:

Cause code indicates the cause or source of the tsunamis.
Valid values: **1 to 12**
1 = earthquake
2 = questionable earthquake
3 = earthquake and landslide
4 = earthquake and volcano
5 = earthquake, volcano and landslide
6 = volcano
7 = volcano and earthquake
8 = volcano and landslide
9 = volcano, earthquake, and landslide
10 = landslide
11 = meteorological
12 = explosion

Event Probability:

Probability of actual tsunami occurrence is indicated by a numerical rating of the validity of the reports of that event:
Valid values: 0 to 4
4 = definite tsunami
3 = probable tsunami
2 = questionable tsunami
1 = very doubtful tsunami
0 = erroneous entry

Tsunami Magnitude:

Tsunami magnitude, Mt is defined in terms of tsunami-wave amplitude by Iida et al. (1967) as:
$Mt = \log_2 Hmax$
Some other formulae are also in use.

Tsunami Intensity:

Tsunami intensity scales have been suggested based on its effect and damage caused by it. There are many formulae for intensity based on tsunami runups. Tsunami intensity is defined by Soloviev and Go (1974) as
$I = \log_2 (2^{1/2} * h)$
where "h" is the maximum run up height of the wave.

Table 2

List of Tsunamis that Affected Indian Region and Vicinity

S. N.	Date	Location	Long.	Lat.	Eq. Mag	Cau	Pro	I	Max Run up (run ups)	Ref.
1	326 B.C.	Indus delta /Kutch region				1	4			Lisitzin (1974)
2	About 500 AD	Poompuhar, Tamilnadu (probably due to Krakatau eruption)	79.52	11.12			4			Wikipedia
3	900 AD	Nagapattinam, Tamilnadu (may be from Sunda-Andaman arc)	79.53	10.46			4			Kalaki Krishnamurty
4	1008	Iranian Coast	60	25		1	4			Murty et al. (1999)
5	1762.04.12	Bay of Bengal (Bangladesh)	92	22		1	4		**>2** (1)	Mathur (1988)
6	1819.06.16	Kutch	26.6	71.9	Mw 7.8	1	3			Macmurdo
7	1842.11.11	N.Bay of Bengal	90	21.5		1	4		(3)	Oldham (1883)
8	1845.06.19	Kutch	23.6	68.37		1	3			Nelson
9	1847.10.31	Little Nicobar Island	93.667	7.333	Mw 7.5-7.9	1	3			Berninghausen (1966), Heck,1947
10	1868.08.19	Andaman Islands	92.73	11.67		1	4		**4**	NGDC/NOAA
11	1874	Sunderbans (Bangladesh)	89	22		1	2			Mihir Guha, Free Journal
12	1881.12.31	W. of Car Nicobar	92.43	8.52	Mw 7.9	1	4		**1.2**	Berninghausen (1966), Ortiz and Bilham (2003)
13	Jan. 1882	Sri Lanka (may be from Indonesia)	81.14 E	8.34		1	3			Berninghausen (1966)
14	1883.08.27	Krakatau (Volcanic Eruption)	105.25	-6.06		6	4	4.5	**2**	Berninghausen (1966)

15	1884	W. of Bay Of Bengal								Murty et al. (1999)
16	1935.05.31	Andaman-Nicobar			Mw 7.5	1	4		(1)	NGDC/NOAA
17	1935.11.25	Andaman-Nicobar	94	5.5	Ms 6.5	1	2			NGDC/NOAA
18	1941.06.26	Andaman Islands	92.5	12.1	Mw 7.7	1	4		**1.25**	Bilham et al. 2005
19	1945.11.27	Makran Coast	63.5	25.2	Mw 8.0	1	4		**17**	Murty et al. (1999)
20	1983.11.30	Chagos ridge	72.11	-6.85	Mw 7.7	1	4		**1.5** (2)	NGDC/NOAA
21	2004.12.26	Off west coast of Sumatra and Andaman-Nicobar	95.947	3.307	Mw 9.3	3	4	3.0	**30**	NGDC/NOAA

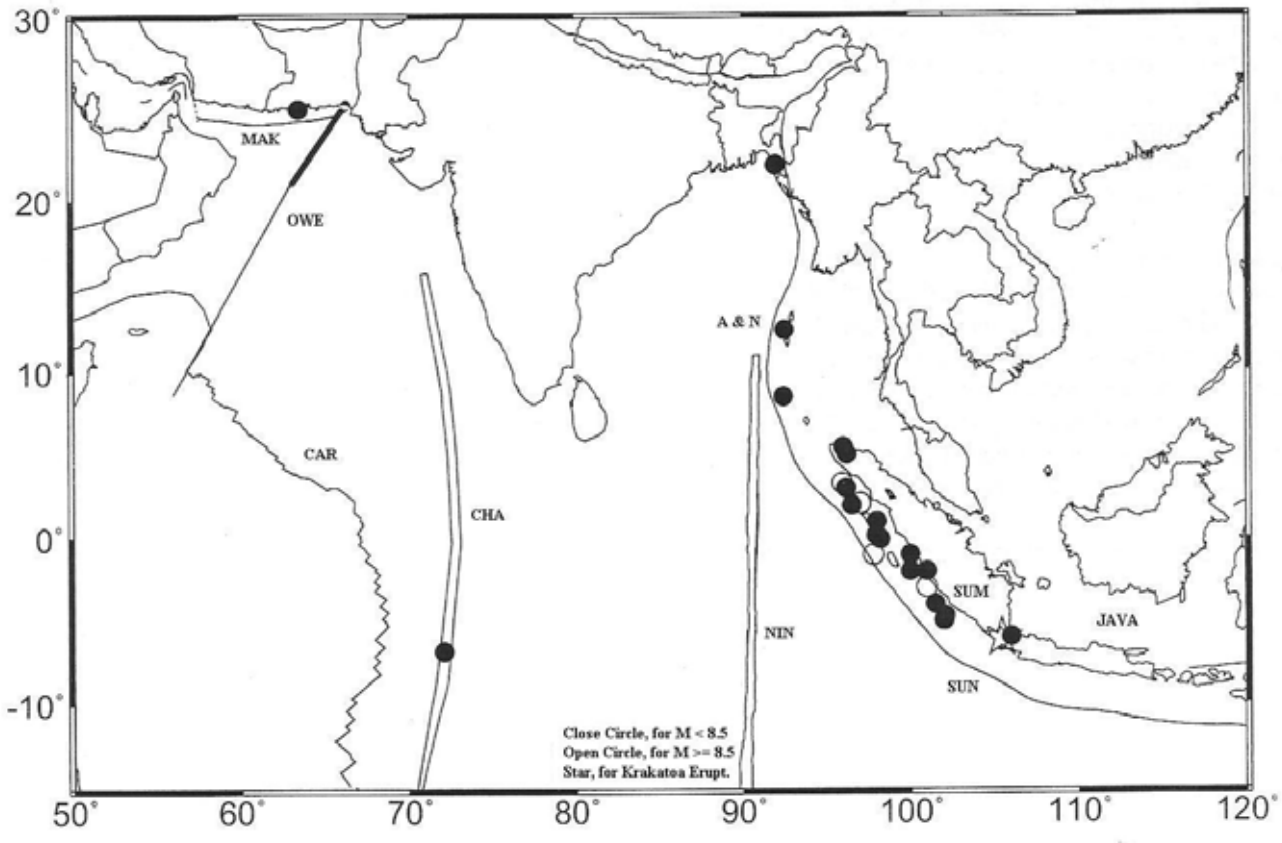

Fig.1. Locations of tsunamis in the Indian Ocean.

MAK - Makran Accretion Zone, OWE – Owen Fracture Zone, CAR – Carlsberg Ridge, CHA – Chagos Archipelago, A & N – Andaman & Nicobar Islands, SUM – Sumatra, NIN – Ninety East Ridge, SUN – Sunda Subduction Zone and JAVA- Java.

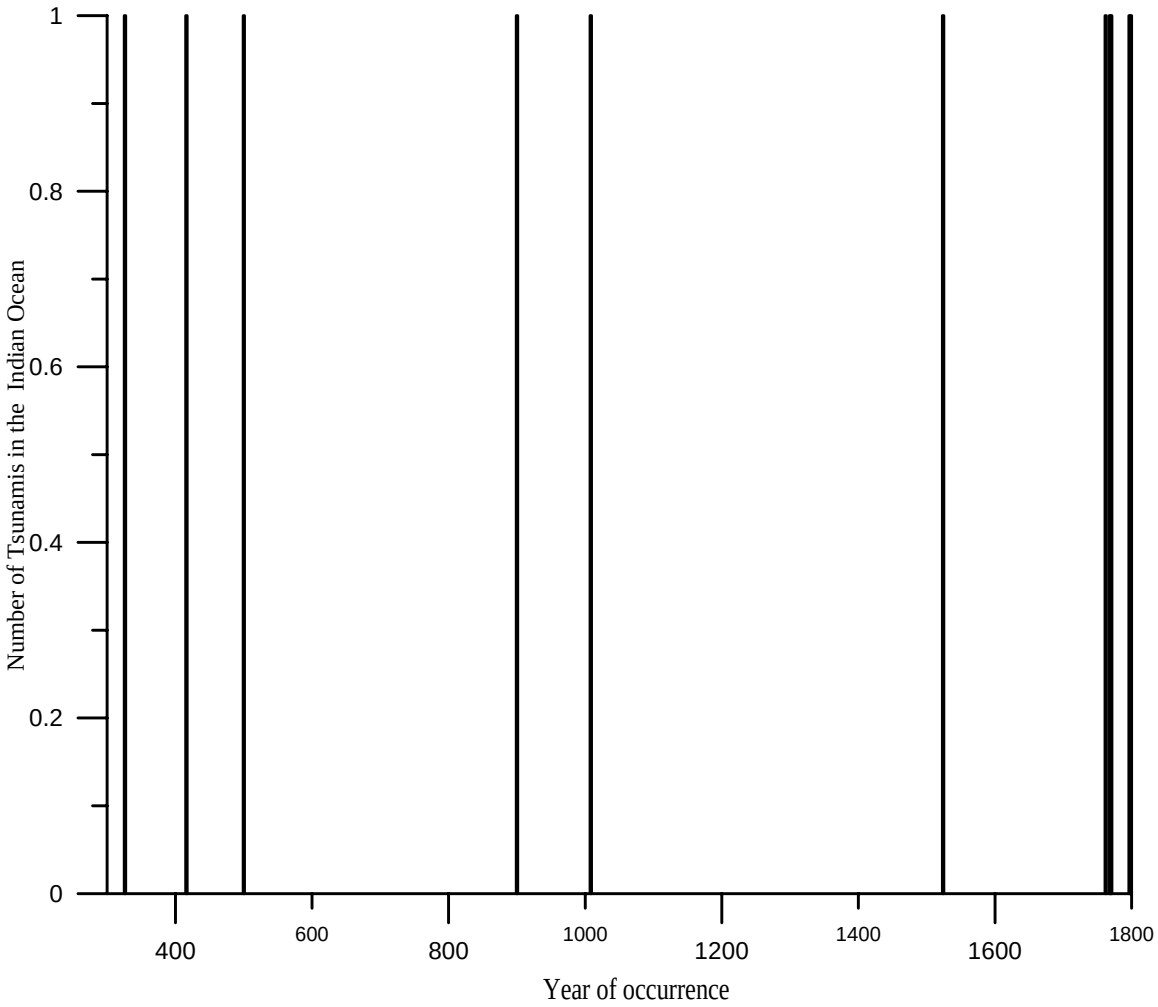

Fig. 2a. No. of Tsunamis in the Indian Ocean vs. Years of occurrences, Prior to 1800.

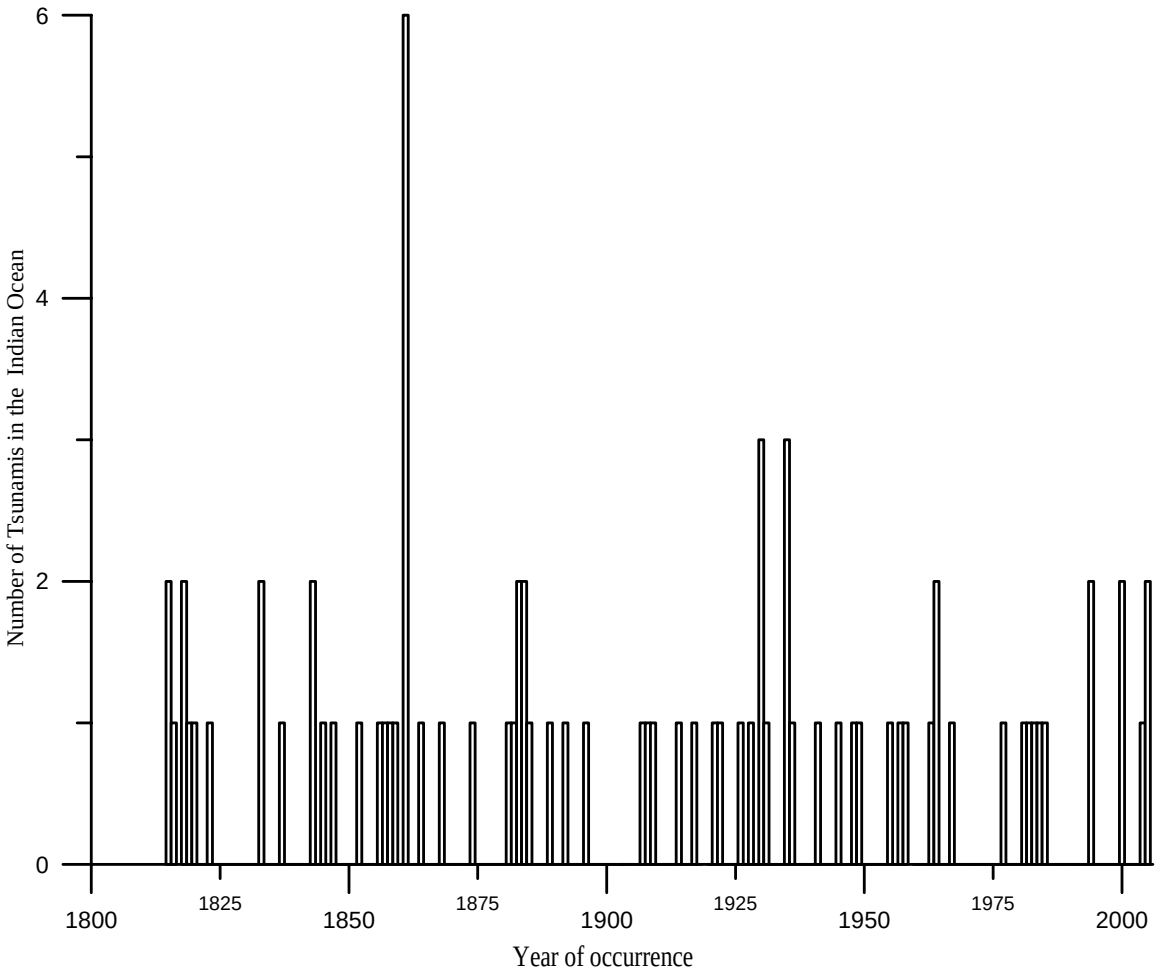

Fig. 2b. No. of Tsunamis in the Indian Ocean vs. Years of occurrences, 1800 Onward to Present.

TSUNAMI HAZARD IN NORTHERN VENEZUELA

B. Theilen-Willige

Technical University of Berlin
Institute of Applied Geosciences
Department of Hydrogeology and Bureau of Applied Geoscientific Remote Sensing (BAGF)
Birkenweg, Stockach, Germany

ABSTRACT

Based on LANDSAT ETM and Digital Elevation Model (DEM) data derived by the Shuttle Radar Topography Mission (SRTM, 2000) of the coastal areas of Northern Venezuela were investigated in order to detect traces of earlier tsunami events. Digital image processing methods used to enhance LANDSAT ETM imageries and to produce morphometric maps (such as hillshade, slope, minimum and maximum curvature maps) based on the SRTM DEM data contribute to the detection of morphologic traces that might be related to catastrophic tsunami events. These maps combined with various geodata such as seismotectonic data in a GIS environment allow the delineation of coastal regions with potential tsunami risk. The LANDSAT ETM imageries merged with digitally processed and enhanced SRTM data clearly indicate areas that might be prone by flooding in case of catastrophic tsunami events.

1. INTRODUCTION

This study is concentrates on tsunami risk mapping for areas where no severe tsunami has occurred recently, but the geomorphologic and topographic features and characteristics are similar to areas hit by recent catastrophic tsunamis as Sumatra and where historical records of tsunamis are available and reliable. The tsunamis can cause severe damage and flood low lands in many segments of the coast. There is a potential of water waves generated by debris avalanches and landslides (Pararas-Carayannis, 2004). Recently found submarine debris avalanches on the sea floor around many islands in the Lesser Antilles suggest that large scale landslides and volcanic island flank collapses must have generated tsunamis in the distant past. The near and far field effects of tsunami waves that can be expected in the future from postulated massive edifice flank collapses of other volcanoes in the Caribbean region and around the world have to be considered when emergency planning is carried out. There can be no doubt that disaster mitigation and prevention measurements are valid in a cost-benefit analysis. Major population shifts to Caribbean coasts and an explosion of tourism are significantly adding to the risk being affected by natural hazards.

2. OBJECTIVES

The main objective of this study is the contribution to the implementation of a Natural Hazard – GIS relating and integrating results from different remote sensing data and ground data to provide a classified risk map that may be used by non-specialist on-site. The focus of this research will be on the contribution to the development of a spatial database to serve primarily for disaster mitigation planning. The aim is to place GIS into the earthquake, mass movement and tsunami prone regions as those of the communities of Northern Venezuela to assist in the management of natural disasters.

3. METHODS AND APPROACH

This study considers the support provided by remote sensing data, including DEM data acquired by Space Shuttle Missions, and a GIS based spatial databases for the delineation of potential tsunami risk sites in North-Venezuela. On a regional scale the areas of potential tsunami risk are determined by an integration of remote sensing data, geologic, seismotectonic and topographic data and reports of historical tsunamis. The evaluation of digital topographic data is of great importance as it contributes to the detection of the specific geomorphologic/ topographic settings of tsunami prone areas. The basic and main geoscientific components in such a Tsunami Hazard GIS and the remote sensing input are described in Fig.1, respectively (Theilen-Willige, 2006 a and b).

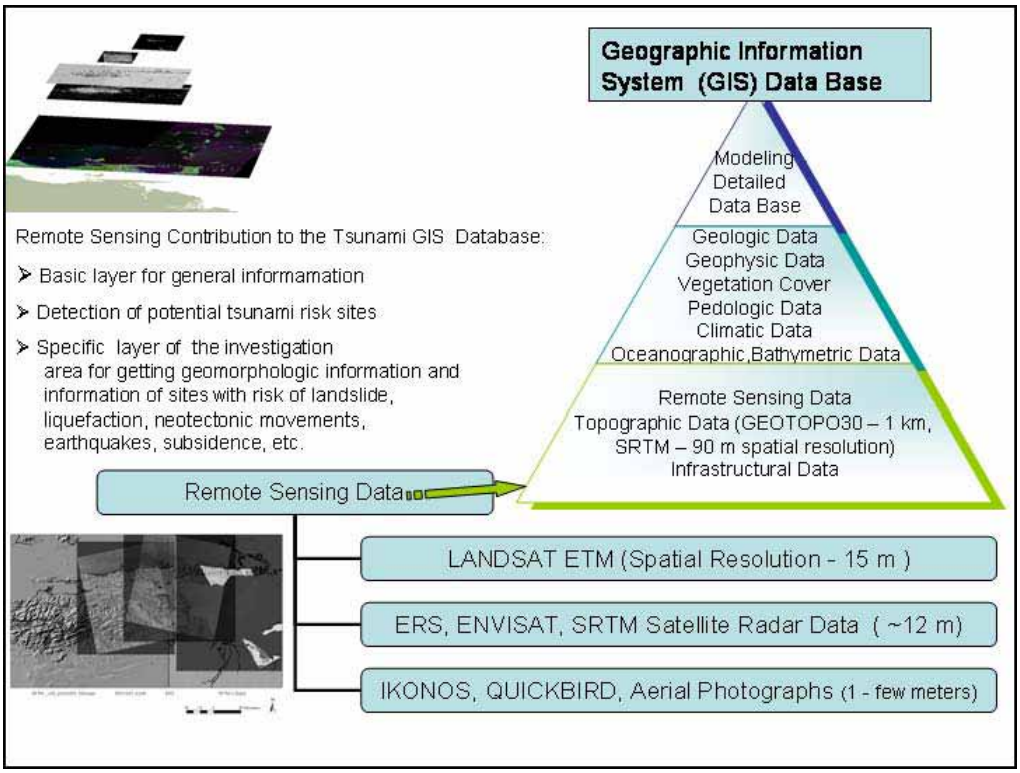

Figure1 : Remote Sensing Contribution to a Tsunami Hazard Information System

The various data sets as NOAA- , LANDSAT ETM- , ERS-, and ENVISAT - data data, topographic, geological and geophysical data from the study regions were integrated as layers into GIS using the software ArcView GIS 3.3 with the extensions Spatial Analyst und 3DAnalyst and ArcGIS 9.1 of ESRI (Fig.2). Other geodata as provided by ESRI ArcIMS Server or USGS Natural Hazards Support System were included, so earthquake data or bathymetric maps. As a complementary tool Google Earth Software was used in order to benefit from the 3D imageries of the various investigation areas (http://earth.google.com/). For the objectives of this study digital elevation data have been evaluated: Shuttle Radar Topography Mission - SRTM, 90 m resolution) data provided by the University of Maryland, Global Land Cover Facility (http://glcfapp.umiacs. umd.edu:8080/esdi/) and GTOPO30 data provided by USGS (http://www.diva-gis.org/Data.htm, 1 km resolution) were used as base maps. Potential risk sites for hazardous tsunami waves were identified by analyzing areas in Venezuela showing heights below 20 m above sea level (Fig.2). These areas below 20 m height were studied then more detailed. The topographic data were merged with LANDSAT ETM data (Band 8: 15 m resolution). For enhancing the LANDSAT ETM data digital image processing procedures have been carried out.

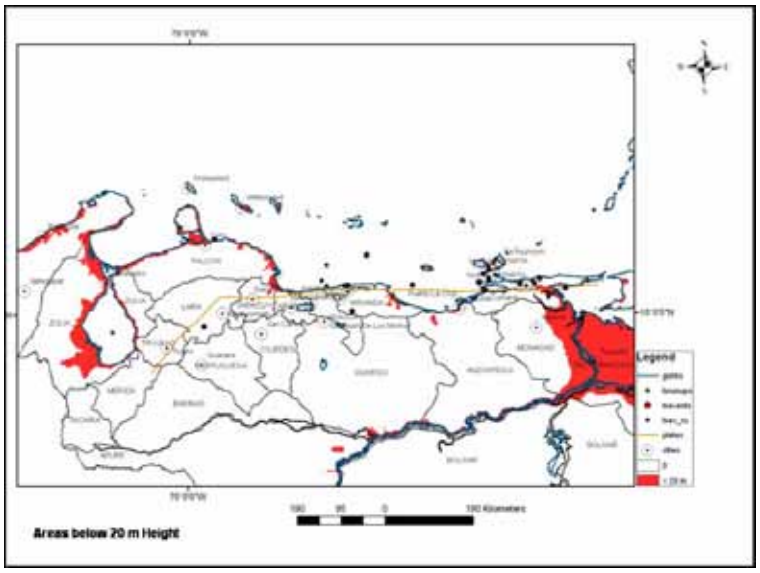

Figure 2: Map of Venezuela indicating areas below 20m height above sea level

A systematic GIS approach is recommended for tsunami risk site detection as described in Figs.3 and 4 extracting geomorphometric parameters based on the SRTM DEM data as part of a Tsunami Information System.

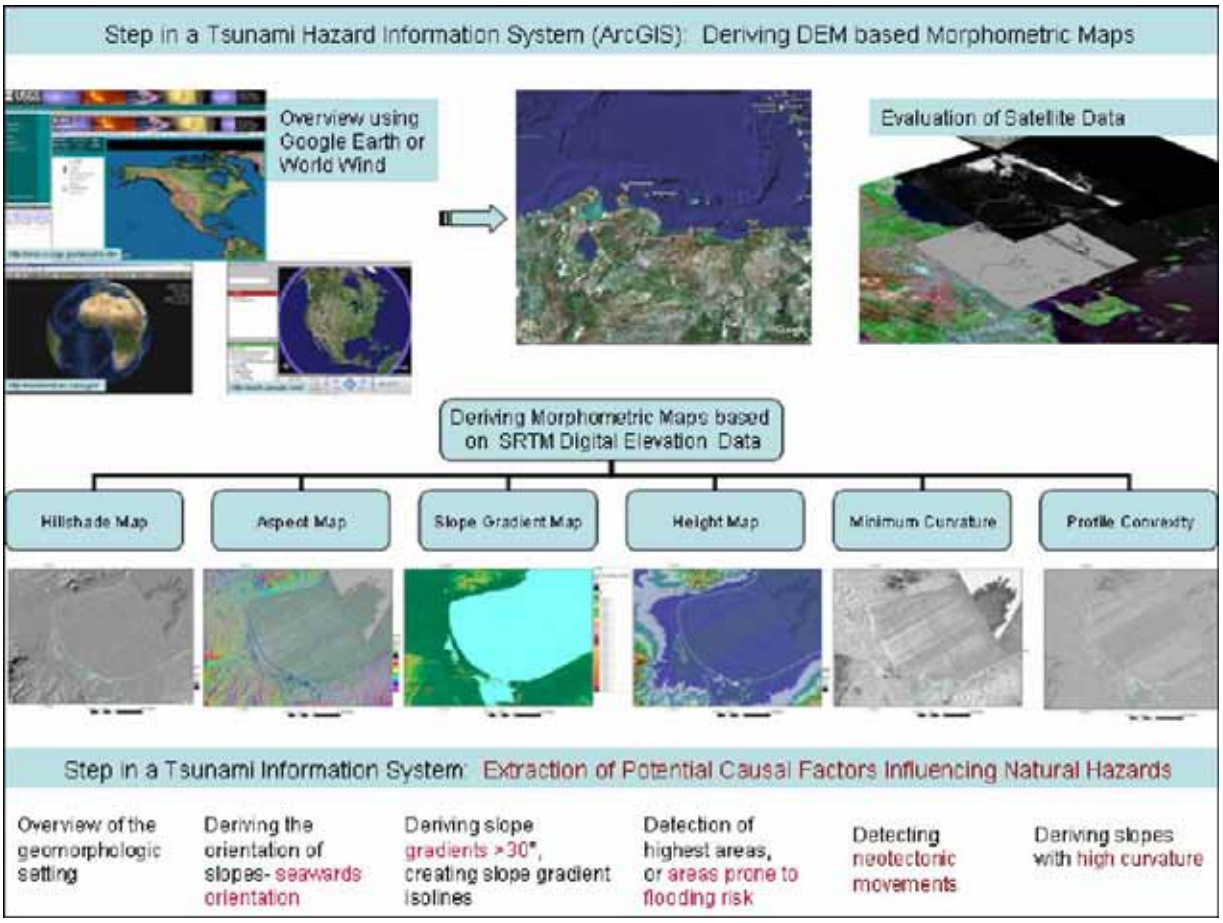

Figure 3: Workflow in a Tsunami Hazard Information System

For getting a geomorphologic overview terrain parameters were extracted from Digital Elevation Model data (DEM) as shaded relief, aspect and slope degree, minimum and maximum curvature or plan convexity. Geomorphometric parameters as slope degree, minimum or maximum curvature provide information of the terrain morphology expressing geomorphologic features (see Fig.) that

might be related to tsunami events. These SRTM derived, morphometric parameters correspond to groups of 0, 1st and 2nd order differentials, where the 1st and 2nd order functions have components in the XY and orthogonal planes (Wood, 1996).

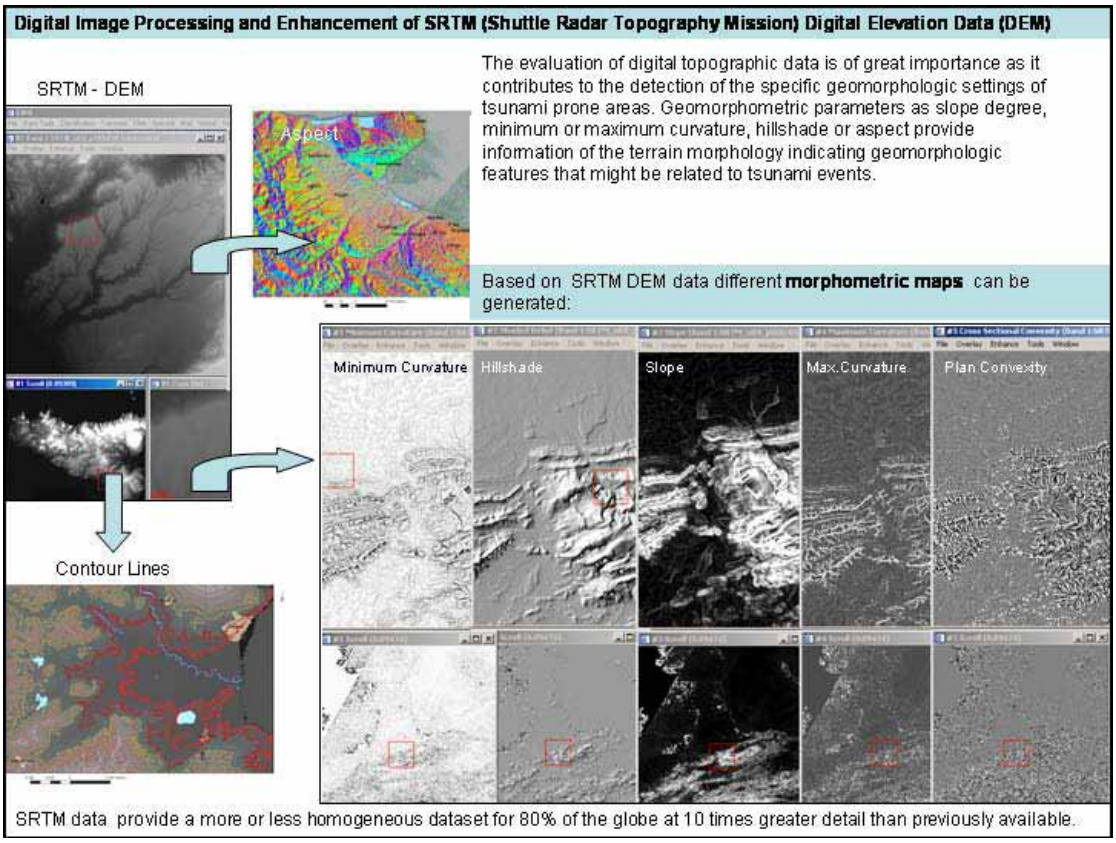

Figure 4 : SRTM based morphometric maps

4. SEISMOTECTONIC SETTING

Presently, the Caribbean region is characterized by convergent, compressional and collisional tectonic activity, which results in frequent occurrences of earthquakes and volcanic eruptions. Often, localized landslides and volcanic island mass edifice failures are collaterally triggered. Most of these events occur near or along the geotectonically active plate boundaries and can generate local tsunamis with complex mechanisms, which represent the characteristics of each particular source. Seismic events in the Eastern Caribbean are principally associated with a subduction zone along a north-south line just east of the main island arc where the Atlantic Plate dips from east to west beneath the Caribbean Plate (Pararas-Carayannis, 2004). Tectonic deformation and active geo-dynamic processes in the Caribbean region have produced distinct seismic and volcanic activity sources capable of generating destructive tsunamis. North- Venezuela lies within the interaction zone of the Caribbean and South America plates. and is being subjected to a stress field characterized by a NNW-SSE maximum horizontal stress and a ENE-WSW minimum horizontal stress (strike-slip regime). This stress tensor, calculated from microtectonic data collected at various sites in Plio-Pleistocene formations, is responsible for present kinematics and activity of sets of faults: east-west right-later al faults, NW-SE right-lateral faults (synthetic to the east-west faults), NNW-SSE normal faults, north-south to NNE-SSW left-lateral faults and ENE-WSW reverse faults (Audemard et al.,1999). The Venezuelan Coast Ranges outline a major transfer zone between the westward-dipping subduction of the Atlantic oceanic lithosphere beneaeth the Lesser Antilles volcanic arc and the westward-dipping subduction of the South American continental lithospere beneath the Andes. At the surface this part is characterized by the occurrence of a major transform fault, the dextral El Pilar-Fault. Northeast-southwest oriented strike-slip faults fragment the Serrania into various blocks. Well expressed at the

surface by the morphologic depression of the Cariaco and Paria Gulfs, the present activity of the El Pilar-fault is reflected in hydrothermal activity and in seiosmicity (Passalaqua et al., 1995). The El Pilar Fault is the easternmost portion of this system, located within an east-west trending topographic depression formed by a graben (Pliocene and early Pleistocene) and since then subjected to right-lateral strike slip movement. It is part of a 5 to10 km-width shear zone.

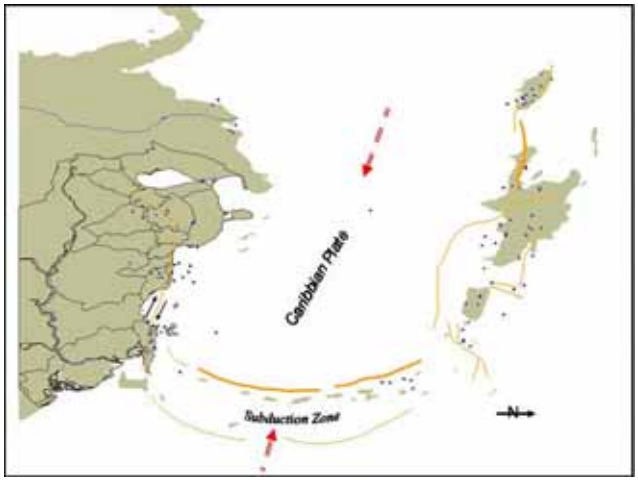

Figure 5: Plate tectonics of Northern Venezuela and earthquake occurrence and distribution

5. EVALUATION OF SRTM AND LANDSAT ETM DATA FROM COASTAL AREAS OF NORTHERN VENEZUELA

Analyzing the images provided by Google Earth from the coastal areas of Venezuela it becomes obvious, that catastrophic flooding events are traced on the satellite imageries. Fig.6 presents an overview of these areas that are investigated more detailed, going from west to east. As there are a lot of rainstorms inducing flash floods, mudflows, debris flows and landslides along the coasts of Northern Venezuela, the traces of these catastrophic events have to be considered, too, for avoiding remote sensing evaluation errors. Debris flows and flash floods on alluvial fans inundated coastal communities as in December 1999. Because most of the coastal zone in Vargas consists of steep mountain fronts that rise abruptly from the Caribbean Sea, the alluvial fans are the only areas where slopes are not too steep to build. Rebuilding and reoccupation of these areas requires careful determination of potential hazard zones including tsunami hazard to avoid future loss of life and property. For tsunami risk site analysis it is very important to investigate very detailed the geomorphologic features that are obviously related to tsunami events. These traces can be mapped based on LANDSAT ETM imageries and some high resolution imageries provided by Google Earth or the University of Maryland, USA without costs. Traces of catastrophic floods visible on satellite imageries, that were derived by comparative investigations of recently tsunami prone areas, can be summarized as shown in Fig.7. Special attention is focused on the traces of high energy waves overrunning the coastal areas with very high velocity and, thus, creating typical features as presented in Fig.8. Among these are the traces of linear and parallel erosion and abrasion, a partly shock-wave like arrangement of sedimentary fans, opened to the sea. One reason for these traces of high velocity - waves might be the focusing of the wave energy towards the coast according to local amplification by refraction and reflection processes. Further on the resonance effects between the various islands, as well to the tsunami propagation in the form of edge waves along the coast have to be taken into account.

As first example in the west the Gulf of Venezuela is presented. The height maps based on SRTM data clearly show the lowest areas (up to 3 m height) in blue colours prone to flooding risk in case of a tsunami. Fig.9 points out where such traces can be observed based on the LANDSAT and SRTM data in the Gulf of Venezuela. In Figs.10 and 11 the potential tsunami hazard risk of this area is

visualized.

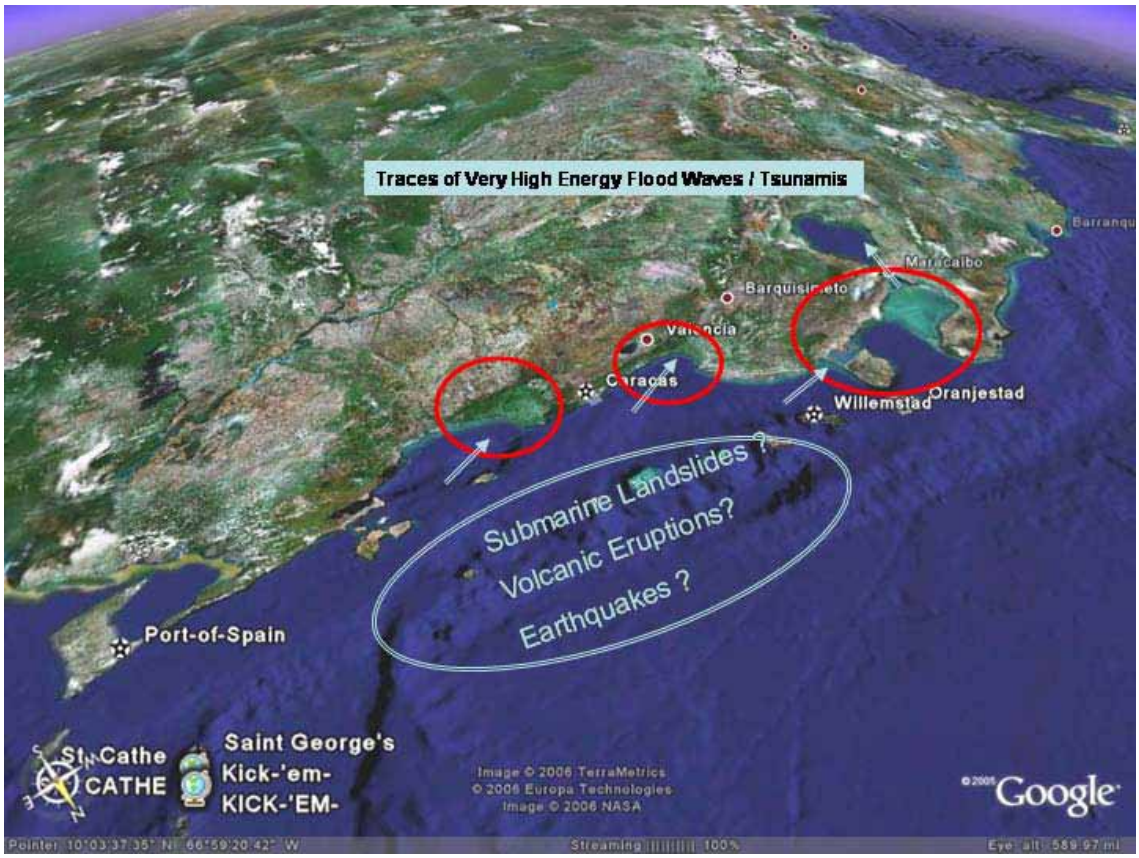

Figure 6: Overview of areas showing traces of catastrophic flooding

There are indications that the Lake of Maracaibo might be affected by tsunami floods as well. In case of a catastrophic tsunami tsunami waves could be “pressed” into the Sea of Maracaibo due to the influence of coastal morphology on water flow and current mechanisms as presented schematically in Fig.9. Fig.10 illustrates that traces of such catastrophic flood waves are visible on LANDSAT ETM imageries of the Gulf of Venezuela. Figs.11 a and b enhance those areas prone to flooding in case of a stronger tsunami.

Figure 7: Typical geomorphologic features of tsunami prone areas

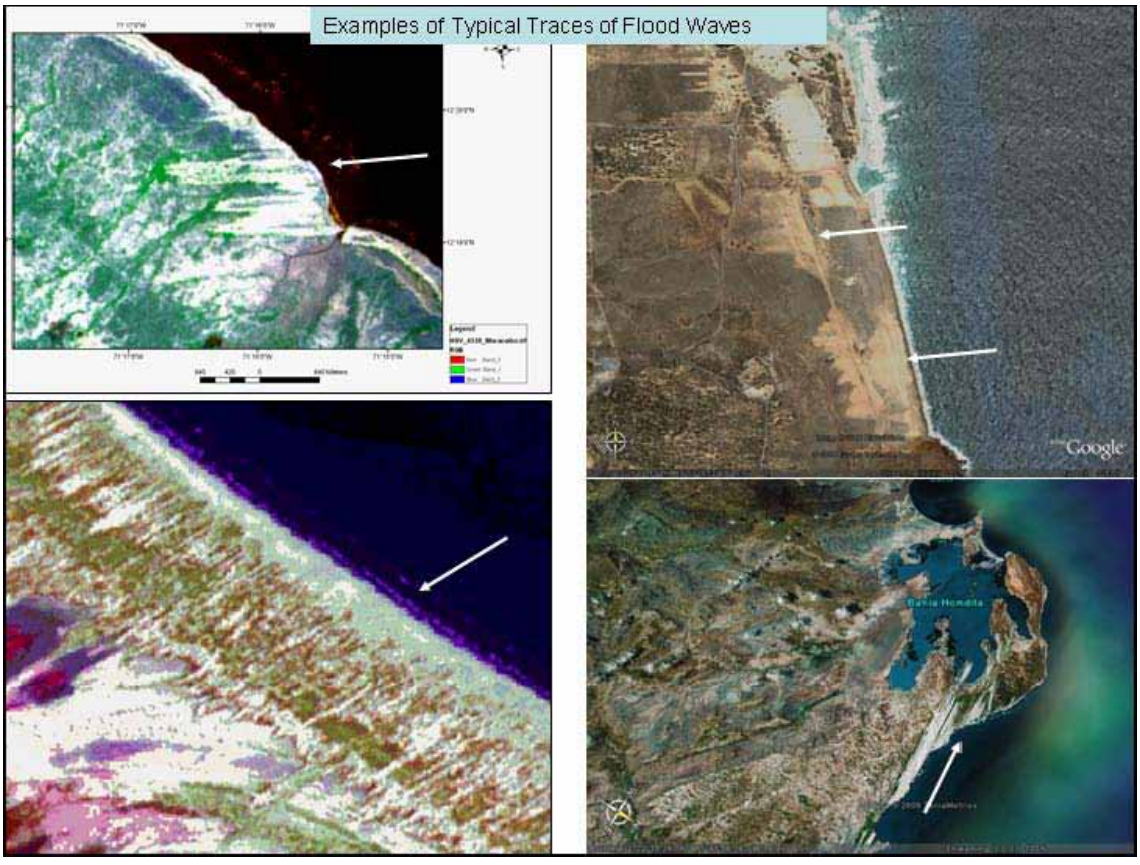

Figure 8: Traces of high energy flood waves after collision with the coast as visible on satellite data from NW-Venezuela Figure 9: Gulf of Venezuela as visible on LANDSAT ETM imageries and SRTM height map indicating areas most susceptible to tsunami flooding

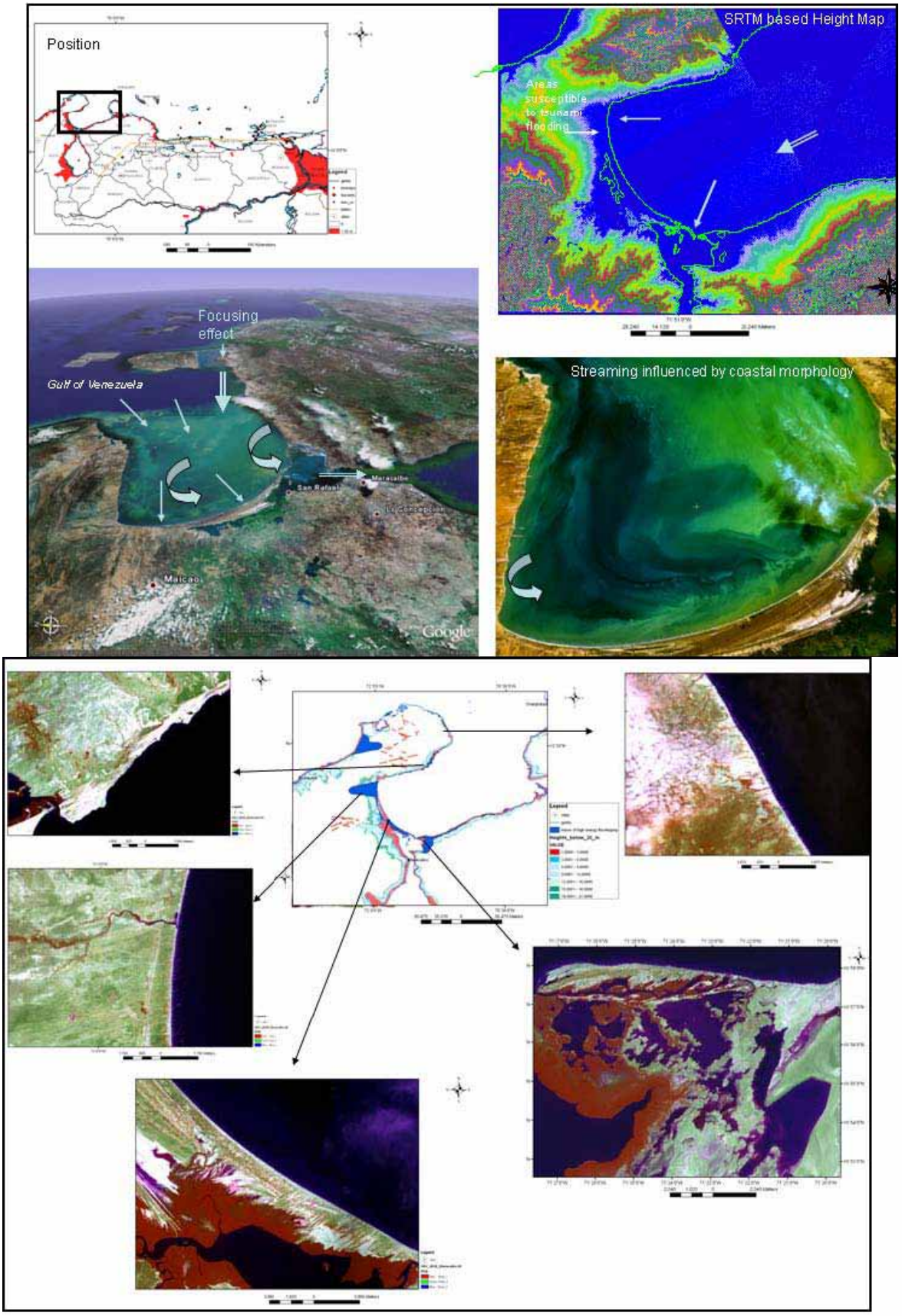

Figure 10: Occurrence of high energetic flood wave traces (dark-blue colours on the map) in the Gulf of Venezuela

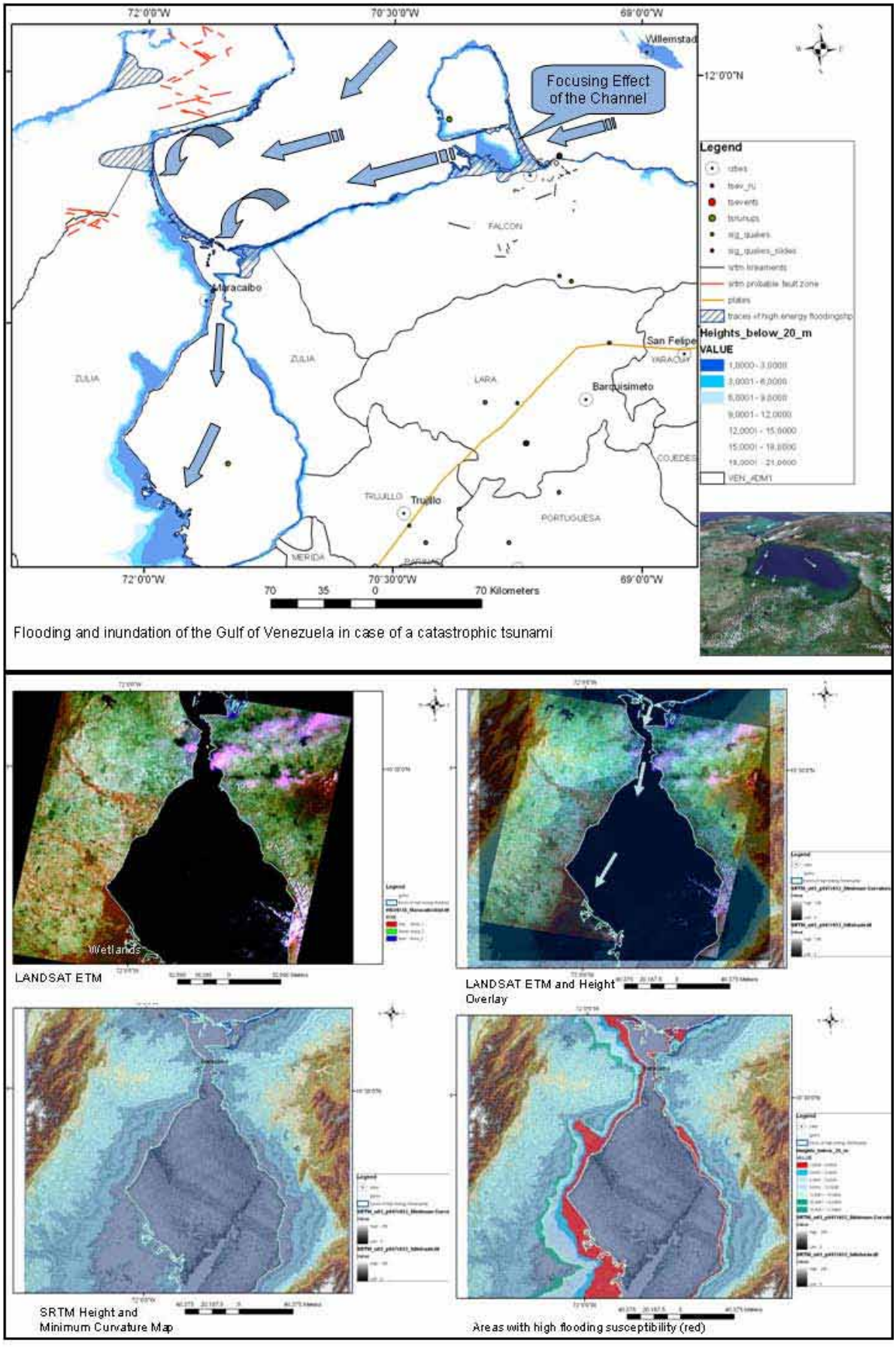

Figure 11 a and b: Detection of areas susceptible to tsunami flooding in the Maracaibo area

The next example shows the eastern part of the Gulf of Venezuela where traces of abrasion due to high velocity flood waves are visible on the LANDSAT ETM imageries.

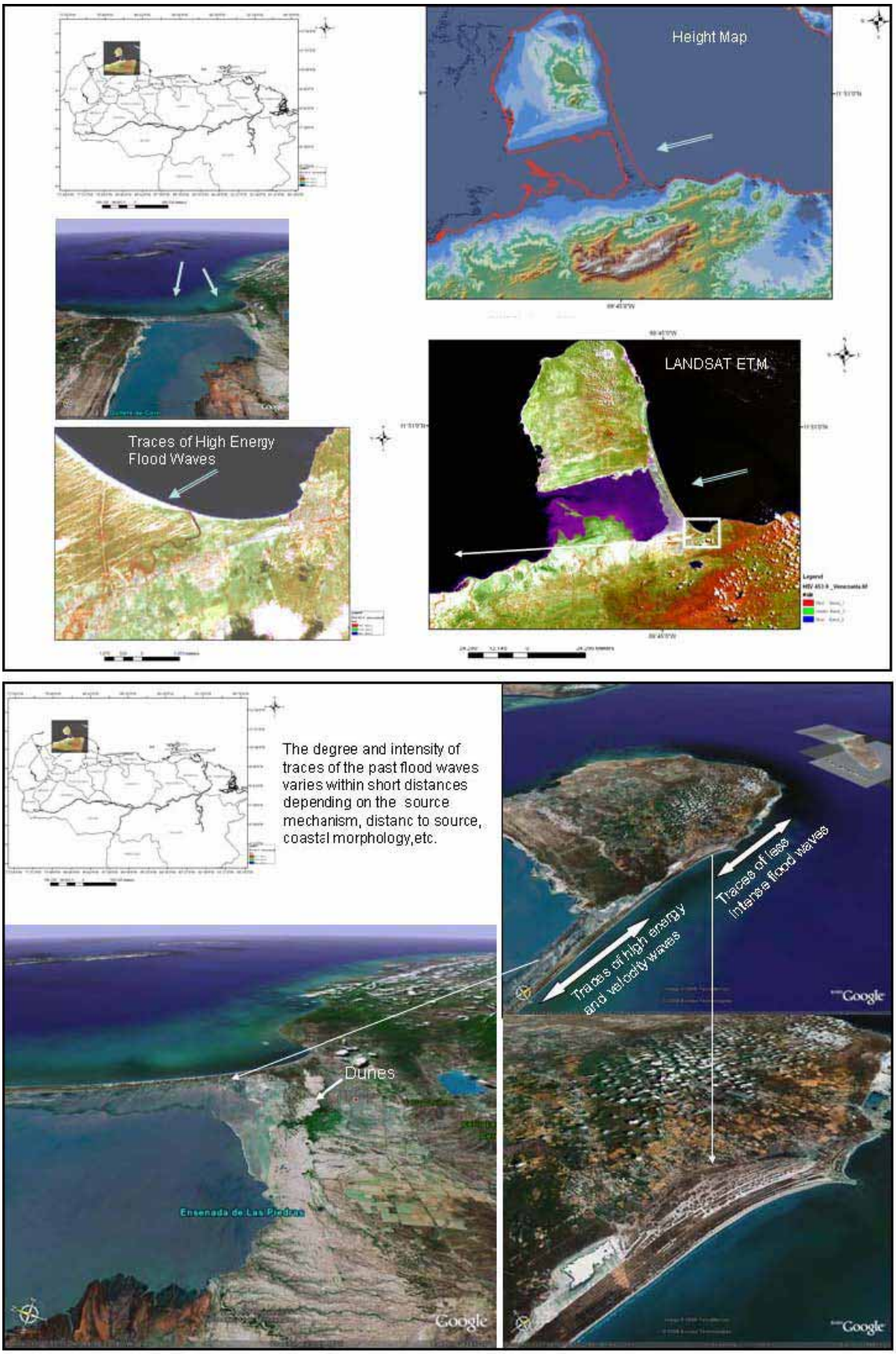

Figure 12 a and b: Traces of high velocity waves and dunes over the abrasion planes indicating a longer period without catastrophic tsunami events

Continuing the analysis of remote sensing data of coastal areas of Venezuela from west to east the following figures show the evaluation results from the central and eastern part of Northern Venezuela. Merging the SRTM height data with the LANDSAT ETM evaluation results areas susceptible to tsunami flooding can be delineated (Fig.13).

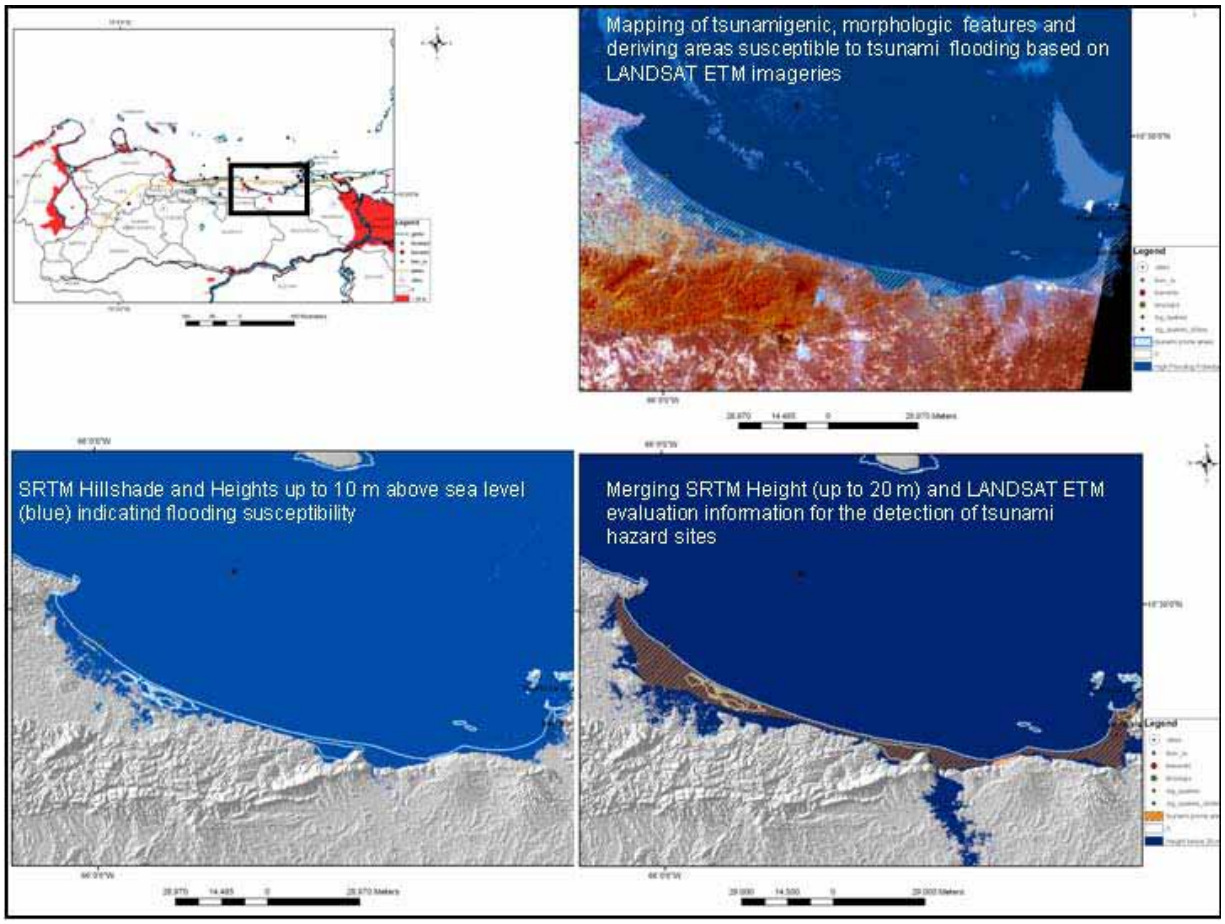

Figure 13: Areas susceptible to tsunami flooding

The next figures 14 and 15 provide an impression of the potential tsunami risk of two cities: Barcelona and Cumana due to their position in low areas near the coast.The perspective 3D-views of the SRTM digital terrain data and of the LANDSAT ETM imagery visualize the situation of these cities. The SRTM Height / LANDSAT ETM data overlay clearly shows those areas that might be flooded in case of a catastrophic tsunami. Fig.16 presents some smaller bays exposed to flooding at the northern coast of the peninsula of Paria. Satellite radar data as ERS and ENVISAT imageries merged with SRTM height data can help to identify flooding prone areas.

6. CONCLUSIONS

The evaluations of different remote sensing data combined with other geodata in a GIS environment allow the delineation of areas susceptible to tsunami flooding and inundation in North-Venezuela as shown in Fig.17. Flooding directions can be derived where erosional features and abrasion are expressed enough on the satellite data. This might contribute to the detection of future potential source regions.

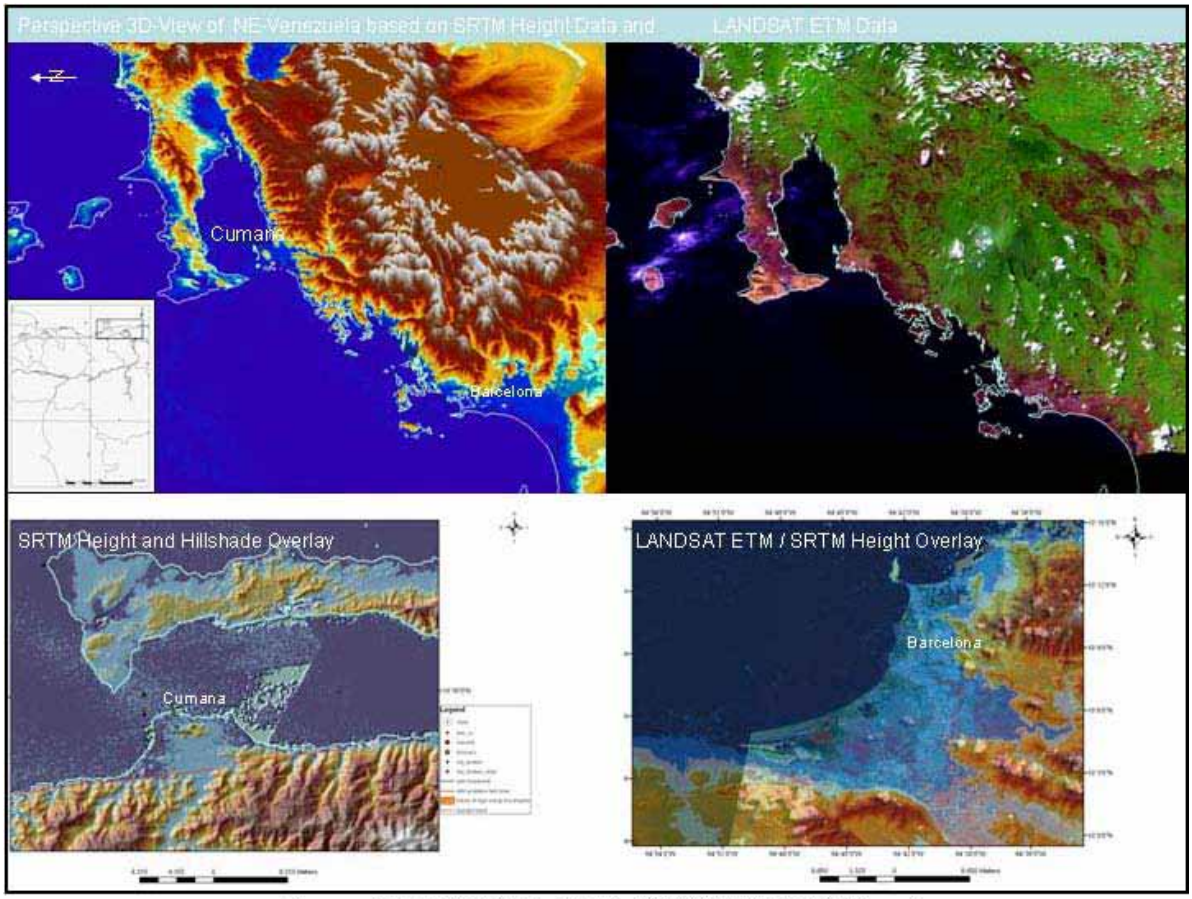

Figure 14: SRTM Height/LANDSAT ETM Overlay

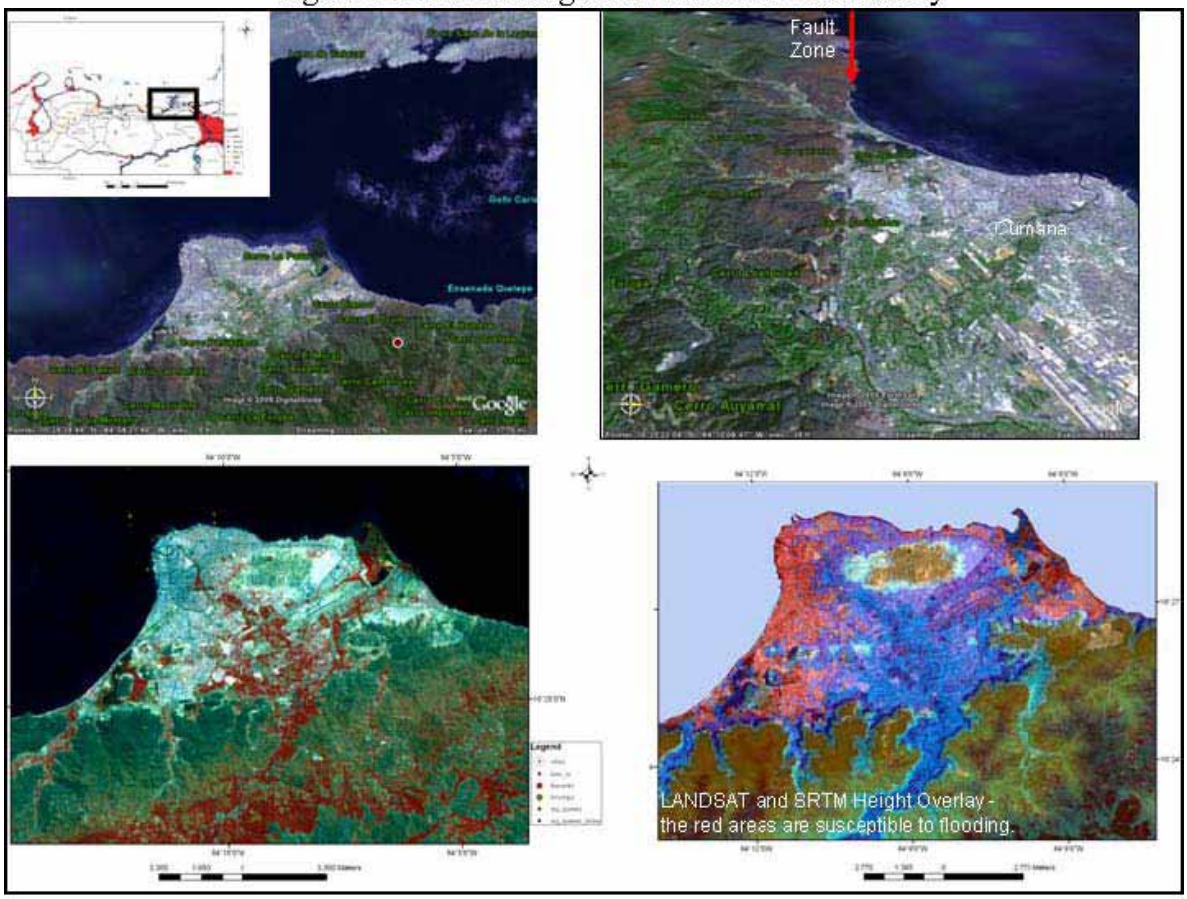

Figure 15: Potential flooding risk sites of Cumana

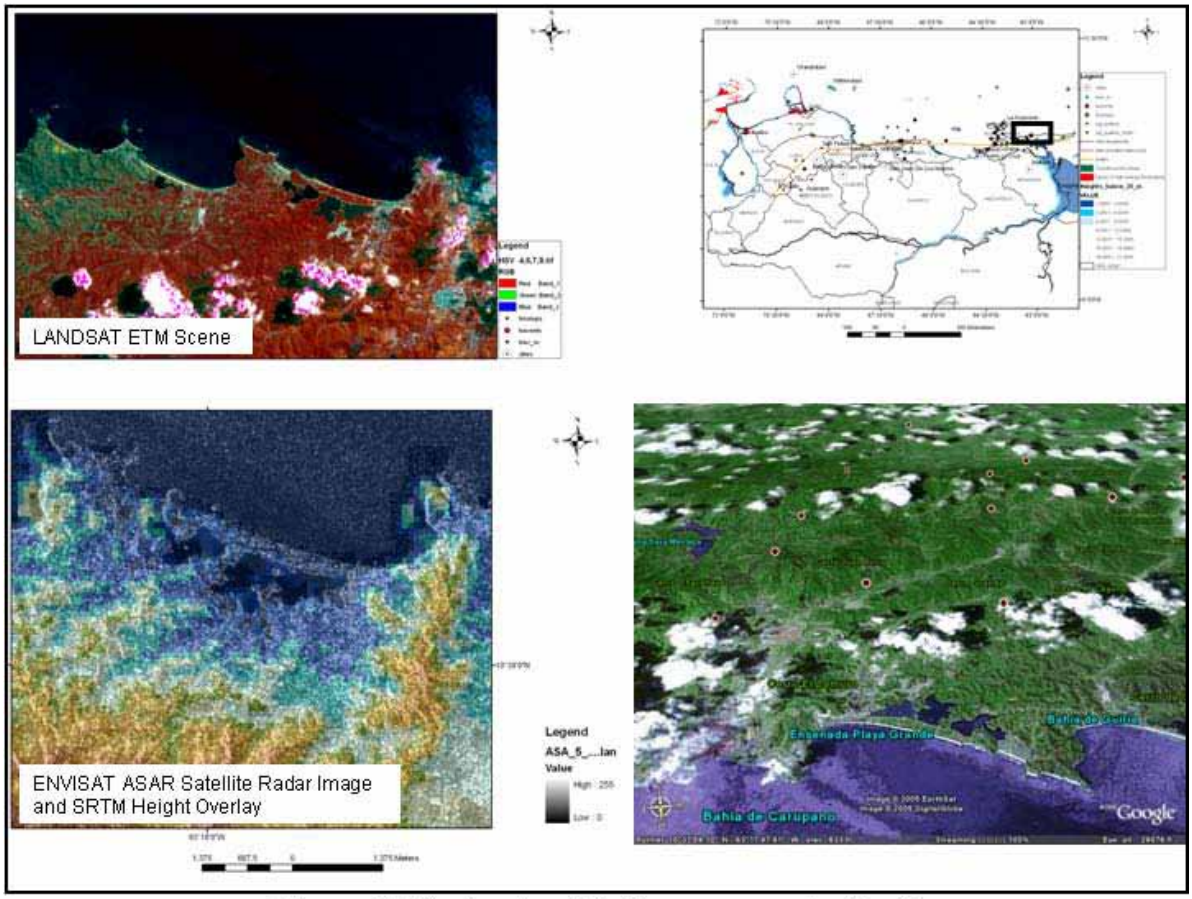

Figure 16: Peninsula of Paria – exposure to flooding

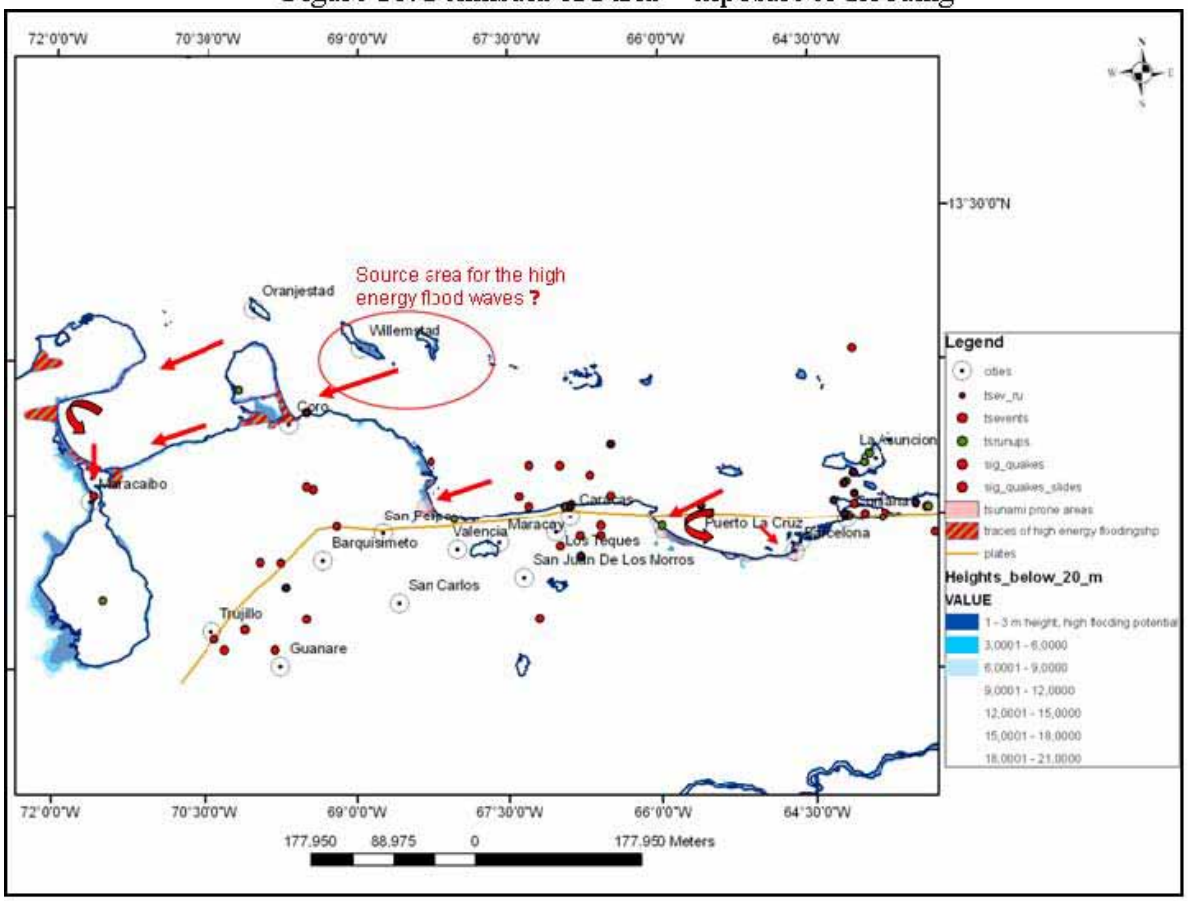

Figure 17: Overview of the tsunami prone areas in N-Venezuela and the flooding directions derived by the traces of erosional features and abrasion

ACKNOWLEDGMENTS

The author thanks ESA/ESRIN and DLR for providing ENVISAT, ERS and SRTM satellite radar and DEM data of NE Venezuela and the Fundación Venezolana de Investigaciones Sismológicas (FUNVISIS ,Venezuelan Foundation for Seismological Research, Caracas) for providing geophysical and geological data. In the scope of the SRTM Mission 2000 the German Aerospace Center (DLR) in Oberpfaffenhofen supported the investigations (AO_029) by providing the necessary SRTM data sets. The same support was given by ESA during the ENVISAT mission (ID AEO.211). The ERS and ENVISAT satellite radar data from ESA were of great value for this study. The University of Maryland, USA is acknowledged for presenting the opportunity to download different satellite data (Global Land Cover Facility).

REFERENCES

Audemard, F., Rendón, H., Romero, G., (1999), Sismicidad, Neotectonica y Campo de Esfuerzo del Norte de Venezuela, FUNVISIS,Caracas.

Bankwitz,P. & Bankwitz,E.(1992): Application of Satellite Data to Seismic Risk Assessment: Strain Analysis of Fault Lineament Systems.- Berliner Geowiss.Abh.,D,1,51-58, Berlin

Baumbach, M.1, Grosser, H.1, Romero, G.2, Rojas, J.3, Sobiesiak, M.1, Welle, W.1, Schmitz, M.(1999): Time and Space Distribution of Cariaco Aftershocks, Focal Mechanisms and Statistical Analysis.- Internet: www.gfz-potsdam.de/pb2/pb1/TaskForce/Einsaetze/Cariaco/cariaco.html

Beltrán, C., (1994), Trazas Activas Y Sintesis Geotectonica de Venezuela A Escala 1:2.000.000, Memorias del VII Congreso Venezolano de Geofísica, pp. 541 – 547.

Beltran,C., Rodriguez,J.A., Singer,A. & Rivero,C. (1999): La Trincheira de las Toscanas. Evidencias Paleosismologicas de Actividad Recente de la Falla de El Pilar entre Casanay y Rio Casanay, Venezuela.- Internet : dptoct@funvisis.internet.ve

Fay O'Loughlin,K. and Lander, J. (2003: Caribbean Tsunamis, A 500-Year History from 1498-1998, ISBN 1-4020-1717-0 edition)

FUNVISIS (Fundación Venezolana de Investigaciones Sismológicas, 1997): The July,9,1997, Cariaco, Eastern Venezuela, Earthquake.- EERI Special Earthquake Report,Oct.1997,

Pararas-Carayannis, G.(2004): Volcanic Tsunami Generation Source Mechanisms in the Eastern Caribbian Region.-Science of Tsunami Hazards, Vol. 22, No. 2, 74-114 (2004), http://library.lanl.gov/tsunami/ts222.pdf

Passalacqua,H., Fernandez,F., Gou,Y. & Roure,F. (1995) : Crustal Arcitecture and Strain Partitioning in the Eastern Venezuelan Ranges.-.- in: TANKARD,A.J. et al.(1995): Petroleum Basins in South America: AAPC Memoir 62, p.667-679

Russo, R. M., Speed, R. C., Okal, E. A., Shepherd, J. B., Rowley, K. C., 1993: Seismicity and tectonics of the southeastern Caribbean. J. Geophys. Res. 93, 14,299-14,319. Schmitz, M.(1999): Time and Space Distribution of Cariaco Aftershocks, Focal Mechanisms and Statistical Analysis.- Internet: http://www.gfz-potsdam.de/pb2/pb21/Task_Force/Einsaetze/Cariaco/cariaco.html

Theilen-Willige,B. (2002): Beitrag der Fernerkundung zur Erdbebenvorsorge – Fernerkundungsmethoden bei der Erfassung von durch Erdbeben und Erdbebenfolgeschäden gefährdeten Bereichen.- in: Fiedler,F., Nestmann,F. & Kohler,M.(2002,Hrsg): Naturkatastrophen in Mittelgebirgsregionen.- Verlag für Wissenschaft und Forschung (VWF), Berlin, 245-270 Theilen-Willige,B. (2006 a): Tsunami Risk Site Detection in Greece based on Remotes Sensing and GIS Methods.- Science of Tsunami Hazards, Volume 24, No. 1, 35-48, http://www.sthjournal.org/241/willige.pdf

Theilen-Willige, B. & Taymaz. T. (2006) Remote Sensing and GIS Contribution to Tsunami Risk Detection of coastal Areas in the Mediterranean
http://www.ewc3.org/upload/downloads/Symposium_MegaEvents_05_Theilen-Willige_057.pdf

Theilen-Willige,B. (2006 b): Emergency Planning in Northern Algeria based on Remote Sensing Data in Respect of Tsunami Hazard Preparedness, Science of Tsunami Hazards, Vol.25, 3-18,
http://sthjournal.org/251/willige1.pdf
http://sthjournal.org/251/willige2.pdf

Wood, J.D. (1996): The geomorphological characterisation of digital elevation models PhD Thesis, University of Leicester, UK, http://www.soi.city.ac.uk/~jwo/phd

SEDIMENT CHARACTERISTICS OF THE M-9 TSUNAMI EVENT BETWEEN RAMESWARAM AND THOOTHUKUDI, GULF OF MANNAR, SOUTHEAST COAST OF INDIA

S.R.Singarasubramanian, M.V.Mukesh, K.Manoharan
S.Murugan, D.Bakkiaraj, A.John Peter
Department of Earth Sciences,
Annamalai University,
Annamalainagar-608002,
Tamilnadu, India
e-mail: laksrs@yahoo.com

P.Seralathan
Department of Marine Geology & Geophysics,
Cochin University of Science and Technology,
Fine Arts Avenue,
Cochin,
Kerala, India

ABSTRACT

On 26th December, 2004, a massive earthquake occurred NW of Sumatra in the seismically active zone close to Sunda Trench at a water depth of about 1300m and with an epicenter located at a shallow depth of 10km below the ocean floor. This earthquake triggered tsunami waves in the Indian Ocean and hit most of the Tamilnadu coast, with wave height varying from 3 to 10m. In the study area dunes were breached. Erosional channels were created. Inundation in the study area ranges between 10 and 600m from the shoreline. The inundated sediment thickness varies from 1 to 30cm and was well preserved. Sediments thickness gets reduced landwards and occurs as set of layers. The sediments were fresh, grey to dark grey in color.

INTRODUCTION :

Tsunamis transport sediments from the offshore and beach, subsequently deposit them over the coastal low lands. Tsunami deposits fine landward, while river deposits generally fine seaward (Nelson et. al. 1996b). Multiple normal graded beds within the deposit suggest deposition by successive tsunami waves rather than a storm surge (Nelson et. al. 1996b). Tsunamis have the potential to deposit sand farther inland or at a higher elevation than storms (Dawson and Shi, 2000). Tsunami deposits may be of three categories (Whelan and Kelletat, 2003) as large clasts, coarse to fine sand and other fairly obscure deposits such as wash over fans. The composition and texture of sand grains can be used to determine a coastal source (Peterson and Darienzo, 1996).

Ancient tsunamis have also been inferred based on sand sheets found in coastal low lands, including those found in Scotland (Dawson et. al., 1988; Long et. al., 1989), Japan (Minoura and Nakaya, 1991), New Zealand (Clague-Goff and Goff, 1999), the Mediterranean (Dominey- Howes et. al, 1999; Minoura, et. al., 2000) and the Pacific Coast of North America (Clague et. al., 2000). Sand sheets are important markers of ancient tsunamis, especially serve as the only record of some prehistoric tsunamis.

The impact of tsunami waves on coastline will be very severe due to their greater wavelengths and wave periods. If there is sufficient sediment supply, tsunami waves are constructive as they move inland, and transport a variety of grain sizes ranging from silt to large boulders. The retreating waves can remobilize and erode sediments (Barbara Keating et al., 2004). The most common tsunami deposits are fine sediments that most frequently occur as sediment sheets. An attempt has been made to decipher the tsunami sediment deposits and its characteristics between Rameswaram and Thoothukudi, Gulf of Mannar, Tamilnadu, India.

STUDY AREA

The present study area forms the part of east coast of India and southern part of Tamilnadu. The study area is located between Rameswaram (Lat. 9.28345 and Long. 79.32142) in the north and Thoothukudi (Lat. 8.44593 and Long. 78.10071) in the south. The study area includes the coastal villages of Ramanathapuram and Thoothukudi districts. (Map No. 1).

The shelf width off Pamban in the Gulf of Mannar is about 25 km and the shelf break occurs more or less at about 200m depth. The shelf is very wide off the coast between Sippikulam and Tuticorin. The 20m depth contour lies at distance of 30 km between Rameswaram island and Valinokkam and about 40-45 km between Valinokkam and Tuticorin. The Rameswaram and Tuticorin coast is characterized by the presence of 21 coral islands with varying sizes and arranged in an en echelon manner within the 20m depth contour. These features have effectively altered by the tsunami waves.

Along the coast several morphological features have induced in the inundation levels. A prominent spit is occurring near Thoothukudi, running few kilometers in length. It joins with main land and forming Tombolo. Beach ridges are found to be

discontinuous. They are varying in length and width. These are distributed for a few kilometers away from the coastline, but lying parallel to the shoreline. These ridges are separated by salt pans and in some places by swales. Beach ridges are compact and almost covered by vegetation.

Sand dunes are formed at interface between sea and land. They bordered the high tide mark and extend inland up to 2 to 5 km. They run parallel to the shoreline separated from each other by marked troughs. The crests are flat and range in height from 0.5 to 2m. They are stabilized by the vegetation. After the mega tsunami event the sand dunes were breached in many places and the coastal geomorphology has changed. In many places the channels were diverted or filled with sediments or new formations of erosional structures were observed. The coastal regions become steep in some places and shallow in some places due to the differential erosion and accretion of sediments by tsunami waves.

METHODOLOGY :

The inundation distance of tsunami waves were marked using Garmin-12 GPS. The distance and height of the waves were noted by observing the water level marks in the walls of houses. Sediment samples were collected along several coastal settings like beaches, intertidal environments, and coastal plains by penetrating 8cm diameter PVC pipes up to 1m depth. Before that a pit was made to study layering and for photography. The collected samples were washed and sieved at ¼ phi interval ASTM sieve sets for 20 minutes. The grain size distribution was studied to determine sedimentary environment with the help of log-probability studies.

SURFICIAL IDENTIFICATION:

Identification of tsunami deposits was based on several criteria, including differences in grain size and color. Sedimentary deposits from the tsunami were found in most places where significant inundation occurred. Tsunami deposits were overlying a known preexisting surface that was texturally distinct, such as from soils identification was fairly simple, where as if the underlying material was beach sand that was similar both texturally and visually, identification was more difficult. In tsunami deposits, grain size generally fines upwards and rip-up clasts may be present. The base of the deposits erodes underlying structures and a heavy mineral layer may be present at the base. Underlying sands were often trampled while tsunami sands were relatively undisturbed. Many of the deposits had multiple layers.

GEOMORPHIC CHANGES:

There are many changes in the geomorphic features after tsunami. It was observed that tsunami sediments were deposited as layers with fining up sequences, indicating repeated wave attack with different wave velocities which brought considerable sediments from near/offshore to land. The thickness of sediments varies from place to place. Tsunamigenic sediment thickness steadily thins landward. Certain coastal segments of the study area (stations 1 to 6) were not affected much by the tsunami waves- only uprush were witnessed by the local communities. Hence inundation level and sedimentation was very less in these segments when compared to the southern sector (Fig.1). Station 7, encountered only erosion but no sedimentation by tsunami.

The southern 5 stations (8-14) were affected by tsunami waves. In station-8, 9 &10) the very thick sedimentation took place along the coast. The shoreline was filled with sediments to an extent of about 120cm thick with 150m length and 20m width along the coast. Tsunami waves entered up to 150m inland. Coastal morphology was completely altered. Thick sedimentation in the northern part of station 8 leads to the extent of beach towards the sea. The sediments were fresh, fine to medium, loosely packed and layered. Here rich heavy minerals were deposited as bands on the surface by tsunami waves. The segregation of heavy minerals into fine and coarse was observed. The coarser heavy minerals were deposited away from the coast and fine near the coast (5 to 20m from the coast).

Stations 11&12 were also affected by the sedimentation due to the tsunami waves. The inundation is up to 75m inland. The sediments were deposited over the normal coarser beach sediments as thin layers. The layering was prominent with thin dark colored bands of sediments. The thickness is about 10 to 15cm only. The fresh sediments brought by tsunami were identified based on their freshness, color and textural difference from the older sediments. Oxidation of fresh sediments was observed. Behind the Harbor Guest House in station 14, the sedimentation was up to 500m inland from the shore. Tsunami waves enter into the inland by eroding a channel of 15m width near the coast and become narrow in inland. The sediments entered through the channel to the inland. Sedimentation took place in and around the channel. Fresh fine and loose, layering of sediments was noticed in the inland. The thickness is about 50cm. Dark banding of sediments is prominent. In station 15, near the AMD plant, the tsunami waves enter inland into the dense scrubs. The inundation is up to 60m inland. Erosion along the shore line is prominent. Fine sediments with layering were deposited over the eroded surface along the coast. The thin dark colored bands of sediments were observed. The thickness of fresh fine sediments deposited over the coarser fragments is about 30cm.

The Gulf of Mannar coast was affected by the diffracted tsunami waves from the southern Sri Lankan coast. Tsunami inundation along the southern Mannar coast is moderate. Tsunami impact along the northern Gulf of Mannar coast between Thanushkodi and Tuticorin is rather very meager due to the presence of 21 coral islands. The coast is considered as raised coast consisting of coralline terraces.

In general, the study area encountered good sedimentation in some locations depending upon their geomorphological setup. From the study, it was observed that the tsunami waves propagation was almost from south east and flowed to north west. These waves are diffracted, since the region is located in and near the shadows of Sri Lanka. The wave velocity is also less due to the shallow nature of the coasts.

GRANULOMETRIC STUDIES:

The grain size distribution is believed to be considered of several normal subpopulations representing the sediments transported by the process of rolling, suspension and saltation (Inman, 1949). The combination of two or more of these processes produces characteristics log probability curve shapes. The mentioned characteristics of the sediments and the mechanisms were utilized to study the size analysis. Textural attributes of sediments and sedimentary rocks viz. mean (Mz),

standard deviation (σ1), skewness (SkI) and kurtosis (K_G) are widely used to reconstruct the depositional environments of sediments and sedimentary rocks (Amaral, 1977). Correlation between size parameters and transport processes/depositional mechanisms of sediments has been established by exhaustive studies from many modern and ancient sedimentary environments (Folk and Ward, 1957; Mason and Folk, 1958; Friedman, 1961, 1967; Visher, 1969; Valia and Cameron, 1977; Wang et. al, 1998; Asselman, 1999; Malvarez et.al., 2001). Mean size is the average size of the sediments influenced by the source of supply, transporting medium and the energy conditions of the depositing environment.

The phi mean size of the samples varies from 0.830 to 3.153 Φ with an average mean of 2.143Φ (Fig.2) (Table 1). The majority of the sediments (67%) samples fall in fine sand category and the rest in medium sand category. The mean size indicates that the fine sands were deposited at a moderately low energy conditions and the medium sand were deposited at a moderate energy conditions. The variation in phi mean size, therefore, reveals the differential energy conditions leads to the deposition of these kinds of sediments in different locations.

Standard deviation (σ1) measures the sorting of sediments and indicates the fluctuations in the kinetic energy or velocity conditions of the depositing agent (Sahu, 1964). The standard deviation values of the sediments range between 0.463 and 0.717 Φ with an average value of 0.630 Φ (Fig.2). The sorting of sediments range from well sorted to moderately sorted character. About 50% of the samples fall under moderately well sorted nature. Well sorted nature was represented by rest of the samples. This kind of sorting nature of the sediments may be due to the intermixing and influx of the sediments from sea as well as the river. The presence of fine sand and well sorted nature suggests effective wave action to scour the sediments from the shelf region during the break of tsunami waves. Skewness (Ski) measures the asymmetry of a frequency distribution. The skewness values range between -0.159 (Station -11) and 1.145 (Station-1) with an average value of 0.029 (Fig.2). The symmetry of the samples varies from strongly fine skewed to strongly coarse skewed nature. The strongly fine skewed and fine skewed sediments generally imply the introduction of fine material or removal of coarser fraction (Friedman, 1961) or winnowing of sediments (Duane, 1964). The predominant fine skewed nature of sediments indicates excessive riverine input. The positive skewness (50%) of sediments indicates the unidirectional transport (channel) or the deposition of sediments in sheltered low energy environment (Brambati, 1969).

Values of the fourth moment kurtosis(K_G) ranging between 0.871 (Station-9) and 1.949 (Station-4) with an average of 1.276 (Fig.2). Majority (75%) of the samples falls under leptokurtic to very leptokurtic nature of distributions. Friedman (1962) suggested that extreme high or low values of kurtosis imply that part of the sediment achieved its sorting elsewhere in a high energy environment. The variation in the kurtosis values is a reflection of the flow characteristics of the depositing medium (Seralathan and Padmalal, 1994; Baruah et. al., 1997). Finer in size and dominant leptokurtic nature of sediments reflect maturity of the sand and variation in the sorting values are likely due to continuous addition of finer/ coarser materials in varying proportions (Prabhakara Rao et. al., 2001).

The size analyses of vertical core sample show a distinct difference between the deposition of sediments by normal cycle of waves and by tsunami waves. In Taruvaikulam, sediments were showing a sudden increase in mean size from 1.137 to 1.757 at a depth of about 40cm and 1.947 at the top. The bottom sediments having a maximum mean size of 1.307 at a depth of 80cm. The average mean size of the bottom sediments between 40 and 100 cm depth was only 1.214, where as the average above 40cm depth is 1.794 (Fig.3). Likewise there was a remarkable change in other size parameters also. This clearly indicates the sudden input of sediments during tsunami in the Taruvaikulam region.

According to Sahu (1964), the variations in the energy and fluidity factors seem to have excellent correlation with the different processes and the environment of deposition. Sahu's linear discriminant functions of Y1 (Aeolian, beach), Y2 (Beach, shallow agitated water), Y3 (shallow marine, fluvial) and Y4 (turbidity, fluvial) were used to decipher the process and environment of deposition. With reference to the Y1 and Y2 values, six samples (50%) fall in beach process (Y1) and ten (83%) samples deposited by shallow agitated water (Y2) respectively. Eleven samples (92%) were showing the Y3 values fall in shallow marine environment. The Y4 values show that about 42% of the samples were deposited by fluvial action and 58% by turbidity action (Table-2). The results indicate that most of the sediments were deposited under shallow marine environment by beach and fluvial processes by a near shore whirlpool agitating turbidity action of water.

Fig. 1 Showing inundation distance of tsunami waves towards inland

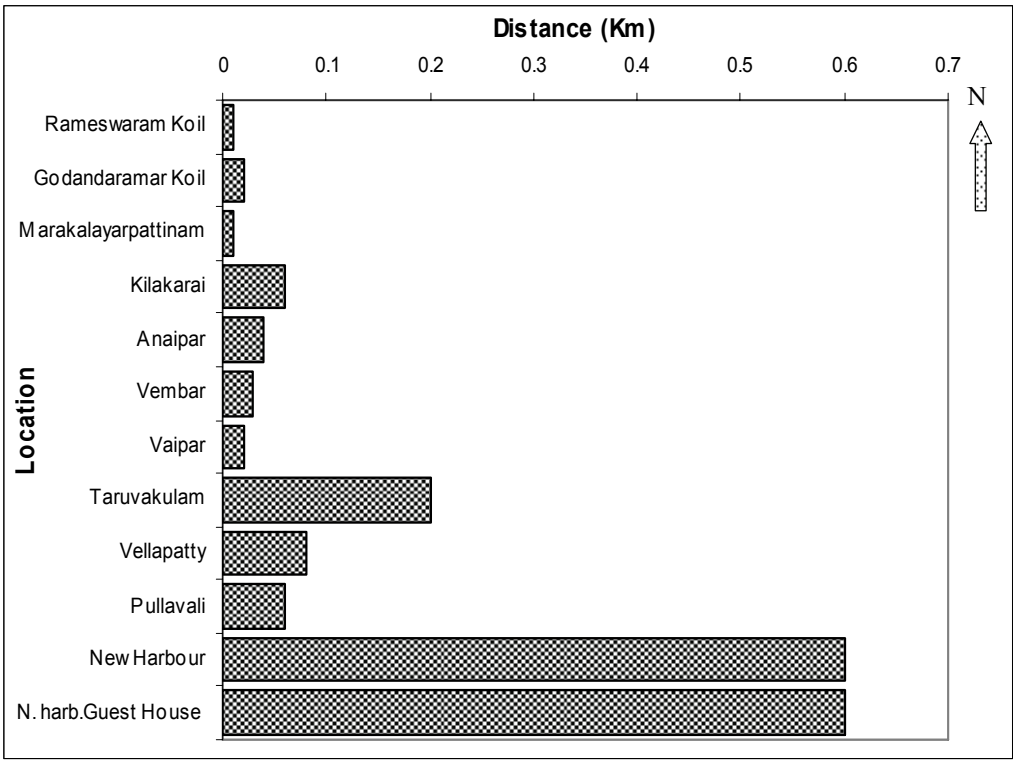

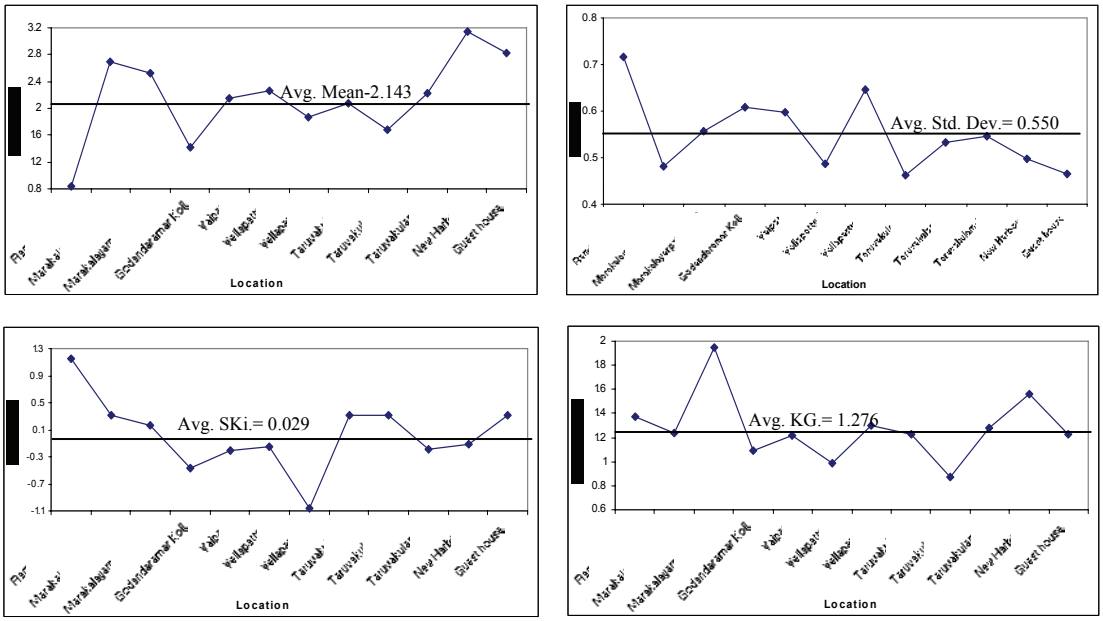

Fig-2 Showing horizontal variation of size parameters in various locations

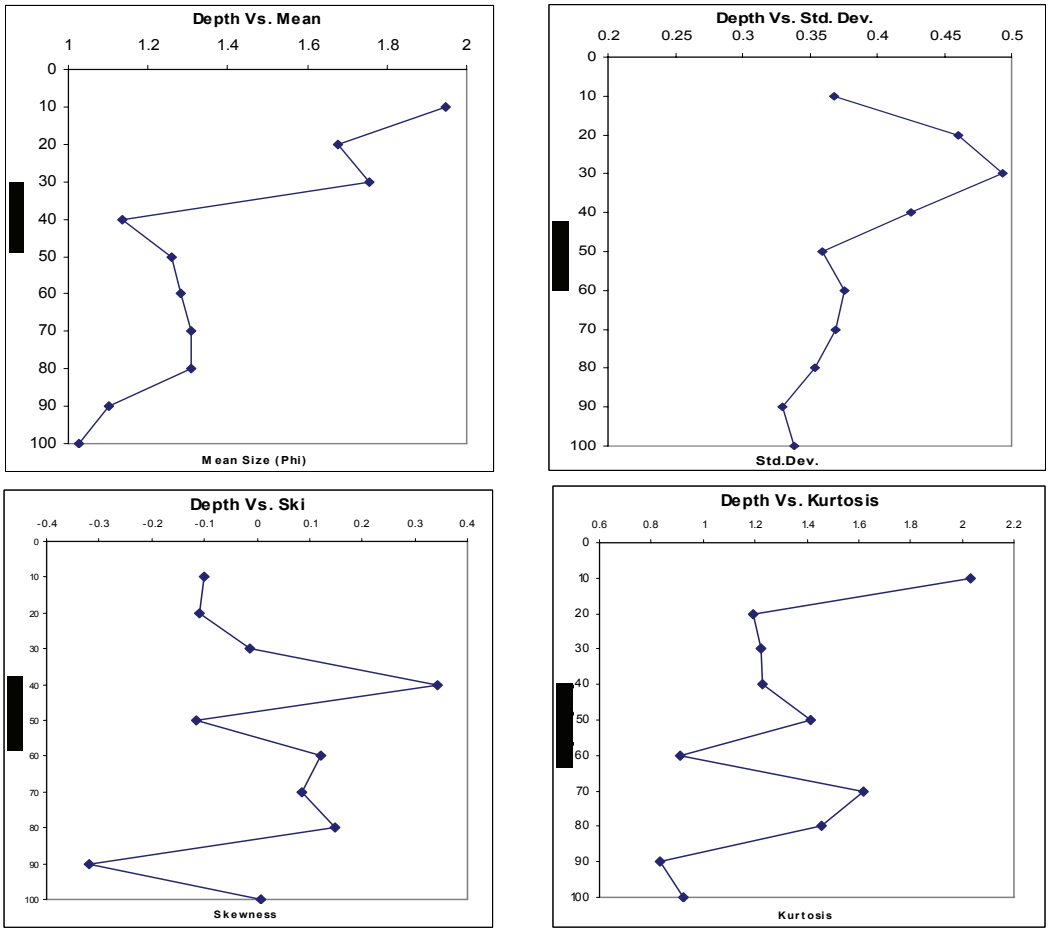

Fig-3 Showing vertical variation of size parameters

SUMMARY AND CONCLUSION

The catastrophic waves generated by tsunami on 26th December, 2004 in the Indian Ocean devastated the Tamilnadu and parts of Andhra and Kerala coasts. Houses built along the coastal belt, coastal landforms and beaches were heavily damaged by strong tsunami inundation. The tsunami waves alter severely the mouth and estuary regions. The tsunami waves enter inland from the SSE direction in the study area as diffracted waves. The inundation varies from 0.01km to 0.6km.

The waves alter the sediment dynamics when enter the coastal zone, thus altering the coastal geomorphology by breaching coastal dunes, eroding beaches to form new channels, filling of estuaries and backwater channels by sediments. This preliminary investigation gives an idea about the sedimentological evidence preserved between Rameswaram and Thoothukudi.

The coastal morphology in Taruvaikulam and Thoothukudi harbor were altered by breaching of coastal dunes, erosion along the beach and deposition of fines along the coast. Effect of tsunami waves was more along the projected and flat beaches. The shallow shelf beaches were not affected by the tsunami waves. Beach erosion is also prominent in the flat beaches. Thick and extensive sediment deposition was observed at Taruvaikulam, where the coast is slightly projected towards the sea in the northern part. The northern part hence received a good sedimentation than the southern part, where there was no much change.

In general the tsunami sedimentation in the study area indicate that they were deposited at different time intervals at different inundation distances. They were thinning landward. Multiple grading of sediment deposition was prominent, indicating that the deposition took place at different time intervals and by successive waves.

From the granulometric analysis of sediments indicates a moderately well sorted nature of the sediments and moderate energy condition in the depositional environment. This is well supported by the mean size of sediments which vary from fine to medium in size and the standard deviation of sediments indicating that they were well sorted to moderately sorted characters. The sorting character infers that the sediments were from beach and not from rivers. The predominant positive skewness of the sediments indicating a unidirectional transport or deposition in sheltered low energy. The mesokurtic to leptokurtic nature of sediments refers to the continuous addition of finer or coarser materials and retention of their original characters during deposition. The size distribution of sediments indicate that a bimodal or polymodal distribution. The histogram indicates wide range of size distribution and asymmetrical nature of sediments, but predominantly the finer clastics are more and the lacking by coarser clastics.

From the energy process discriminant functions of Sahu (1964), the sediments were deposited by beach and fluvial processes under shallow agitating environment and carried by turbidity action. The results indicate that most of the sediments were deposited by beach processes than by fluvial influence under a nearshore whirlpool agitating environment.

Acknowledgment:

Author whole heartedly acknowledges DST-SERC for providing financial assistance in the form short term project. He also thanks to co-authors and university authorities for providing necessary infrastructure facilities for this research.

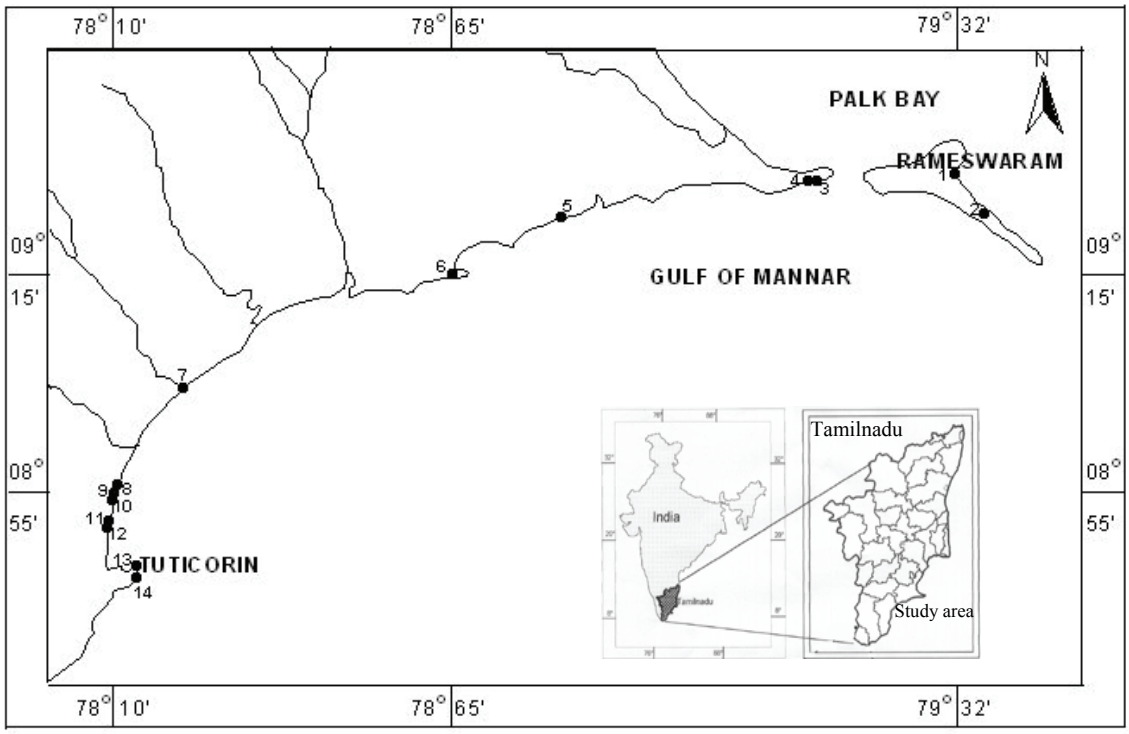

Map -1 Showing study area and sampling locations

Table – 1 Showing the Statistical Analysis of surface samples

Stn. No	Mean	Std. Dev	Skewness	Kurtosis	Remarks
1.	0.830	0.717	1.145	1.375	Coarse sand, Moderately Sorted, St. Fine Skewed, Leptokurtic
2.	1.410	0.608	-0.473	1.093	Medium sand, Moderately Well Sorted, St.Coarse Skewed, Mesokurtic
3.	2.697	0.482	0.307	1.237	Fine Sand, Well Sorted, St. Fine Skewed, Leptokurtic
4.	2.517	0.558	0.173	1.949	Fine Sand, Moderately Well Sorted, Fine Skewed, Very Leptokurtic
5.	1.784	0.754	-0.179	1.324	Medium sand, Moderately, Coarse Skewed, Leptokurtic
6.	1.987	0.654	-0.241	1.056	Medium Sand, Moderately Well Sorted, Coarse Skewed, Mesokurtic
7.	2.154	0.598	-0.215	1.215	Fine Sand, Moderately Well Sorted, Coarse Skewed, Leptokurtic
8.	2.083	0.463	0.313	1.230	Fine sand, Well Sorted, St. Fine Skewed, Leptokurtic
9.	2.233	0.546	-0.185	1.277	Fine Sand, Moderately Well Sorted, Coarse Skewed, Leptokurtic
10.	2.267	0.486	-0.159	0.984	Fine Sand, Well Sorted, Coarse Skewed, Mesokurtic
11.	1.877	0.646	-1.055	1.296	Medium Sand, Moderately Well Sorted, St. Coarse Skewed, Leptokurtic
12.	3.153	0.498	-0.123	1.557	Very Fine Sand, Well Sorted, Coarse Skewed, Very Leptokurtic
13.	2.817	0.464	0.306	1.230	Fine Sand, Well Sorted, St. Fine Skewed, Leptokurtic
14.	1.770	0.556	0.203	0.853	Medium Sand, Moderately Well Sorted, Fine Skewed, Platykurtic

Table -2 Showing Linear discriminant function values (after Sahu, 1964)

Stn.No.	Y1	Y2	Y3	Y4	Remarks			
					Y1	Y2	Y3	Y4
1.	0.8442	92.9487	-9.8033	15.3775	Beach	Sh. Agitated water	Fluvial (deltaic)	Fluvial (deltaic)
2.	0.7216	58.0221	-0.4691	3.4689	Beach	Beach	Shallow Marine	turbidity
3.	-5.5512	85.9317	-2.7087	10.4661	Aeolian	Sh. Agitated water	Shallow Marine	Fluvial (deltaic)
4.	-2.1212	99.0565	-2.7624	13.1707	Beach	Sh. Agitated water	Shallow Marine	Fluvial (deltaic)
5.	0.2317	86.5409	-3.5319	6.8605	Beach	Sh. Agitated water	Shallow Marine	turbidity
6.	-1.7197	74.3849	-1.9501	5.2279	Beach	Sh. Agitated water	Shallow Marine	turbidity
7.	-2.1341	75.8050	-1.4078	6.3932	Beach	Sh. Agitated water	Shallow Marine	turbidity
8.	-3.4607	75.1198	-2.7562	10.0337	Aeolian	Sh. Agitated water	Shallow Marine	Fluvial (deltaic)
9.	-2.5055	74.8232	-1.0080	7.0043	Beach	Sh. Agitated water	Shallow Marine	turbidity
10.	-3.8223	66.3357	-0.5972	5.6781	Aeolian	Sh. Agitated water	Shallow Marine	turbidity
11.	1.0720	61.6815	2.1043	0.9429	Beach	Beach	Shallow Marine	turbidity
12.	-5.2313	92.2353	-0.5965	9.5876	Aeolian	Sh. Agitated water	Shallow Marine	turbidity
13.	-6.0622	86.5436	-2.5207	10.5158	Aeolian	Sh. Agitated water	Shallow Marine	Fluvial (deltaic)
14.	-2.9382	67.4795	-3.1556	7.0338	Aeolian	Sh. Agitated water	Shallow Marine	Turbidity

Plate- I

Plate – I A- Distribution of fresh layered sediments after tsunami along the coast for 4" inch at Vellapatty; B- Distribution of fresh sediments and deserted trees by tsunami waves about 50m inland at Vellapatty; C- Deposition of heavy minerals by tsunami waves along the shore at Taruvaikulam; D- Deposition of fresh sediments and creation of water bodies by erosion due to tsunami waves at Taruvaikulam; E- Erosional land surface and formation of water bodies to a distance of 70m rom the shore at Thoothukudi ; F- Deposition of fine sediments in channel (150m from the shore) during the inundation of tsunami waves.

REFERENCES

Amaral, E.J. (1977): Depositional environment of the St. Peter sandstone deduced by textural analysis. Jour. Sed. Pet. 47, pp. 32-52.

Asselman,N.E.M. (1999): Grain size trends used to asses the effective discharge for flood plain sedimentation. River Waal, The Netherlands. *Jour. Sed. Research*. 69. p. 51-61.

Barbara K., Whealan.F., and J.Balley-Brock (2004): Tsunami deposits at Queen's beach, Oahu, Hawaii- Initial results and wave modeling. *Science of Tsunami Hazards,* V. 22; No. 1. p. 23-43

Baruah,.J. Kotoky.P. and Sarma.J.N. (1997): textural and geochemical study on river sediments: A case study on the Jhanji river , Assam. *Jour. Indian Assoc. Sedimentologists.* 16. p. 195-206.

Brambati.A. (1969): Stratigraphy and sedimentation of Siwaliks of North Eastern India. *Proc. Inter. Sem. Intermontane Basins: Geology and Resources*, Chiang Mai, Thailand. P.427-439.

Chague-Goff, C., and J.R. Goff (1999): Geochemical and sedimentological signature of catastrophic saltwater inundations (tsunami), New Zealand. *Quaternary Australasia*. 17. p.38-48.

Clague, J.J., P.T. Bobrowsky and I. Hutchinson (2000): A review of geological records of large tsunamis at Vancouver Island, British Columbia and implications for hazard. *Quaternary Sci. Rev.* 19. p.849-863.

Dawson, A.G. and S.Z.Shi (2000): Tsunami deposits. *Pure Appl. Geophys., 157,* 875-897.

Dawson, A.G., D.Long and D.E.Smith (1988): The Storegga slides: evidence from eastern Scotland for a possible tsunami. *Mar.Geol.,* 82. p.271-276.

Dominey-Howes,D., A.Cundy and I.Croudace (1999): High energy marine flood deposits on Astypalaea Island, Greece: Possible evidence for the AD1956 southern Aegean tsunami. Mar. Geol., 163. p. 303-315.

Duane, D.B. (1964): Significance of skewness in recent sediments, western Pamlico Sound, North Carolina; *Jour. Sed. Pet.*, v.34.p.864-874.

Folk. R.L. and Ward, W.C. (1957): Brazos River Bar: a study in the significance of grain size parameters. *Jour. Sed. Pet.,* 27. p. 3-26.

Friedman, G.M., (1961): distinction between (*sic*) dune, beach, and river sands from their textural characteristics: *Jour. Sed. Pet.,* v.31.p.514-529.

----------(1962): On sorting, sorting coefficients and the log normality of the grain-size distributions of sandstones. *Jour. Geol*. 70. p. 737-753.

----------(1967): Dynamic processes and statistical parameters compared for size frequency (*sic*) distribution of beach (*sic*) and river sands. *Jour. Sed. Pet*. 37. p.327-354.

Inman, D.L.(1949) Sorting of sediments in the light fluid mechanics, J*our. Sed. Pet.*, 19, pp.51-70

Long, D., D.E.Smith and A.G. Dawson (1989): A Holocene tsunami deposits in eastern Scottland. Jour.Quaternary Sci.,4 p.61-66.

Malvarez.G.C., Cooper.J.A.G. and Jackson.D.W.T. (2001): Relationship between wave induced currents and sediment grain size on a sandy tidal flat. *Jour. Sed. Research.* 71., p. 705-712.

Mason.C.C. and Folk,R.L. (1958): Differentiation of beach, dune and eolian flat environments by size analysis, Mustang Island, Texas. *Jour. Sed. Pet.,* 28. p.211-226.

Minoura,.K. and S.Nakaya (1991): Traces of tsunami preserved in inter-tidal lacustrine and marsh deposits: Some examples in northeast, Japan. Jour. Geology, 99. p.265-287.

Minoura, K. F.Imamura, U.Kuran, T.Nakamura, G.A. Papadopoulos, T.Takahashi and A.C.Yalciner (2000): discovery of Minoan tsunami deposits. Geology, 28, p. 59-62.

Nelson, A.R., I Shennan, and A.J.Lonh (1996 b): Identifying coastal subsidence in tidal wetland stratigraphic sequences at Cascadia subduction zone of western North America. *J. Geophys. Res., 101 (B3)*, 6115-6135

Peterson, C.D. and M.E.Dareinzo (1996): Discrimination of climatic, oceanic and tectonic mechanisms of cyclic marsh burial. *In assessing Earthquake Hazards*.

Prabhakara Rao.A., Anilkumar.V., Yugandhar Rao.A., Ravi.G.S. and Krishnan.S. (2001): Grain size parameters in the interpretation of deposistional environments of coastal sediments between Bendi Creek and Vamsadhara river, East Coast, India. *Jour. Indian Assoc. Sedimentologists.* V.20.no.1. p. 106-116.

Sahu, B.K. (1964): Depositional mechanisms from the size analysis of clastic sediments. *Jour. Sed. Pet.*, v.34.p.73-83.

Seralathan.P. and Padmalal.D (1994): Textural studies of the surficial sediments of Muvattupuzha river and central Vembanad Estuary, Kerala. *Jour. Geol. Soc. India*. 43. p. 179-190.

Valia. H.S. and Cameron, B. (1977): Skewness as paleoenvironmental indicators. Jour. Sed. Pet. 4. p.784-793

Visher, G.S. (1969): Grain size distributions and depositional process. Jour. Sed. Pet., 39. p. 1074-1106.

Wang.P., Davis.R.A. and Kraus.N.C.(1998): Cross shore distinction of sediment texture under breaking waves along low energy coasts. *Jour. Sed. Research*. 68. .497-506.

Wedephol, K.H. Ed. (1974): *Handbook of Geochemistry*, Springer Verlag Berlin, Heidelberg, New York.

Whelan, F. and Kelletat, D. (2003): Analysis of tsunami deposits at Trafalgar, Spain, using GIS and GPS technology. *Essener Geographische Arbeiten* 35; P.25.

STRATEGIC GEOGRAPHIC POSITIONING OF SEA LEVEL GAUGES TO AID IN EARLY DETECTION OF TSUNAMIS IN THE INTRA-AMERICAS SEA

Joshua I. Henson[1)], Frank Muller-Karger[1)], Doug Wilson[2)]
Steven L. Morey[3)], George A. Maul[4)], Mark Luther[1)], Christine Kranenburg[1)]

[1)] College of Marine Science
University of South Florida
140 7th Ave S. St. Petersburg, FL 33705 United States

[2)] Office of Atmospheric Research
National Oceanic and Atmospheric Administration
NOAA Chesapeake Bay Office Annapolis, MD 21403 United States

[3)] Center for Ocean-Atmospheric Prediction Studies
Florida State University
Tallahassee, FL 32306 United States

[4)] Department of Marine and Environmental Systems
Florida Institute of Technology
150 W. University Blvd Melbourne, FL 32901 United States

ABSTRACT

The potential impact of past Caribbean tsunamis generated by earthquakes and/or massive submarine slides/slumps, as well as the tsunamigenic potential and population distribution within the Intra-Americas Sea (IAS) is examined to help define the optimal location for coastal sea level gauges intended to serve as elements of a regional tsunami warning system. The goal of this study is to identify the minimum number of sea level gauge locations to aid in tsunami detection and provide the most warning time to the largest number of people. We identified 12 initial, prioritized locations for coastal sea level gauge installation. Our study area approximately encompasses 7ºN, 59ºW to 36ºN, 98ºW. The results of this systematic approach to assess priority locations for coastal sea level gauges will assist in developing a tsunami warning system (TWS) for the IAS by the National Oceanic and Atmospheric Administration (NOAA) and the Regional Sub-Commission for the Caribbean and Adjacent Regions (IOCARIBE-GOOS).

INTRODUCTION

Historical data suggest that tsunamis have occurred in the Intra-Americas Sea (IAS) region approximately once every 3-yr, and destructively once every 21-yr [*O'Loughlin and Lander*, 2003]. According to Bryant [2005], approximately 14% of all tsunamis have occurred in the Caribbean. When considering only Hawaii, Alaska, the U.S. West Coast, and the Caribbean, about 2,590 victims or 83% of all tsunami fatalities in these regions over the last 150 years occurred in the Caribbean [*O'Loughlin and Lander*, 2003]. As a result of these recorded fatalities and the rise of Caribbean population by almost 300% from 1950 to 2000 [*CIAT, et al*., 2005], protection of human life is a primary reason for establishing a TWS in this region. In this work, historical tsunamis in the IAS are analyzed with the aid of a numerical ocean model and the results are used to suggest locations for coastal sea level gauges for the most efficient implementation of a TWS for the IAS region.

A tsunami is a series of large amplitude, shallow water gravity waves generated by an event capable of displacing a huge volume of water. Whether a gravity wave is considered to be a shallow or deep-water wave depends on the ratio between its wavelength and the depth of water.

Deep-water wave: $\lambda < 2\,H$
Shallow-water wave: $\lambda > 20\,H$
where, λ = wavelength and H = water depth

While tsunamis are usually generated in deep water, they are considered shallow-water waves because the typical wavelength of a tsunami is 220,000-m and the average depth of the Caribbean is approximately 2600-m.

Tsunamis propagate at the shallow water gravity wave phase speed of $c = (g\,H)^{1/2}$, which can be in excess of 222 m s^{-1} (~ 800 km hr^{-1}), until they dissipate or encounter a shelf and shallow coastal water where they slow to 8 – 14 m s^{-1} (~ 30 – 50 km hr^{-1}) [*NOAA and USGS Fact Sheet*, 2005]. Tsunami dissipation primarily depends on the magnitude and character of the tsunamigenic event, although bottom topography and bottom type also play important roles. Eventually, the tsunami is likely to impact a shoreline where life and property are then endangered. This study seeks to understand how and where tsunamis are generated in the IAS, how they travel through this region, and where a minimum number of sensors should be located to most efficiently warn the public of an impending tsunami.

A comprehensive warning system typically uses a seismometer to detect a geological event capable of generating a tsunami, and then utilizes near-by sea level gauges to determine whether a tsunami was generated. The system also should be able to predict potential impact locations and wave height, and disseminate that information to decision-makers. Different types of tsunami warning systems/networks are currently being successfully employed to measure, record, and telemeter both oceanographic and meteorological data. Standard means of telemetry include satellite, radio, cellular, telephone line, or Internet. One type of tsunami monitoring system involves Real-Time Kinematic Global Positioning System (RTK-GPS) technology [*Kato, et al.*, 2001]. Curtis [2001] suggests a multi-sensor approach. The Pacific TWS utilizes a combination of coastal sea level gauges and Deep-ocean Assessment and Reporting of Tsunamis (DART) buoys to acquire data for tsunami detection and for propagation and coastal run-up prediction.

The predominant tsunamigenic events are earthquakes; however landslides, avalanches, submarine slumps or slides, volcanic eruptions, volcano flank failure, and oceanic meteor impact can also cause a tsunami [*Lander, et al.*, 2002; *McCann*, 2006; *Pararas-Carayannis*, 2004]. Often, a tsunami is the result of coinciding events, thus it can be difficult to identify the actual tsunamigenic mechanism(s). Seismic and/or volcanic activity can produce a submarine landslide, which can in turn generate a tsunami. When analyzing events from pre-instrument periods it can be difficult to determine if a submarine slump or slide occurred, and the actual direct tsunamigenic event, such as this, may remain undetected. The manner in which a tsunami is generated will affect the warning time available [*Lander, et al.*, 1999]. This warning time can be maximized by predicting how and where the next IAS tsunami is most likely to occur. In general, the closer a sea level gauge is to a tsunami origin, the more warning time available to other locations around the Caribbean basin.

When designing a TWS it is critical to understand the types of tsunamigenic mechanisms, the coastlines that are more likely to be affected by a tsunami, tsunami travel time to those coasts, and the resulting effects from historical tsunamis [*Lander, et al.*, 1999]. However, the historical record is incomplete. In this study, we simulate tsunamigenic events with the potential to have far-field (greater than 1000-km) destructive impacts. The results of the numerical simulations are combined with information on human population concentrations around the Caribbean to determine the most critical and advantageous locations for the installation of coastal sea level gauges.

Discussed later, most sub-aerial landslides and volcanic tsunami origins are only locally destructive and are therefore not considered in this study. In order to determine if a tsunami is truly destructive at a location, high resolution bottom topography and a model with run-up capability is required to predict the extent of inundation. Wave height along the coast is not analyzed in this study because local effects dictate the necessity of very high bathymetric and model grid resolution to determine wave amplitude at the seashore. Run-up results along a coastline can vary by a factor of 10 [*Hwang and Lin*, 1969; *Smith and Shepherd*, 1994].

Historical Tsunamis in the IAS Region

Shallow earthquakes, magnitude 6.5 or greater, cause the majority of Caribbean tsunamis [*McCann*, 2006]. O'Loughlin and Lander [2003] describe 127 reported tsunamis in the Caribbean basin over approximately the past 500-yr. Of those reported, the authors find that 53 are almost certainly true tsunamis and another 8 are most likely true. These tsunami events were generated by various sources including but not limited to earthquakes, submarine slides/slumps, volcanic eruptions, and more likely a combination of those three. Understanding how past tsunamis have affected the region will help determine how future tsunami disasters can be mitigated.

The historical record of tsunami origins and affected areas is sparse. The data used in this study is from both O'Loughlin and Lander [2003] and the National Geophysical Data Center [*NGDC*, 2005]. These original tsunami origin data have 0.1° precision [*Dunbar*, 2005, personal correspondence], and while there are historical records of areas affected by some of these events, for others there is no information regarding effects or arrival location. Therefore, a numerical model is used to simulate historical tsunamis. Criteria used to select the events that are simulated are discussed under Methods ("Creation of Tsunamigenic Events List"). The simulations are performed with the Navy Coastal Ocean Model (NCOM), described under Methods ("Modeling").

The Caribbean and Surrounding Tectonic Plates

In order to fully understand the nature of the earthquakes that may generate tsunamis, the plate boundaries and their movement must also be understood. Tectonic activity due to plate movement is the principal cause of earthquakes, 80% of which occur along the plate boundaries in the oceanic crust [*Woods Hole*, 2005]. Figure 1 shows the plates in the Caribbean region, their boundaries, and summarizes their interactions. The Caribbean (CA) plate is bordered to the north and east by the North American (NA) and South American (SA) plates, to the south by the SA, North Andes (ND), Panama (PM), and Cocos (CO) plates, and to the west by the CO plate [*Bird*, 2003; *Lander, et al.*, 2002; *McCann*, 2006; *O'Loughlin and Lander*, 2003; *Pararas-Carayannis*, 2004]. Sitting on the CA plate are the islands of Hispaniola, Puerto Rico, and Jamaica to the north, the Lesser Antilles to the east, and to the west is Central America. The South American continent boarders the CA plate to the south [*Bird*, 2003; *McCann*, 2006].

The CA plate is moving eastward approximately 20 ± 3 mm yr^{-1} relative to the NA and SA plates [*Demets*, 1993; *Grindlay, et al.*, 2005; *Lander, et al.*, 2002; *McCann*, 2006; *O'Loughlin and Lander*, 2003; *Pararas-Carayannis*, 2004; *ten Brink, et al.*, 2004]. Some estimates are as high as 37 mm yr^{-1} [*Mercado and McCann*, 1998; *Sykes, et al.*, 1982]. The NA and SA plates are subducting under the eastern margin of the CA plate, leading to the formation of the Lesser Antilles volcanic arc. At the northern boundaries, the CA plate is sliding past the NA plate leading to transpressional motion (compressive loading as a result of shear stresses) and uneven or oblique subduction near Puerto Rico [*Lander, et al.*, 2002; *McCann*, 2006; *O'Loughlin and Lander*, 2003]. The southern boundary is characterized by a complex convergent margin near Venezuela and strike-slip faults on land [*McCann*, 2006]. The CO plate is subducting under the CA plate on the western boundary, which also forms a chain of volcanic activity [*Lander, et al.*, 2002]. Further explanation on the tectonic regime of the CA and adjacent plates can be found in McCann [2006] and Grindlay et al. [2005].

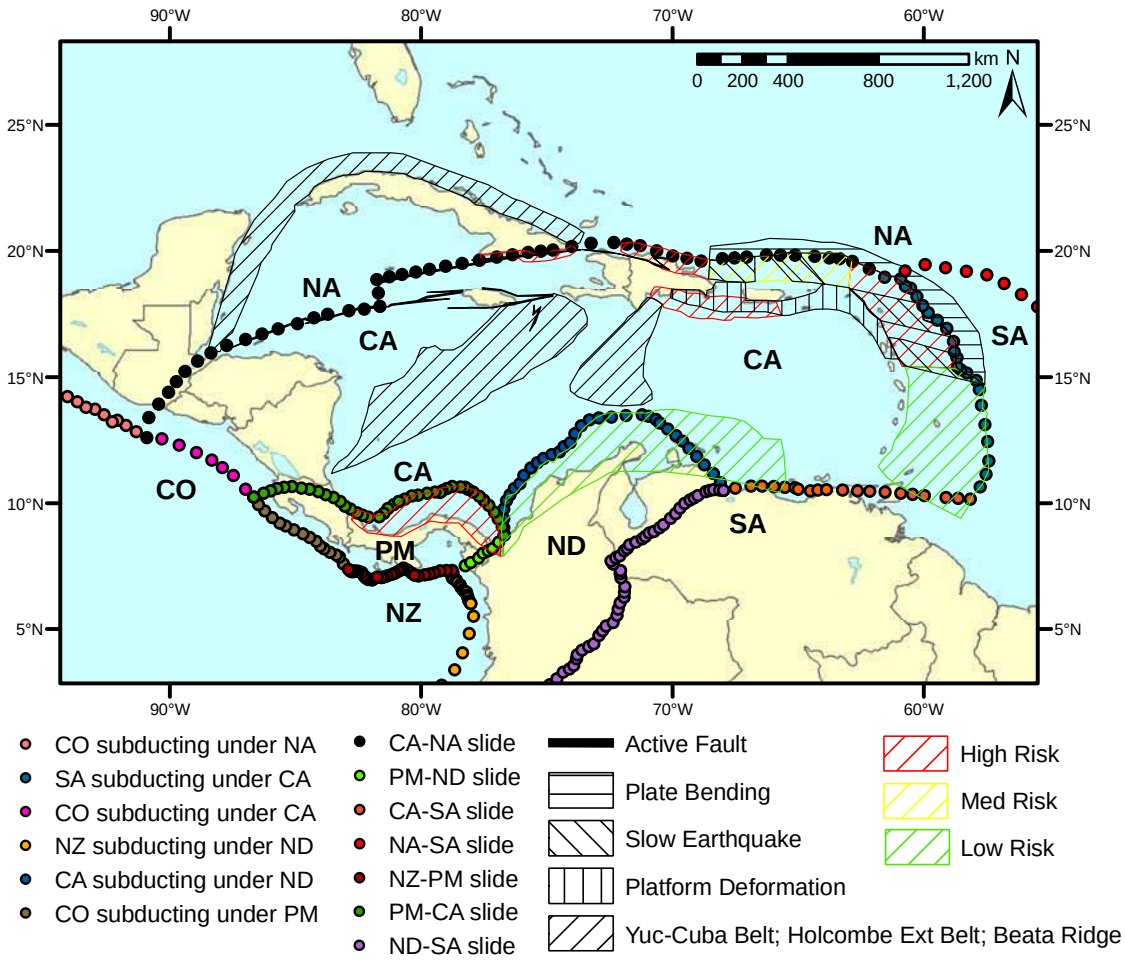

Figure 1 – Plate boundaries and interactions from Bird [2003] and tsunamigenic source regions from McCann [2006].

Tsunamigenic Earthquakes

There is a range of possible outcomes due to seismic activity in the Caribbean, some of which are more likely to produce a tsunami [*Grindlay, et al.*, 2005; *McCann*, 2006; *Mercado and McCann*, 1998]. The nature in which a tsunamigenic earthquake occurs will dictate the attributes of a resulting tsunami. Typically, significant vertical deformation of the sea floor (i.e. a dip/slip earthquake) is required for tsunami generation. This deformation can be due to either isostatic rebound of an accretionary prism near a subduction zone or a change in crustal elevation [*McCann*, 2006; *Okal, et al.*, 2003]. The direction of movement, depth of deformation, length and width of the deforming fault or plate boundary, deformation dip and slip angles, and focal depth will determine the size of the tsunami [*McCann*, 2006; *Polet and Kanamori*, 2000; *Zahibo, et al.*, 2003a]. For example, a shallow subduction zone earthquake or an earthquake with a more vertical angle of deformation will usually displace a larger volume of water and consequently generate a larger tsunami [*Bilek and Lay*, 2002; *Polet and Kanamori*, 2000]. The overlying geology also determines whether a tsunami will result from an earthquake [*Bilek and Lay*, 2002; *Kanamori*, 1972]. There may be stronger motion at the sea floor than the measured seismic moment would

typically represent if a rupture occurs within a sedimentary wedge or the rupture velocity is slow [*Okal, et al.*, 2003; *Polet and Kanamori*, 2000].

Regions where there is potential for an earthquake with a slow rupture velocity, or slow earthquake, to occur have a higher potential to produce a tsunami larger than a seismometer would otherwise indicate [*Polet and Kanamori*, 2000; *Todorovska and Trifunac*, 2001]. When the sea floor deformation velocity is on the same order as tsunami velocity (i.e. a slow earthquake, slide, or slump) the tsunami may be amplified by an order of magnitude [*Todorovska and Trifunac*, 2001]. The amplification may be caused by constructive interference as the tsunami is produced, since a slow rupture velocity will yield a longer duration earthquake [*Bilek and Lay*, 2002].

McCann [2006] defines seismic tsunamigenic threats in the Caribbean (see Figure 1) into the following categories: platform deformation, plate bending, slow earthquake, belts and ridges, active faults, and low to high tsunamigenic risk. These regions are based on the geologic and tectonic regime of the IAS, and the plate boundaries/interactions from Bird [2003] coincide with McCann's [2006] tsunamigenic zones.

Tsunamigenic Submarine Slides, Slumps and Landslides

These types of tsunamigenic events are typically initiated by an earthquake, hurricane, or volcanic event such as an eruption or flank failure, but they may also be initiated without an apparent catalyst [*Jiang and LeBlond*, 1992; *Lander, et al.*, 1999; *McCann*, 2006; *O'Loughlin and Lander*, 2003; *Pararas-Carayannis*, 2004; *von Huene, et al.*, 1989; *Grilli and Watts*, 2005]. Therefore, it may be difficult to determine whether a slide or an earthquake is the source of a tsunami. For example, the tsunami can be caused by a slide or slump that may or may not be related to an earthquake.

Many tsunamis have been generated in areas of the Caribbean where strike/slip plate movements dominate tectonic activity [*McCann*, 2006]. This suggests a slide or slump as either the primary or secondary tsunamigenic mechanism because vertical deformation of the sea floor is not typically associated with strike/slip plate movement. Grindlay et al. [2005] shows historic evidence of massive slumps or slides along the northern Puerto Rico margin which most likely generated tsunamis, and cracking on the eastern edge of the Mona rift that may lead to mass failures in the future, similar to past events.

Understanding how a tsunami forms helps determine their propagation and destructive potential. Since slide or slump tsunami-like waves have a much shorter period than a more typical dip/slip type tsunami, they dissipate faster and are typically only locally dangerous [*Fryer and Watts*, 2000; *Fryer, et al.*, 2001; *Pararas-Carayannis*, 2004; *Watts, et al.*, 2003]. Without detailed ocean bottom mapping and analysis it is difficult to determine the potential for a massive slide or slump. Hence, the slide or slump tsunamigenic potential of the IAS is not considered in this work.

Tsunamigenic Volcanic Events

Volcanoes along the Lesser Antilles chain are the most likely source for volcanic tsunamigenic events in the Caribbean Sea. Overall, approximately 5% of tsunamis are volcanic in origin [*O'Loughlin and Lander*, 2003; *Sigurdsson*, 1996]. There are many different volcanic tsunamigenic mechanisms from eruption to structural failure. O'Loughlin and Lander [2003] and Pararas-Carayannis [2004] review case studies of such events, including tsunamis that were generated by the Soufrière Hills volcano on Montserrat Island, the Mt. Pelèe volcano on

Martinique, the La Soufrière volcano on St. Vincent, and Kick'em Jenny, a submarine volcano north of Grenada affecting Montserrat, Martinique, St. Vincent, and Grenada, respectively.

Most tsunamis of volcanic origin have relatively local destructive effects and/or are predictable. This limits how useful a basin wide TWS will be to protect the public from volcanic tsunamigenic events. Therefore, these events are not considered in this study. The best defense against local tsunamis is public education.

Sea Level Gauges in the Caribbean and Adjacent Regions

Over approximately the past 10-yr, some 60 sea level gauge stations were installed in the Caribbean and surrounding countries by NOAA, programs such as RONMAC (Water Level Observation Network for Latin America) and CPACC (Caribbean Planning for Adaptation to Global Climate Change), and other locally and internationally-funded programs to examine local sea level changes and other weather related research. Government organizations, educational institutions, and independent companies had offered to maintain these stations, but as of February 2006, most stations are in various states of disrepair. The majority of which no longer collect data, and in many cases, installations are missing equipment. To contribute to a tsunami warning network, most stations will need to be replaced, while others need to be upgraded with additional hardware such as a Global Positioning System (GPS) receiver and/or Geostationary Operations Environmental Satellite (GOES) transmitter [*Henson and Wilson*, 2005].

As of February 2006, of the 60 stations that had been deployed historically throughout the IAS region, 17 are fully operational and transmitting data, 16 are not operational but the equipment was accounted for, and 10 are questionably operational. The remaining stations are either no longer operational or missing altogether [*Air-Sea Monitoring Systems*, 2006; *Henson and Wilson*, 2005]. Groups such as IOCARIBE, the Puerto Rico Seismic Network (PRSN), and NOAA are working towards the installation of sea level gauges throughout the IAS (see Results and Discussion "Operational Sea Level Gauges in the Caribbean").

METHODS

This study seeks to determine where the minimum number of sea level gauges should be located to maximize the warning time to the largest amount of people. We analyze how and where regionally destructive tsunamis form, propagate, and impact a coastline, as well as the coastal population distribution. We also develop an assessment of where coastal sea level gauges are operational so monitoring efforts will not be duplicated.

Without pinpointing specific tsunami origin locations, we examine areas where a tsunami is more likely to occur by using a tsunamigenic event source map [*McCann*, 2006] and the known or assumed origins of 42 historical tsunamis. This analysis is critical to maximizing warning time because a sea level gauge should be installed closest to a tsunami origin. Propagation, travel time, and impact analyses are accomplished through the simulation of historical tsunamis with the NCOM. There are several sub-studies involved in using the NCOM including parameter sensitivity and initial condition analyses, and travel time calculations [*Henson*, 2006]. The amount of warning time available is derived from a combination of modeling with the NCOM, developing isochrones, and estimating travel time to coastal population centers throughout the region. Isochrones were developed independently and then tested against the NCOM results.

The tsunamigenic risk analysis uses a 1° resolution grid whereas the NCOM uses a 2-arc-minute resolution grid. The former is used to determine where a tsunami is most likely to occur, and the latter is used to understand tsunami propagation and travel time.

Creation of Tsunamigenic Events List

A total of 61 tsunamis have affected the IAS region in the past 500-yr. Event data is taken from both O'Loughlin and Lander [2003] and the NGDC tsunami database [2005]. Since most volcanic and shore-based landslide tsunamigenic events have localized effects, they are omitted from this study [*O'Loughlin and Lander*, 2003; *Pararas-Carayannis*, 2004; *Smith and Shepherd*, 1995]. Events are also discarded if the origin is located inland, the origin latitude and longitude cannot be found, or the event did not originate in the IAS.

Each event is qualitatively rated on a scale of 0 – 4 according to the validity of the historical observations, and we chose the higher of the ratings from the two databases of rankings available [*NGDC*, 2005; *O'Loughlin and Lander*, 2003]. In an effort to create the largest list of probable events, the 42 simulated historical events have a validity rating of 3 or higher. All simulated tsunamigenic sources are assumed to be regionally destructive.

It is necessary to adjust some of the historical origin coordinates to properly initialize the NCOM (due to model bottom topography and grid resolution limitations). Where possible, the origin is moved closer to or along a plate boundary, but in some cases they are moved perpendicular to isobaths. Figure 2 shows the final origin locations of the simulated tsunamis. Table 1 provides a list of the events modeled and notes which origins were adjusted.

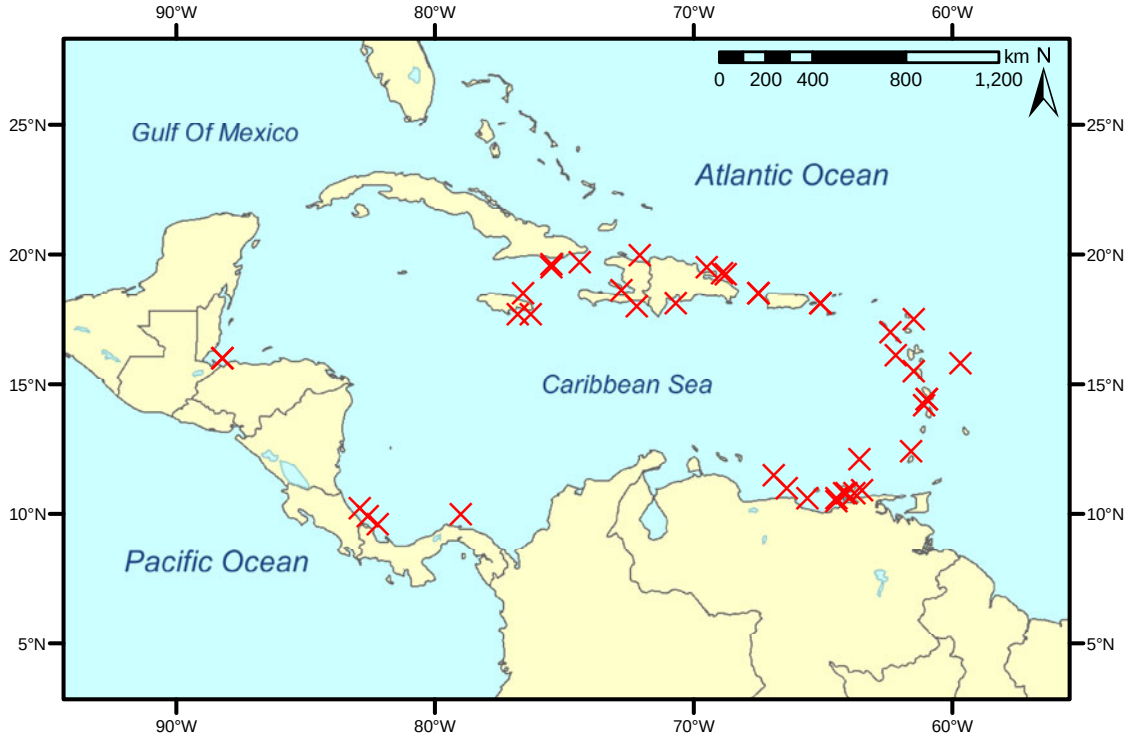

Figure 2 – The locations of the 42 historical tsunamis simulated in this study. The origin of the tsunamigenic events are represented by an "X" (see Table 1). Some events have a similar origin location.

Table 1 – Tsunami events modeled, ordered chronologically (see also Figure 2). Shaded cells denote events whose origin is adjusted, with original coordinates shown in parenthesis. Sources: O'Loughlin and Lander [2003] and the NGDC Tsunami Database [2005]. No information was found for cells that are blank.

Tsunami origin	**Latitude (°N)**	**Longitude (°W)**	**Date**	**Time**	**Validity rating**	**Earthquake magnitude and corresponding scale**	**Source type and brief description**
Venezuela	10.80 (10.70)	64.20 (64.20)	9/1/1530	1430 UT	4		Earthquake
S. Belize	16.00 (16.20)	88.20 (88.50)	11/24/1539	2300 LT	4		Earthquake
Venezuela	10.80 (10.70)	64.10 (64.10)	9/1/1543	2300 LT	4		Earthquake
Leeward Is.	17.50	61.50	4/16/1690		4	Ms 8.0	Earthquake; dispute regarding exact day, found 4/06/1690 as well
Jamaica	17.70 (17.90)	76.80 (76.90)	6/7/1692	1643 UT	4	Ms 7.5	Earthquake induced submarine landslide
Venezuela	10.60 (10.60)	64.50 (64.30)	1726		3		Earthquake
Venezuela	10.50 (10.50)	64.50 (64.30)	1750		3		Earthquake
Hispaniola	18.10 (18.30)	70.70 (70.70)	10/18/1751	1900 UT	4	Ms 7.3	Earthquake
Haiti	18.00 (18.40)	72.20 (72.80)	11/21/1751	0750 LT	3		Earthquake
Martinique and Barbados	14.40	61.00	4/24/1767	0600 UT	3		Shocks
Haiti	18.70 (18.60)	72.63 (72.80)	6/3/1770	1915 LT	4		Earthquake
Costa Rica	10.20	82.90	2/22/1798		4		Earthquake
Venezuela	11.50	66.90	3/26/1812		3		Earthquake

Table 1 (Continued)

Tsunami origin	Latitude (°N)	Longitude (°W)	Date	Time	Validity rating	Earthquake magnitude and corresponding scale	Source type and brief description
Jamaica	17.70 (18.00)	76.30 (76.50)	11/11/1812	1818 UT	3		Earthquake
Costa Rica, Nicaragua, and Panamá	9.60 (9.50)	82.20 (83.00)	5/8/1822	0500 UT	4	Ms 7.6	Earthquake
Martinique	14.40	61.00	11/30/1823	1130 LT	4		Earthquake
Martinique	14.20	61.10	11/30/1824	0330 LT	3		Earthquake
Trinidad and St. Christopher	12.40 (12.40)	-61.60 (61.50)	12/3/1831	1140 UT	4		Earthquake
Hispaniola and Cuba	19.97 (19.50)	72.10 (72.10)	5/7/1842	2200 UT	4	Ms 8.1	Earthquake (no effect in PR)
Guadeloupe	16.10	62.20	2/8/1843	1435 UT	4	Mw 8.3	Earthquake induced landslide
Cumaná, Venezuela	12.10	63.60	7/15/1853	1415 LT	3	Ms 6.7	Earthquake
Honduras	16.00 (16.20)	88.20 (88.50)	8/9/1856		4	Ms 7.5	Earthquake
St. Thomas, St. Croix, Puerto Rico, Dominica	18.10	65.10	11/18/1867	1850 UT	4	Ms 7.5	Earthquake; along the north scarp of the Anegada Trough; 15 to 20-km SW of St. Thomas; St. Croix, St. Thomas, and Isla de Vieques formed a triangle around the epicenter; others believe it may have been of volcanic origin on Little Saba

Table 1 (Continued)

Tsunami origin	Latitude (°N)	Longitude (°W)	Date	Time	Validity rating	Earthquake magnitude and corresponding scale	Source type and brief description
Puerto Rico	18.10	65.10	3/17/1868	1045 UT	4		Earthquake
Venezuela	10.80 (10.70)	63.80 (63.80)	8/13/1868	1137 LT	4		Earthquake
Lesser Antilles	15.50	61.50	3/11/1874	0430 LT	4		Earthquake
Jamaica	19.60	75.50	8/12/1881	0520 LT	4		Earthquake
Panama	10.00	79.00	9/7/1882	1418 UT	4	Ms 8.0	Earthquake (landslide?)
Haiti	19.70	74.40	9/23/1887	1200 UT	4		Earthquake
Venezuela	11.00	66.40	10/29/1900	0842 UT	4	Ms 8.4	Earthquake
Jamaica	18.50 (18.20)	76.60 (76.70)	1/14/1907	2030 UT	4	Ms 6.5	Earthquake induced submarine landslide
Puerto Rico	18.50	67.50	10/11/1918	1414 UT	4	Ms 8.25	Earthquake induced submarine landslide (subduction near the Bronson deep [Mona Canyon]; cables cut in several places)
Puerto Rico	18.50	67.50	10/24/1918	2343 LT	4		After shock from the 10/11/1918 earthquake
Cumaná, Venezuela	10.60	65.60	1/17/1929	1152 UT	4	Ms 6.9	Earthquake (fault activity; slides and collapses)
Cuba	19.50	75.50	2/3/1932	0616 UT	3	Ms 6.7	Earthquake
Hispaniola	19.30	68.90	8/4/1946	1751 UT	4	Ms 8.1	Earthquake

Table 1 (Continued)

Tsunami origin	Latitude (°N)	Longitude (°W)	Date	Time	Validity rating	Earthquake magnitude and corresponding scale	Source type and brief description
Puerto Rico	19.50	69.50	8/8/1946	1328 UT	4	Ms 7.9	2nd shock from 8/4/46 earthquake; this one located 100-km to the NW
Barbados, Antigua, Dominica	15.80	59.70	12/25/1969	2132 UT	4	Ms 7.7	Earthquake
Leeward Is.	17.00	62.40	3/16/1985	1454 UT	4	Ms 6.3	Earthquake (possible landslide)
Puerto Rico	19.23 (18.90)	68.77 (63.80)	11/1/1989	1025 UT	3	Ms 5.2	Earthquake
Costa Rica, Panama	9.90 (9.60)	82.60 (83.20)	4/22/1991	2156 UT	4	Ms 7.6	Earthquake
Venezuela	10.90 (10.60)	63.50 (63.50)	7/9/1997	1924 UT	3	Mw 7.0	Earthquake

Determination of IAS Tsunamigenic Potential

This study simulates events with the potential to have far-field (greater than 1000-km) destructive consequences and illustrates where impacts are possible. The proximity of the islands to each other makes it difficult for tsunami energy to propagate out of the region (or, in the case of origins outside of the region, to move into the Caribbean Sea). The tsunamigenic potential is an index that considers both the spatial frequency of tsunamigenic events and the geologic and tectonic regime of the region. This index helps identify where the next tsunamigenic event is likely to occur. In order to quantitatively measure the tsunamigenic potential of events it is necessary to place the data into bins. Through experimentation it was determined that 1° resolution is optimal because it is large enough to encompass more than one event but small enough to discern distinct geologic and tectonic areas.

The McCann [2006] tsunamigenic event source map (see Figure 1) is used to incorporate the geologic and tectonic regime of the region. Assigning a weighting system (Table 2) to the event source map, based on source type, allows it to be used as a relative tsunamigenic risk map. The weights, although subjective, allow for a quantification of the tsunamigenic event potential. High, medium, and low risk can be directly translated into weights (3, 2, and 1 respectively) but slow earthquake potential, plate bending, or platform deformation regions as well as active faults and geologic belts and ridges also increase the potential for a region to produce a tsunami and are therefore assigned a weight of 1.5. This tends to be more important where areas of high, medium, and low risk overlap these regions.

Table 2 – Weight assignments to the tsunamigenic event source map [*McCann*, 2006].

High risk	**Medium risk**	**Low risk**	**Slow earthquake, belt or ridge, plate bending, platform deformation, active fault**
3	2	1	1.5

The weight attributes of each source type are applied to the 1° resolution grid (Figure 3) and when a grid cell or bin is not completely covered by a source type, the fractional area each source type encompasses is calculated. This is multiplied by the weight of the source type to determine the weight of the bin. Multiple weight types in a single bin are combined in superadditive process. For example, if a bin contains 1/3 high risk, 1/5 slow earthquake, and 1/3 platform deformation the resulting weight is: (1/3 * 3) + (1/5 * 1.5) + (1/3 * 1.5) = 1.8. The fractional areas can be both greater than or less than 1 since source types overlap. The final value of each bin is calculated by adding the spatial frequency to the potential bin weights (Figure 4).

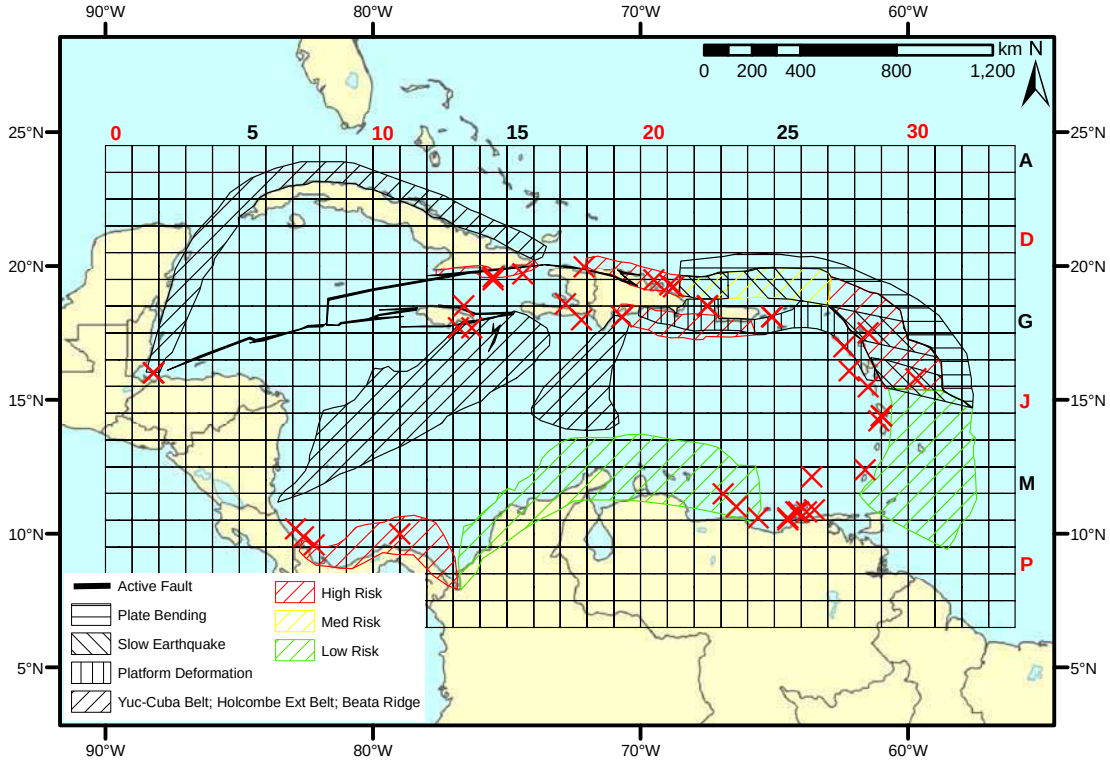

Figure 3 – 1° resolution grid, map of the IAS, historical tsunami origins, and tsunamigenic source regions. "X" represents the location of the historical origins.

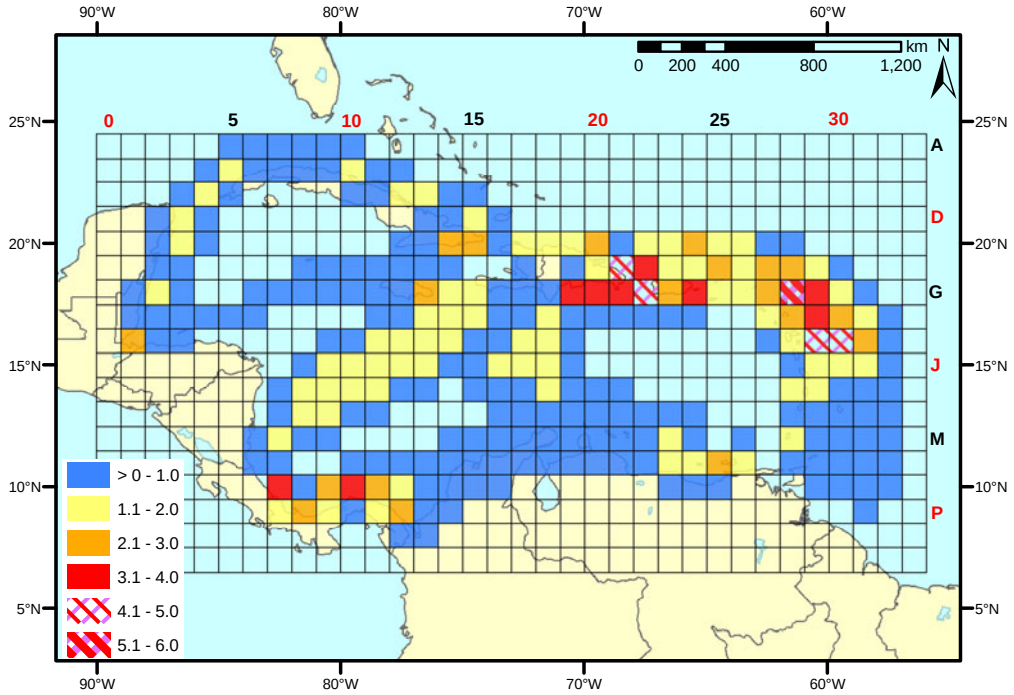

Figure 4 – Sector total weights. Result of binned historical tsunami origins and weight assignments to 1° resolution grid. Bins without coloring have a value of zero.

Modeling

A numerical simulation of the historic tsunamis helps explain tsunami propagation throughout the region, determine which coastlines are likely to be affected, and measure the travel time to those locations. Initial conditions (Table 3) are the same for every tsunami simulation due to a lack of specific historical data.

The NCOM is a three-dimensional model featuring flexibility of model grid discretization and numerical methods [*Martin*, 2000; *Morey, et al.*, 2003b; *Morey, et al.*, 2003a]. Other studies of historical tsunamis in the Caribbean have used different models but these are based on the same basic equations used by the NCOM [*Mader*, 2001; *Mercado and McCann*, 1998]. Some of the basic equations of motion that NCOM solves are listed here in Cartesian coordinates from Morey et al. [2003b] (Equations 1 – 4). Although the Coriolis term is accounted for in the NCOM, its contribution is relatively small given the simulation duration (6-hr).

$$\frac{\partial u}{\partial t} = -\nabla \bullet (\mathrm{V}u) + Qu + fv - \frac{1}{\rho_0}\frac{\partial p}{\partial x} + F_u + \frac{\partial}{\partial z}\left(K_M \frac{\partial u}{\partial z}\right) \quad (1)$$

$$\frac{\partial v}{\partial t} = -\nabla \bullet (\mathrm{V}v) + Qv + fu - \frac{1}{\rho_0}\frac{\partial p}{\partial y} + F_v + \frac{\partial}{\partial z}\left(K_M \frac{\partial v}{\partial z}\right) \quad (2)$$

$$\frac{\partial p}{\partial z} = -\rho g \quad (3)$$

$$\nabla \bullet \mathrm{v} = \frac{\partial u}{\partial x} + \frac{\partial v}{\partial y} + \frac{\partial w}{\partial z} = Q \quad (4)$$

$$\rho = \rho(T, S, z)$$

where,

u, v = velocity vector terms (m s^{-1}) ∇ = del operator V = unit vector
Q = a volume source or sink term (m^3 s^{-1}) t = time (s) f = coriolis parameter
ρ_0 = reference water density (kg m^{-3}) p = pressure (Pa) S = salinity
F_u, F_v = friction vector terms (N) x, y, z = coordinate directions
T = potential temperature (^{o}C) g = gravitational acceleration (m s^{-2})
K_M = vertical eddy coefficient for momentum

A leap-frog, semi-implicit time stepping integration scheme is used for the tsunami simulations. This allows the use of larger time steps while maintaining stability and accuracy [*Morey, et al.*, 2003b; *Rueda and Schladow*, 2002]. However, if too large a time step is used and the Courant, Friedrichs, and Lewy (CFL) condition is violated, gravity waves (such as those modeled for this research) may be slowed down [*Bartello and Thomas*, 1996; *Dupont*, 2001]. The CFL condition states that the time step must be smaller than the time it takes for a wave to propagate from one grid point to the next (Equation 5).

$$C < 1$$
$$C = \frac{c\Delta t}{\Delta x} \quad (5)$$

where, c = wave celerity (m s^{-1}); Δt = time step (s); and Δx = grid space (m)

Although it is a three-dimensional model, for these simulations the NCOM is run as a barotropic model with one depth-averaged vertical grid cell. Tidal components are not included and the temperature and salinity remain constant. All tsunamis are assumed to be shallow water waves. Sea boundaries are open and allow perturbations to radiate out of the model domain. Land boundaries are closed and act as vertical walls with heights equal to the adjacent ocean grid cell depth (typically 4-m). Land elevation is set to 20-m above sea level, and to avoid dry cell conditions as a wave reaches the coast, the minimum water depth is set to 4-m. Wave run-up on land is outside the scope of this study due to a lack of high resolution bottom and coastal topography for the study area, and a lack of high quality historical observations/measurements to ground truth model results. The grid resolution is set to 2-arc-minutes to match the resolution of the ETOPO2 [*NGDC*, 2001] global bathymetric and topographic dataset, which is used as the model bottom topography.

Initial Conditions

Known as an inverse tsunami problem, a method of determining some of the initial conditions for a tsunamigenic event is to back-calculate them from historical observations of tsunami impacts [*Mader*, 2001; *Murty*, 1977]. However, the historical record for tsunamis in the Caribbean region is poor and it is difficult to reconstruct such events with any accuracy. Some works have used a seismic or initial condition model [*Mercado and McCann*, 1998; *Meyer and Caicedo O.*, 1998] to determine the initial wave parameters while other models such as NCOM and MOST (Method of Splitting Tsunamis) can also run with user-defined initial conditions. For this study, several sensitivity tests were run to determine initial wave amplitude and e-folding radius, bottom roughness height, model time step, surface field output interval, and total run time. Results are summarized in Table 3.

Table 3 – Sensitivity test results summary

Initial amplitude (m)	**e-folding radius (m)**	**Bottom roughness height (m)**	**Time step (s)**	**Surface field output interval (s)**	**Total run time (hr)**
4	10,000	0.003	7.5	45	6

The surface field output interval depends on the temporal resolution required to consistently identify the exact moment of tsunami impact. A surface field output interval of 45-sec was sufficient to obtain adequate temporal resolution. The sensitivity experiments converged on a model time-step of 7.5-sec and a grid spacing of 2-arc-minutes, which also satisfies the CFL condition (see Equation 5). Based on a celerity of 222 m s^{-1} (~ 800 km hr^{-1}), two time steps will pass as a wave moves from one grid point to another.

The shape of the initial wave adds the most uncertainty to the results of the simulations presented here. However, too little is known about the initial conditions of all of the events simulated. Therefore, in order to compare the output from each model run, the same initial conditions are used to initialize all of the historical tsunami simulations. Zahibo et al. [2003b] has also used the same initial conditions for 19 historical events, and a time step and grid spacing of 6-sec and 3000-m, respectively.

Each tsunami is modeled as a point source using a normalized Gaussian dome with an amplitude of 4-m and an e-folding radius of 10,000-m (see Table 3; Equations 6 – 11). This assumes that the entire water column is composed of an incompressible fluid and that the tsunami-genesis process is instantaneous [*Okada*, 1985]. This assumption is based on previous works such as Kowalik and Whitmore [1991], Shuto [1991], and Mercado and McCann [1998].

The initial shape of the sea surface η is given by,

$$\eta(r) = A * e^{\left(\frac{-r^2}{2*R^2}\right)} \qquad (6)$$

where, A is the initial maximum height of the wave above a resting sea surface (m); R is the e-folding radius (m); and r is the radius from the center of the perturbation (m). Given the location for the center of the initial perturbation, $\eta(r)$ can be readily mapped onto the ocean model grid space.

Determination of Coastal Grid Points (CGP), Population Data Integration, and Time Series Analysis

Analyses of population data within the model study region are conducted to determine the approximate population densities along the coastlines. In the model, 10,623 grid points adjacent to land are identified in an area approximately from 7ºN, 59ºW to 36ºN, 98º W (Figure 5A). A close up of CGP's around Puerto Rico illustrates resolution (Figure 5B). Population data is obtained from the Latin American and Caribbean Population Database (LACPD) [*CIAT, et al.*, 2005]. This database encompasses the Caribbean and South and Central American regions at a mean resolution of 33,000-m. The resolution varies from country to country and is generally 9,000- to 53,000-m. Each CGP is assigned the value of the LACPD population cell closest to it.

Figure 5A – All 10,623 coastal grid points used in the initial time series analysis study.

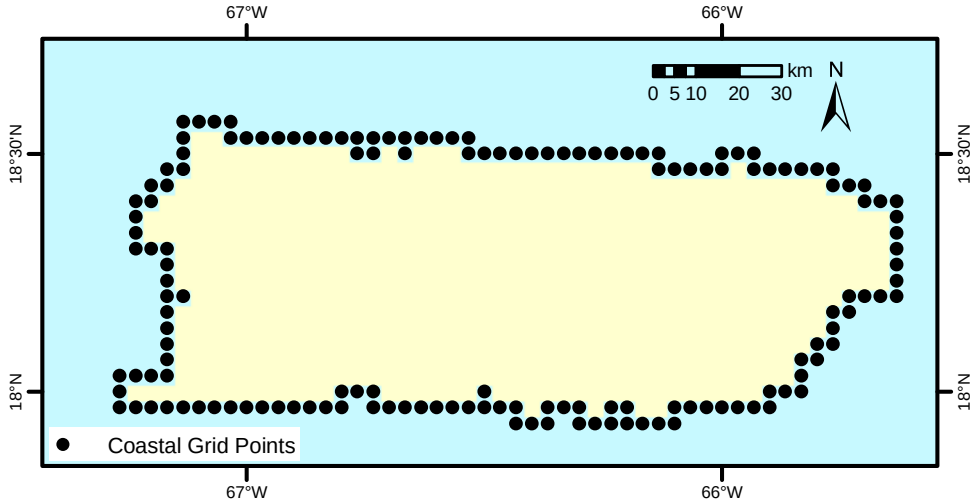

Figure 5B – Inset of figure 5A; Close-up view of CGPs around Puerto Rico

The CGP's bordering the continental United States are not used because, as it is shown later (see Results and Discussion), the travel time to where the continental US is impacted by the simulated tsunamis is at least 4-hr (Figure 6). Sea level gauges throughout the Caribbean would identify the threat of a destructive tsunami impact along the continental US with at least 3-hr of warning time eliminating the need to analyze those CGP's for this part of the study.

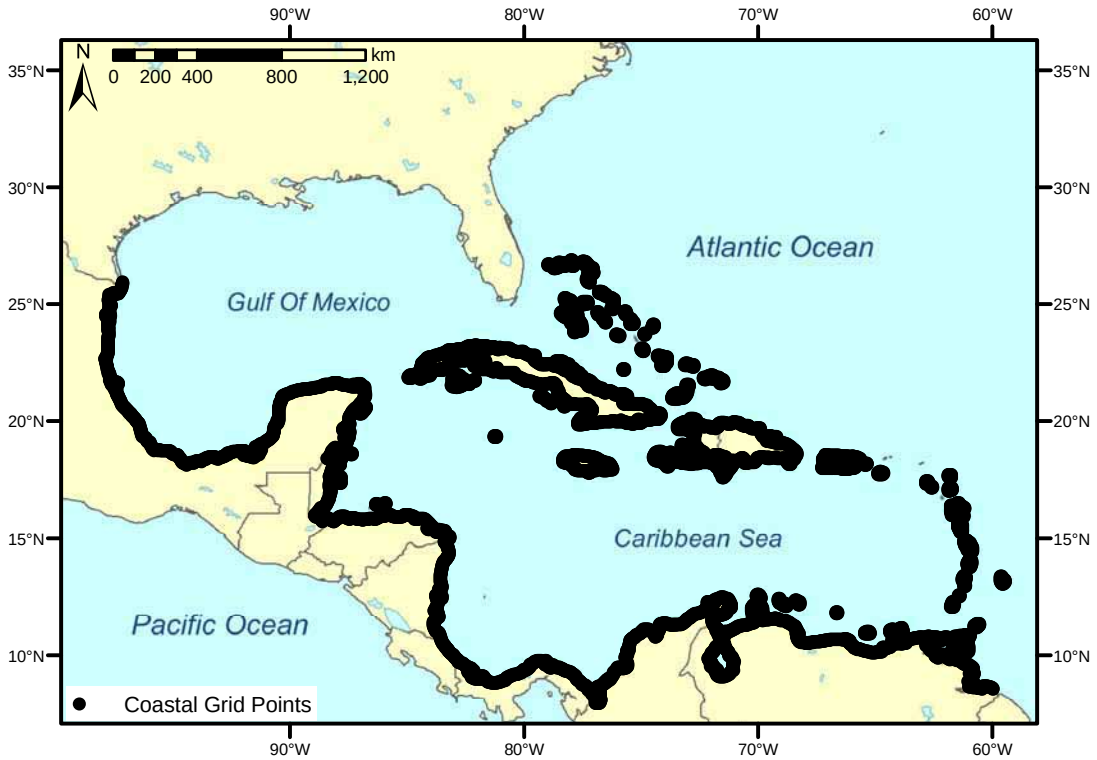

Figure 6 – Locations of the 8009 CGP's with population data attributes. The CGP's bordering the continental United States seen in figure 5A are not shown here.

Efficient use of a limited number of sea level gauges requires that each gauge warn the greatest number of people possible. This is achieved through the use of population centers. A population center, due to the high and variable resolution of the population data set, is defined as a CGP having a population of over 500. Once these points are identified, the dataset is edited to eliminate replicates and points in close proximity to each other. It is necessary to supplement this list with major tourist locations since these do not necessarily have high populations. The resulting dataset is summarized in table 4 and displayed in figure 7.

Table 4 – List of population centers. * denotes added tourist location; Coordinates from www.fallingrain.com and adjusted to nearest CGP.

St. Johns, Antigua and Barbuda*	Near Old Harbour, Jamaica
Basseterre, Saint Kitts and Nevis*	Kingston, Jamaica
Basse-Terre, Guadeloupe (France)*	Ponce, Puerto Rico
Christiansted, St. Croix (Virgin Islands)*	Les Cayes, Haiti
Marigot, Sint Maarten (Neth. Ant.)*	Mayagüez, Puerto Rico
Roseau, Dominica*	Fajardo, Puerto Rico
Fort-de-France, Martinique (France)*	Santo Domingo, Dominican Republic
Castries, St. Lucia*	Near Jeremie, Haiti
Bridgetown, Barbados*	Near St. Marc, Haiti

Table 4 (Continued)

Kingstown, St. Vincent and the Grenadines*	Cap-Haïtien, Haiti
St. George's, Grenada*	Santiago De Cuba, Cuba
Puerto Limon, Costa Rica*	South Beach, Bahamas (New Providence)
Portobelo, Panama*	Near Barcelona, Venezuela
Cancun, Mexico*	Near Puerto Cabello, Venezuela
Playa del Carmen, Mexico*	Near Carúpano, Venezuela
Willemstad, Curaçao*	Pampatar, Venezuela
Cartagena, Colombia	La Ceiba, Honduras
Barranquilla, Colombia	San Juan, Puerto Rico
Santa Marta, Colombia	Port-of-Spain, Trinidad and Tobago
near Oranjestad, Aruba	Havana, Cuba
Puerto Cortes, Honduras	Manzanillo, Cuba

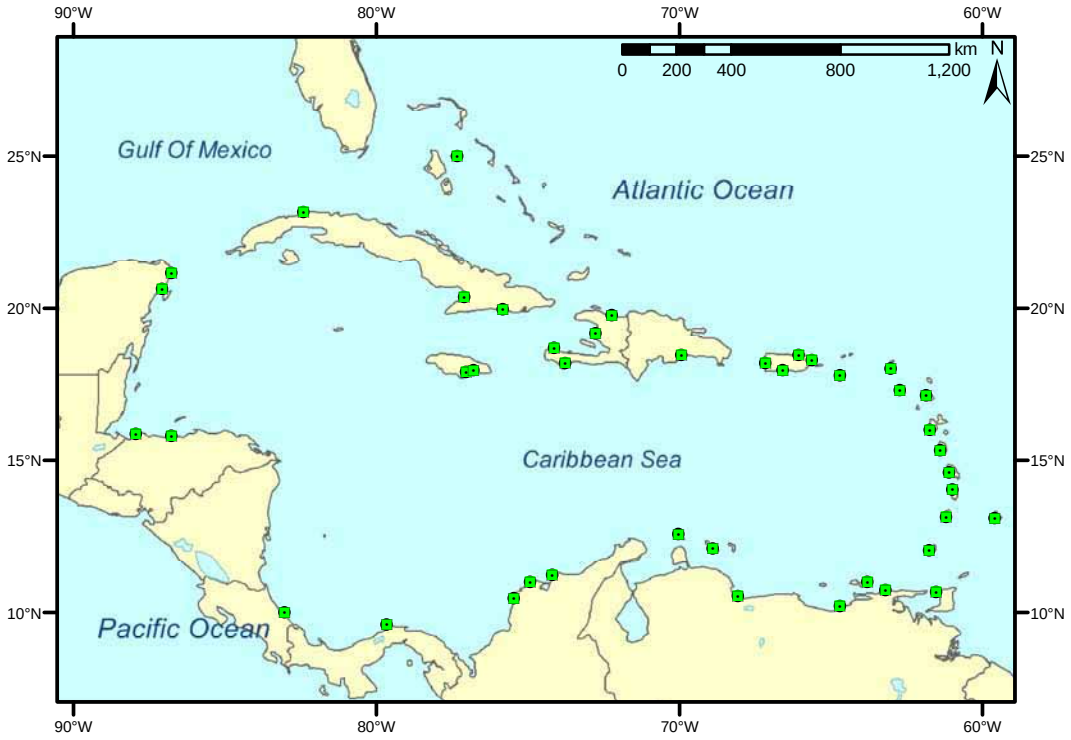

Figure 7 – Population centers (represented by the squares).

A time series of model sea level are extracted for each CGP, and from them, tsunami travel time is calculated. A CGP is determined to have been impacted by the tsunami if the criterion

$$(\eta_n - \eta_{n-2})^2 > 10^{-5}\ \mathrm{m}^2 \qquad (7)$$

is met, where n is any output record number (at 45-sec intervals). Condition (7) is true when the time rate of change of the sea level at a CGP exceeds some threshold. Travel time is defined as the

time between the model initialization and the time when the first peak or trough above the threshold reaches the CGP. Both peaks and troughs are considered to determine travel time because, due to the initial condition uncertainty, phase error may be present. A peak or trough is identified when the time series meets the criteria set forth in both (7) and the condition

$$\frac{\eta_{m+1} - \eta_m}{\eta_m - \eta_{m-1}} < 0 \qquad (8)$$

where, m is any output record number (at 45-sec intervals).

Sea Level Gauge Location Determination

A sea level gauge for a TWS should be positioned to maximize warning time. Several factors such as population centers, locations where a tsunami may occur, travel time or propagation speed, and wave dissipation are considered when calculating warning time. The first Pacific Ocean DART buoy detection array was designed to detect a tsunami within 30-min after the generating earthquake [*Bernard, et al.*, 2001]. The IAS TWS proposal, accepted by the IOC (Intergovernmental Oceanographic Commission), recommends at least 15-min of warning time [*IOC-UNESCO*, 2005]. This study calculates warning time by subtracting travel time to the population center from the travel time to a sea level gauge. A population center is considered warned if it can be notified within 30-min after tsunami generation. In general, the closer the gauge is to the tsunami origin, the more warning time available to population centers.

Knowing where a tsunami will originate is essential to determining where a gauge should be installed. The McCann [2006] tsunamigenic source map, used in part to create the tsunamigenic risk map (Figure 4), appears to have a gap in a tsunami risk region just north of Venezuela in sectors N25 and N26 (Figure 3). Based on McCann's methodology for classifying risk or source areas, and the frequency of historical tsunamis occurring in those sectors, they should be within a region of low risk. This additional low risk value is added to the value of sectors N25 and N26 as if completely covered by a low risk area. The rest of the bins or sectors without values are discarded and the upper ~ 5%, or 15 of the remaining sectors are considered to be where tsunami-genesis risk is relatively highest (Figure 8).

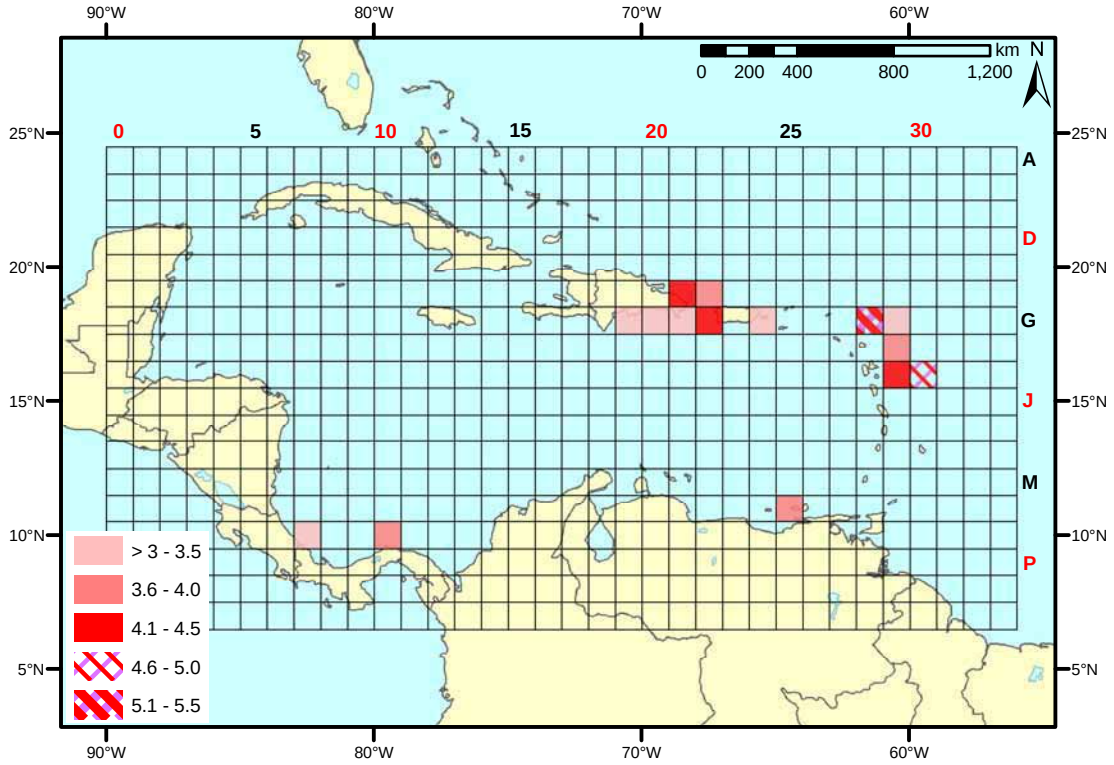

Figure 8 – Top 5% of risk sectors. The color bar shown here is different than that shown in figure 4.

Travel time is measured from the center of the shaded sectors in Figure 8 to the nearest point of land and to the population centers using a series of isochrones. The recommended gauge location corresponds to the point of land nearest to the center of the relatively higher risk tsunamigenic sectors. With this strategy, each point closest to a high-risk sector should receive a sea level gauge resulting in 15 locations. However, some sectors are closest to the same point of land and the final number of locations identified is discussed later. For simplicity, gauge locations are referred to as the sector they correspond to.

Location Priority for Coastal Sea Level Gauges

Through an iterative experimental process a simple decision matrix is developed to evaluate the relatively highest risk sectors in the following categories:

i. Sector risk value
ii. Number of population centers the sector's gauge can warn in time
iii. Number of population centers less than 1000-km away
iv. Number of sectors closest to one potential gauge location
v. Number of sectors sharing a border

Each sector is assigned a rank in all categories, the ranks are added together, and the sector with the lowest number is assigned an overall rank of 1, the second lowest a rank of 2, etc. The final priority list includes all aspects with equal consideration since all ranks are simply added together.

The sector risk values are ranked so the sector with the highest relative risk receives first priority. This means that, to a first order, a sea level gauge is most useful within or nearest to a sector that is the most likely to generate a tsunami. This location, though, may not be able to warn as many population centers as another, reducing its effectiveness.

According to the warning time criteria of 30-min, each location has the potential to warn a certain number of population centers. However, in the Caribbean, the risk to population centers is low if they are at least 1000-km away from the tsunami origin [*Zahibo, et al.*, 2003b]. A direct line distance is used in this study, since the resulting complex island reflections and refractions soon after tsunami generation make it difficult to perform accurate ray tracing. The list of population centers each gauge can warn is reduced to those less than or equal to approximately 1000-km away from the center of the sector. The sector and corresponding gauge that warns the most population centers less than or equal to approximately 1000-km away is given higher priority.

In some cases, different risk sectors are closest to the same point of land (Figure 10). It is more efficient to install a sea level gauge on a point of land closest to more than one sector. This gives the gauge the ability to warn of a tsunami originating from multiple sectors. Higher priority is allocated to sectors that share a gauge location.

Population centers near multiple higher risk sectors have increased potential to be impacted by a tsunami. To account for this sector density or clusters of higher risk sectors, the number of borders each sector shares with another sector is counted. In this manner, higher priority is skewed towards the clusters of risk centers.

RESULTS and DISCUSSION

Our systematic approach to assess sea level gauge location and priority should assist in developing an IAS TWS. Here we review the modeling decisions and results, vulnerability of the IAS coastline to tsunami impact, sea level gauge installation location and priority, and currently operational sea level gauges within the IAS.

Modeling Validity

Major aspects of modeling include choosing the correct model, the accuracy of the initial conditions, and the validity of assumptions. Depending on the model used for both propagation and initial displacement there may be differences in calculated wave amplitudes. However, previous studies have not evaluated whether the choice of model affects travel time estimates [*Mercado and McCann*, 1998; *Whitmore*, 2003; *Zahibo, et al.*, 2003a]. Travel times estimated here, in general agree with those calculated in both Weissert [1990] and Mercado and McCann [1998] and observed by Reid and Taber [1919].

Weissert [1990] developed an isochron time chart for the 1867 Virgin Islands tsunami (see Table 1). Travel times are in reasonable agreement for open areas, but less in regions of more complicated bottom topography. For example, he estimated a travel time of 100- to 120-min to the Northeast coast of Cuba, but the NCOM travel time calculation was approximately 250- to 350-min. This significant difference may have been a result of a coarser bottom topography used in Weisserts' study (ETOPO5), or the breakdown of that model's ability to simulate a tsunami in shallow water, as explained by the author.

Mercado and McCann [1998] simulated the 1918 Puerto Rico tsunami (see Table 1) and show a sea level time series for three Puerto Rico locations: Aguadilla, Mayagüez, and Boquerón.

These three time series are compared to those generated from the NCOM output. As in this study, travel time to these locations is taken as the time corresponding to the first peak or trough on the Mercado and McCann [1998] sea surface elevation time series. Reid and Taber [1919] report observations of the 1918 Puerto Rico tsunami. The travel times they and Mercado and McCann [1998] report generally agree with those produced in this study.

Any discrepancies with Mercado and McCann [1998] may be because they use a higher bathymetric and grid resolution, more accurate bottom topography, and run-up capability (Mercado and McCann use a 3-arc-second grid resolution where a 2-arc-minute resolution is used in this study). In addition, the location and shape of the initial wave is also different. They generate the tsunami along a multi-segment fault line whereas it is considered a point source here.

Tsunami Travel Time and IAS Coastline Vulnerability

Based on the temporal frequency of historical tsunamigenic events, the IAS region is likely to experience another destructive tsunami at any moment [*O'Loughlin and Lander*, 2003; *Pararas-Carayannis*, 2004; *Zahibo, et al.*, 2003b; *Zahibo, et al.*, 2003a]. Several works have discussed the local nature of devastating effects from many historical tsunamis [*Mercado and McCann*, 1998; *Meyer and Caicedo O.*, 1998; *Pararas-Carayannis*, 2004; *Zahibo, et al.*, 2003a]. It has also been shown that tsunamis generated in the Caribbean can be destructive as far away as 2- to 3-hr [*Zahibo, et al.*, 2003b]. In order to determine the IAS coastline vulnerability, here it is assumed that these tsunamis can be destructive up to 6-hr away.

Figure 9 displays where 42 historical tsunamis have had the potential to impact (based on the model experiments), and indicates the frequency of impact at those locations. To show where the continental United States has had the potential to be impacted, all 10,623 CGP's are included in figures 9 – 11. Some areas are never hit and some are hit by every tsunami modeled. The two main factors controlling this are the origin location and bottom topography. To incorporate travel time with impact frequency, the mean travel time is displayed in Figure 10. It can be inferred that where the mean travel time is low (≤30-min), the majority of tsunamis impacting that location originated close to it. The opposite can be inferred where the mean travel time is high (>1.5-hr).

The median travel time helps understand what locations may be more vulnerable to a regional tsunami regardless of impact frequency (Figure 11). Compared to mean travel time, the median tends to be lower at locations that are hit more frequently. The mean travel time is longer than the median 64% of the time, suggesting that there are more locations that are hit more often from tsunamis that travel long distances. This is an indication of their vulnerability to regional tsunami impact.

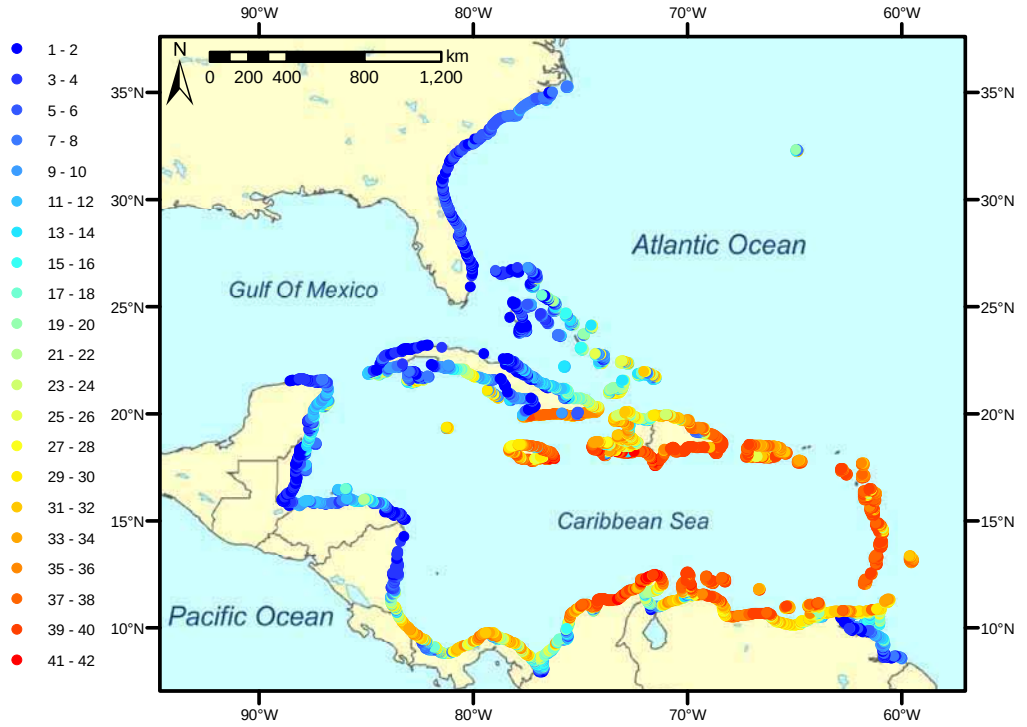

Figure 9 – Impact frequency. Locations where a CGP was impacted by at least one of the 42 historical tsunamis. Colors denote frequency of impact at that location.

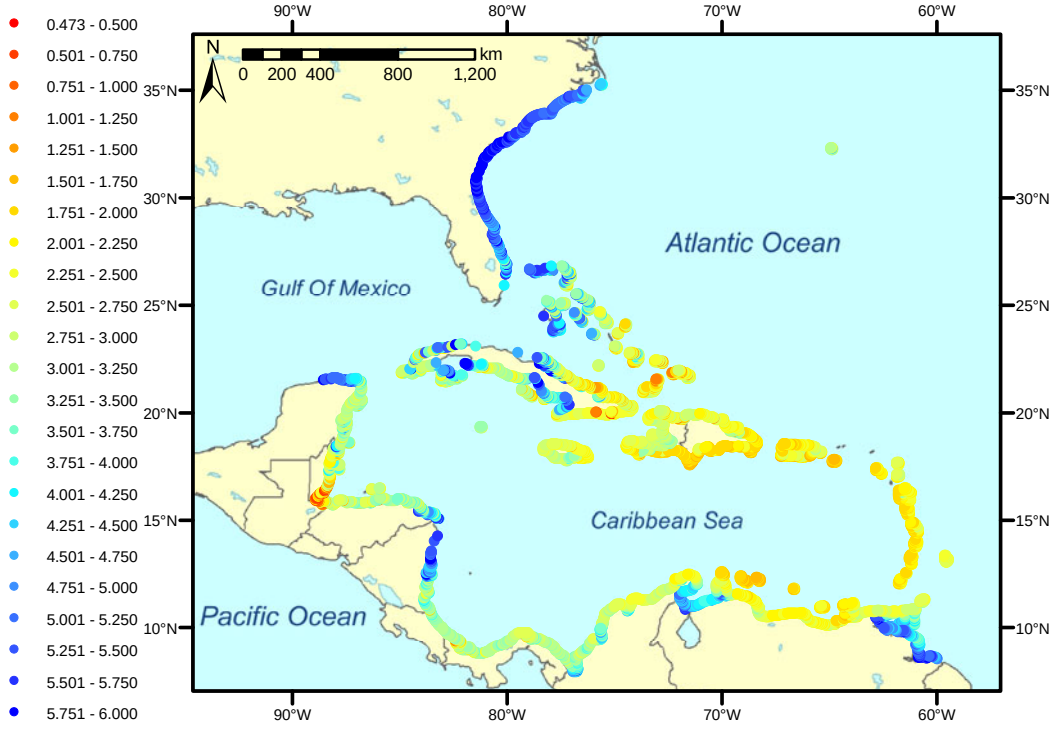

Figure 10 – Mean travel time. Similar to figure 9 but here colors denote mean travel time in hr to that location.

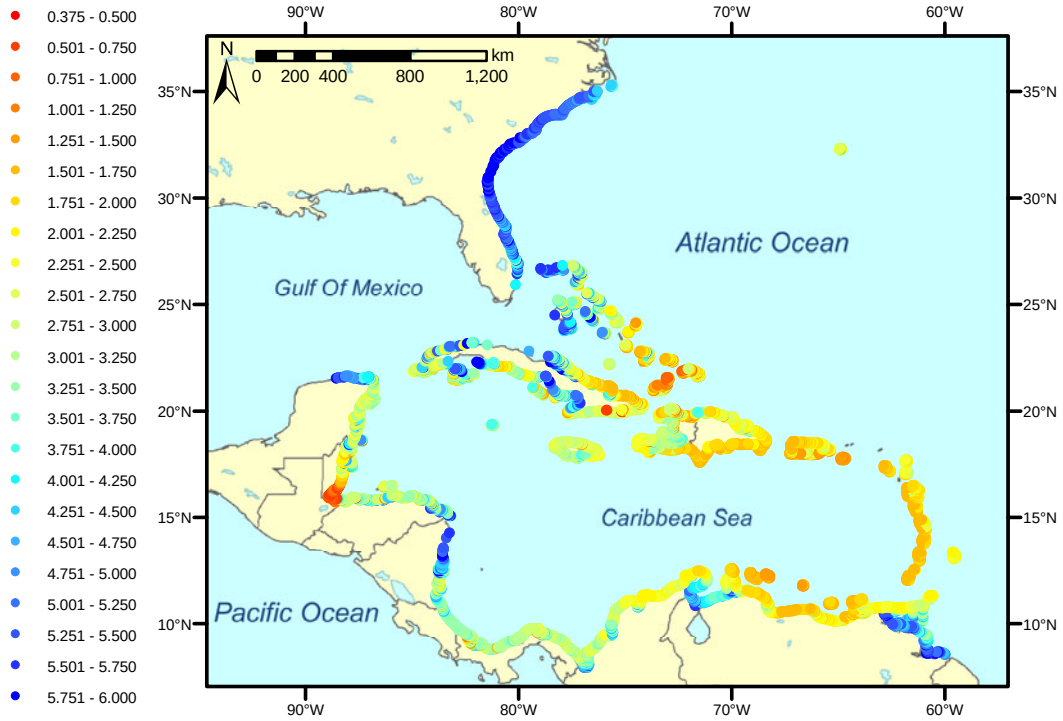

Figure 11 – Median travel time. Similar to figure 9 but here colors denote median travel time in hr to that location.

Sea Level Gauge Location Priority

This study uses a two-pronged approach to determine the IAS regional tsunami risk. One assumes that a tsunami impact has the potential for destruction up to 6-hr from the origin and the other assumes that a tsunami will only be destructive within approximately 1000-km from the origin. The former is important when determining what locations have historically had the potential for impact and the latter is considered when optimizing and prioritizing gauge locations.

Table 5 summarizes the rank of the higher risk sectors by the factors dictating the installation location priority. These factor ranks are combined in a linear fashion to determine an overall rank (Table 6). In the event two sectors have the same value, they are assigned the same rank. The gauge corresponding to the sector with the highest overall rank should be installed first. The insertion of the low risk area over sectors N25 and N26 described in Methods ("Sea Level Gauge Location Determination") led to the addition of sector N25 to the list of relatively higher risk sectors.

Table 6 shows the prioritized list of initial locations for sea level gauges recommended to provide an efficient warning system. When two sectors share the same potential gauge location and have a different priority, the higher priority rank is applied to both sectors. Several sectors share priority and two different locations are recommended for sector G22. Priority sharing can be resolved in a number of ways. The importance of one factor can be increased or decreased, a multiplier can be applied to a factor, or other factors can be included in the decision matrix such as site infrastructure, security of a site, and maintainability. As explained earlier, this study assesses regional tsunami risk of impact based on historical tsunamigenic events, the geologic and tectonic regime of the region, wave propagation dynamics, and the location of major population centers

within a range of 1000-km from the center of the higher risk sectors. Nonetheless, a complete warning system should also consider exactly where run-up and inundation would occur and to what extent.

Table 5 – Decision rank matrix. The sectors are arranged in alphabetical order.

Sector	Risk value	# of sectors with same closest land	# of higher risk sectors sharing a border with another higher risk sector	# warned < 1000-km away	Total
F21	5	3	1	2	11
F22	8	3	1	5	17
G19	15	3	2	4	24
G20	13	3	1	1	18
G21	11	3	1	3	18
G22	3	3	2	4	12
G24	14	3	3	6	26
G28	1	2	2	8	13
G29	12	2	1	9	24
H29	9	1	1	10	21
I29	4	1	1	8	14
I30	2	1	2	11	16
N25	6	3	3	7	19
O7	10	3	3	12	28
O10	7	3	3	12	25

Table 6 – List of initial sea level gauge locations recommended for a TWS. Locations listed in order of highest to lowest priority groups. Coordinates should only be used as a guideline.

Sector	Approximate location for gauge installation	Priority
F21	Arena Gorda, Dominican Republic (18.78°N, 68.52°W)	1
G22	Isla Mona, Puerto Rico (18.09°N, 67.89°W) or Boquerón, Puerto Rico (18.02°N, 67.17°W)	2
G28, G29	Barbuda (17.64°N, 61.80°W)	3
H29, I29, I30	La Désirade, Guadeloupe (16.32°N, 61.05°W)	4
F22	Aguadilla, Puerto Rico (18.50°N, 67.15°W)	5
G20 G21	Boca Chica, Dominican Republic (18.45°N, 69.61°W) Isla Saona, Dominican Republic (18.11°N, 68.57°W)	6
N25	Punta Arenas, Venezuela (10.97°N, 64.4°W)	7
G19	Las Calderas, Dominican Republic (18.20°N, 70.5°W)	8
O10	Portobelo, Panamá (9.55°N, 79.65°W)	9
G24	Isla de Vieques, Puerto Rico (18.10°N, 65.45°W)	10
O7	Punta Manzanillo, Costa Rica (9.63°N, 82.64°W)	11

Changing the number and location of population centers, as well as the decision criteria, may affect the suggested gauge priority. The population centers are selected based on population

and tourism alone and may not need to be warned if they are protected by a wide continental shelf or other wave energy dissipation medium. In addition, the number of warnable population centers will increase if tsunamis have destructive capability at distances greater than 1000-km. Answers to these possibilities require higher resolution bottom topography, modeling more origins (including those that are hypothetical in areas of higher tsunamigenic potential), as well as calculating run-up and inundation.

The installation location coordinates depend on where the center of the higher risk sectors are and should therefore only be used as a guideline. The locations selected are based on the top 5% of the relatively higher risk sectors and do not constitute a finite list. Additional areas should be considered for sea level gauge installations, including Venezuela near the west coast of Margarita Island, the southeast coast of Jamaica, and the southeast coast of Cuba.

Although table 6 lists only one location per sector, in some cases two or three sensors may be more effective. It may take only one gauge to determine if the seismic event caused a tsunami, but this is a binary approach. It may not give enough information as to where else and to what extent the tsunami may impact on a larger scale. More sea level gauges can be used to detect a tsunami originating on either side of an island, and/or also improve travel time and wave height predictions.

A more general approach to a warning system is the installation of DART buoys. They have the potential to yield better predictions because, unlike a coastal sea level gauge, they receive a tsunami signal without being compromised by local effects or coastal noise. Although a DART buoy may prove more useful in propagation and wave height prediction as well as cover a larger origin area, they may not provide as much warning time. This approach cannot warn locations that are the same distance from the tsunami origin as the buoy, because a tsunami will reach both locations at about the same time. This reduces their usefulness and requires that a robust warning system employ a combination of both coastal and open ocean sea level gauges.

Operational Sea Level Gauges in the Caribbean

Figures 12a and b show the locations of some of the fully operational and proposed gauges as well as the recommended locations seen in table 6. The IAS TWS proposal [*IOC-UNESCO*, 2005] recommends that 31 sea level stations become tsunami ready to operate within the IAS TWS. The PRSN group has begun installing ten sea level gauges [*von Hillebrandt-Andrade*, 2006, personal correspondence]. A base station located in Mayagüez, Puerto Rico, will be capable of processing data from these and other sea level stations throughout the IAS. The NOAA National Ocean Service (NOS) has seven sea level gauges installed throughout Puerto Rico and the US Virgin Islands. Two of the PRSN tsunami ready gauges (Aguadilla and Isla Mona) and one of the NOAA NOS gauges (9752695) coincide with locations recommended by this study.

Any sea level gauges used for tsunami warning must be supported as a part of an operational system and regularly maintained. Support can come from a variety of sources because coastal sea level gauges are typically a component of a larger station capable of collecting various other data including wind speed and direction, relativity humidity, air temperature, water temperature, barometric pressure, precipitation, salinity, dissolved oxygen, water clarity, solar radiation, and current flow. These stations therefore have many applications, such as storm surge warnings and studies, hurricane forecasting, geostrophic current analysis, land subsidence, plate tectonics, commercial and recreational fishing and diving, search and rescue operations, and commercial shipping.

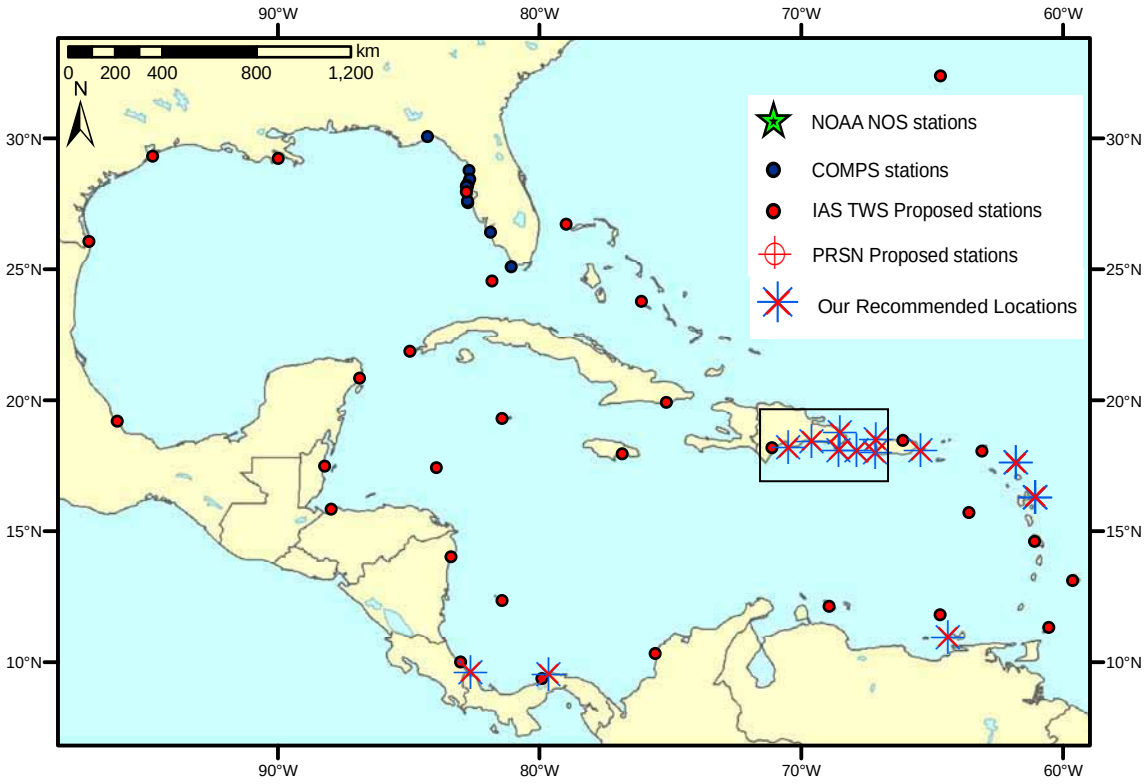

Figure 12a – Selection of operational and recommended sea level gauge stations in the IAS. There are 12 operational sea level gauges sponsored by the NOAA NOS, 13 locations for sea level gauges recommended by this study, 31 IAS TWS proposed locations, 10 PRSN locations proposed for the Puerto Rico Tsunami Ready Tide Gauge Network, as well as 11 Coastal Ocean Monitoring and Prediction System (COMPS) gauges shown in the figure. The alternate location for sector G22 is also shown. Box in northern Caribbean is enlarged in figure 12b.

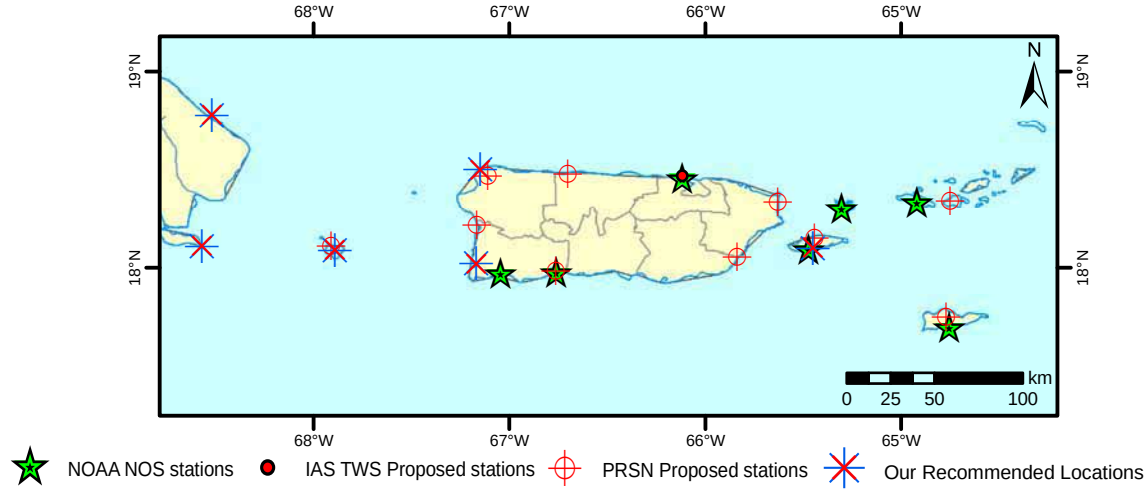

Figure 12b – Inset of figure 12a; Close up view of stations around PR, the USVI, and the Dominican Republic. Illustrates the proximity of the locations recommended in this study with those already installed by NOS and those recommended by the PRSN.

CONCLUSIONS and RECOMMENDATIONS

The goal of a TWS is to mitigate loss of life and property caused by a tsunami. Different types of systems/networks are currently being successfully employed to measure, record, and telemeter both oceanographic and meteorological data for tsunami warning. This study determined prioritized locations for coastal sea level gauges in the IAS based on tsunami generation risk factors, tsunami propagation throughout the region, population distribution, and tsunami travel time to population centers. These locations will give the maximum warning time to the largest number of people in the most efficient manner.

A database of all sea level gauges installed or thought to be installed was compiled and used to coordinate the recommended locations. The expansion of the IAS regional tsunamigenic event risk analysis was accomplished by combining the spatial frequency of 42 historical tsunamis with a modified tsunami source map from McCann [2006]. This study assumes that the 42 tsunamis were generated by either a dip/slip earthquake or massive slide/slump and were regionally destructive. Each historical tsunami was modeled with the NCOM to show which coastal locations could have been affected by historical tsunamis and to estimate the respective travel times. Animations of select simulations are available at http://imars.usf.edu/tsunami/. Throughout this work a GIS database was created which will also be useful to those planning the IAS tsunami warning system.

This study established that, initially, 12 sea level gauges are recommended, and 3 of these locations already have or are planned to have a gauge. These locations correspond to the land closest to the center of the relatively higher risk sectors and should serve as a guide for installation. The list provided in Table 6 is not all-encompassing, but represents a start and will primarily warn against tsunamis that originate in the higher risk sectors. To determine exactly where a sea level gauge should be installed a thorough site evaluation is necessary. During the site evaluation, factors that need to be considered are those such as access to open water, proximity to a reef or other shoaling feature, infrastructure and security of site, and ease of station installation and maintenance.

It is difficult to predict where a tsunami will occur and how much damage it will do. Quantifying damage prediction for affected areas requires a better understanding of tsunamigenic event origins, higher resolution bottom topography, propagation modeling in the littoral zone, and inundation mapping. Run-up and/or inundation calculations must be performed for areas most susceptible to tsunami impact (see Figures 9 – 11). Mercado and McCann [1998] have begun doing this for Puerto Rico and this is already a viable product for areas around the Pacific at the Pacific Tsunami Warning Center [*Titov, et al.*, 2001].

Sea level gauges are a part of a larger system that records, processes, and telemeters data. These stations can provide meteorological and oceanographic data to support other projects such as hurricane and storm surge monitoring and prediction, climate change monitoring, and assist in improving numerical models [*Alverson*, 2005]. These types of systems in other areas around the US are already used by harbor pilots, ship captains, the U.S. Coast Guard, recreational and commercial divers and fishermen, the surfing and sailing industry, scientists, and the general public. Therefore, to guarantee continued existence and viability, these stations must have a multi-mission purpose to garner multifaceted support because thankfully, tsunamis do not occur very often.

ACKNOWLEDGEMENTS

Many people have contributed their time and experience to this work. I thank them for their dedication and especially their patience. They are Carrie Wall, Jesse Lewis, Judd Taylor, Brock Murch, Remy Luerssen, Dr. Chuanmin Hu, Dr. Luis Garcia-Rubio, Dr. Chris Moses, Zhiqiang Chen, Digna Rueda, Dr. Paul Zandbergen, Damaris Torres-Pulliza, Inia Soto, and Laura Lorenzoni. We also thank Vembu Subramanian, Jeff Scudder, Cliff Merz, Rick Cole, and Jay Law for their support and expertise with ocean/met systems. We gratefully thank Drs. Paul Martin and Alan Wallcraft at the U.S. Navy Research Lab for the development of the NCOM. This work was funded by NOAA grant number EA133R-05-SE-5280.

REFERENCES

Air-Sea Monitoring Systems (2006), Assessment and restoration of the MACC sea-level monitoring stations travel report. (http://www.air-seasystems.com/macc/Sea%20Level%20Monitoring%20Stations%20Assesment%20Report.pdf)

Alverson, K. (2005), Watching over the world's oceans, *Nature*, *434*, 19-20.

Bartello, P., and S. J. Thomas (1996), The cost-effectiveness of semi-Lagrangian advection, *Monthly Weather Review*, *124*, 2883-2897.

Bernard, E. N., et al. (2001), Early detection and real-time reporting of deep-ocean tsunamis, paper presented at International Tsunami Symposium, Seattle Washington.

Bilek, S. L., and T. Lay (2002), Tsunami earthquakes possibly widespread manifestations of frictional conditional stability, *Geophysical Research Letters*, *29*, 1673.

Bird, P. (2003), An updated digital model of plate boundaries, *Geochemistry, Geophysics, Geosystems*, *4*, 1027-1079.

Bryant, E.A. (2005), *Natural Hazards*, 2nd ed., 312 pp., Cambridge Univ. Press, Cambridge, New York, Melbourne.

CIAT, et al. (2005), Latin American and Caribbean Population Database, Version 3, Centro Internacional de Agricultura Tropical (CIAT).

Curtis, G. D. (2001), A multi-sensor research program to improve tsunami forecasting, paper presented at International Tsunami Symposium, Seattle, Washington.

Demets, C. (1993), Earthquake slip vectors and estimates of present-day plate motions, *Journal of Geophysical Research*, *98*, 6703-6714.

Dunbar, P. (2005), Personal Correspondence, National Geophysical Data Center (NGDC). National Oceanic and Atmospheric Administration (NOAA)/ National Environmental Satellite, Data, and Information Service (NESDIS).

Dupont, F. (2001), Comparison of numerical methods for modeling ocean circulation in basins with irregular coasts, Dissertation thesis, McGill University, Montreal.

Fryer, G. J., and P. Watts (2000), The 1946 Unimak tsunami: Near-source modeling confirms a landslide, *EOS, Transactions, American Geophysical Union*, *81*, 748.

Fryer, G. J., et al. (2001), Source of the tsunami of 1 April 1946: A landslide in the upper Aleutian Forearc, in *Prediction of underwater landslide hazards*, edited by P. Watts, et al., Balkema, Rotterdam.

Grilli, S. T., and P. Watts (2005), Tsunami Generation by Submarine Mass Failure. I: Modeling, Experimental Validation, and Sensitivity Analyses, *J. Waterway, Port, Coastal, and Ocean Engineering*, *131*, 15.

Grindlay, N. R., et al. (2005), High risk of tsunami in the northern Caribbean, *EOS, Transactions, American Geophysical Union*, *86*, 121, 126.

Henson, J. I. (2006), Strategic Geographic Positioning of Sea Level Gauges to Aid in Early Detection of Tsunamis in the Intra-Americas Sea, Masters thesis, 68 pp, University of South Florida, St. Petersburg.

Henson, J. I., and D. Wilson (2005), Preliminary status report on tide gauges and observing stations in the Caribbean and adjacent waters, paper presented at The Group of Experts on the Global Sea Level Observing System (GLOSS) ninth session, IOC UNESCO, Paris, France, 24 − 25 February.

Hwang, L., and A. C. Lin (1969), Experimental investigations of wave run-up under the influence of local geometry., in *Tsunamis in the Pacific Ocean*, edited by W. M. Adams, pp. 407-425, East-West Centre Press, Honolulu.

IOC-UNESCO (2005), An Intra-Americas Sea Tsunami Warning System Project Proposal, edited, UNESCO Intergovernmental Oceanographic Commission.

Jiang, L., and P. H. LeBlond (1992), The coupling of a submarine slide and the surface waves which it generates, *Journal of Geophysical Research*, *97*, 12,731–712,744.

Kanamori, H. (1972), Mechanism of Tsunami Earthquakes, *Physics of the earth and planetary interiors 6*, 346-359.

Kato, T., et al. (2001), A new tsunami monitoring system using RTK-GPS, paper presented at International Tsunami Symposium, Seattle, Washington.

Kowalik, Z., and P. M. Whitmore (1991), An investigation of two tsunamis recorded at Adak, Alaska, *Science of Tsunami Hazards*, *9*, 67-83.

Lander, J. F., et al. (2002), A Brief History of Tsunamis in the Caribbean Sea, *Science of Tsunami Hazards, 20*, 57.

Lander, J. F., et al. (1999), Use of tsunami histories to define the local Caribbean hazard, paper presented at International Symposium on Marine Positioning, Melbourne, Florida, December.

Mader, C. L. (2001), Modeling the 1755 Lisbon tsunami generation and propagation across the Atlantic Ocean to the Caribbean, *Science of Tsunami Hazards, 19*, 93-98.

Martin, P. J. (2000), A description of the Navy Coastal Ocean Model Version 1.0, 39 pp, Naval Research Laboratory, Stennis Space Center, MS.

McCann, W. R. (2006), Estimating the threat of tsunamigenic earthquakes and earthquake induced-landslide tsunami in the Caribbean, paper presented at NSF Caribbean Tsunami Workshop, World Scientific, San Juan, Puerto Rico.

Mercado, A., and W. McCann (1998), Numerical simulation of the 1918 Puerto Rico tsunami, *Natural Hazards, 18*, 57-76.

Meyer, H., and J. H. Caicedo O. (1998), Evaluation of tsunami worse scenarios in the Caribbean Sea and simulation of wave weights – a TIME project activity (Oral Poster), paper presented at Okushiri Tsunami/UJNR Workshop.

Morey, S. L., et al. (2003b), Export pathways for river discharged fresh water in the northern Gulf of Mexico, *Journal of Geophysical Research, 108*, 3303-3318.

Morey, S. L., et al. (2003a), The annual cycle of riverine influence in the eastern Gulf of Mexico basin, *Geophysical Research Letters, 30*, 1867-1871.

Murty, T. S. (1977), Seismic Sea Waves: Tsunamis, *Bulletin of the Fisheries Research Board of Canada, Bull. 198*.

NGDC (2001), 2-Minute Gridded Global Relief Data (ETOPO2), edited, National Geophysical Data Center, NOAA Satellite and Information Service.

NGDC Tsunami Database (2005), edited, National Geophysical Data Center, NOAA Satellite and Information Service.

NOAA and USGS Fact Sheet (2005), Tsunami Detection and Warnings, edited, United States Department of Commerce, United States Department of the Interior.

O'Loughlin, K. F., and J. F. Lander (Eds.) (2003), *Caribbean Tsunamis: A 500-Year History from 1498-1998*, 263 pp., Kluwer Academic Publishers, Dordrecht.

Okada, Y. (1985), Surface deformation due to shear and tensile faults in a half space, *Bulletin of the Seismological Society of America*, *75*, 1135-1154.

Okal, E. A., et al. (2003), The deficient T waves of tsunami earthquakes, *Geophysical Journal International*, *152*, 416-432.

Pararas-Carayannis, G. (2004), Volcanic tsunami generating source mechanisms in the eastern Caribbean region, *Science of Tsunami Hazards*, *22*, 74-114.

Polet, J., and H. Kanamori (2000), Shallow subduction zone earthquakes and their tsunamigenic potential, *Geophysical Journal International*, *142*, 684-702.

Reid, H. F., and S. Taber (1919), The Porto Rico earthquake of 1918, House of Representatives, 66th Congress, 1st Session, Washington D.C., United States.

Rueda, F. J., and S. G. Schladow (2002), Quantitative comparison of models for barotropic response of homogeneous basins, *Journal of Hydraulic Engineering*, *128*, 201.

Shuto, N. (1991), Numerical simulations of tsunamis – its present and near future, *Natural Hazards*, *4*, 171-191.

Sigurdsson, H. R. (1996), Volcanic Tsunamis, Summary Report for the UNESCO IOC IOCARIBE Tsunami Warning Workshop, UNESCO IOC IOCARIBE, Paris.

Smith, M. S., and J. B. Shepherd (1994), Explosive submarine eruptions of Kick'em Jenny volcano: Preliminary investigations of the potential tsunami hazard in the eastern Caribbean region, paper presented at Caribbean Conference on Natural Hazards; volcanoes, earthquakes, windstorms, floods, St. Ann's Trinidad and Tobago, October 11-15.

Smith, M. S., and J. B. Shepherd (1995), Potential Cauchy-Poisson waves generated by submarine eruptions of Kick 'em Jenny volcano, *Natural Hazards*, *11*, 75-94.

Sykes, L. R., et al. (1982), Motion of Caribbean plate during the last 7 million years and implications for earlier cenozonic movements, *Journal of Geophysical Research*, *70*, 5065-5074.

ten Brink, U. S., et al. (2004), New seafloor map of the Puerto Rico Trench helps assess earthquake and tsunami hazards, *EOS, Transactions, American Geophysical Union*, *85*, 349-360.

Titov, V. V., et al. (2001), Project SIFT (Short-term Inundation Forecasting for Tsunamis), paper presented at International Tsunami Symposium, Seattle, Washington.

Todorovska, M. I., and M. D. Trifunac (2001), Generation of tsunamis by slowly spreading uplift of the sea floor, *Soil Dynamics and Earthquake Engineering*, *21*, 151-167.

von Hillebrandt-Andrade, C. (2006), Personal Correspondence, Puerto Rico Tsunami Ready Tide Gauge Network; Puerto Rico Seismic Network.

von Huene, R., et al. (1989), A large tsunamigenic landslide and debris flow along the Peru trench, *Journal of Geophysical Research*, *94*, 1703-1714.

Watts, P., et al. (2003), Landslide tsunami case studies using a Boussinesq model and a fully nonlinear tsunami generation model, *Natural Hazards and Earth System Sciences*, *3*, 391-402.

Weissert, T. P. (1990), Tsunami travel time charts for the Caribbean, *Science of Tsunami Hazards*, *8*, 67-78.

Whitmore, P. M. (2003), Tsunami amplitude prediction during events: A test based on previous tsunamis, *Science of Tsunami Hazards*, *21*, 135-143.

Woods Hole, Oceanographic Institution (2005), Major Caribbean earthquakes and tsunamis a real risk, edited, SCI/TECH. YubaNet.com.

Zahibo, N., et al. (2003b), Estimation of far-field tsunami potential for the Caribbean coast based on numerical simulation, *Science of Tsunami Hazards*, *21*, 202-222.

Zahibo, N., et al. (2003a), The 1867 Virgin Island tsunami: observations and modeling, *Oceanologica Acta*, *26*, 609-621.

Science of Tsunami Hazards, Vol 25, No. 3 (2006) ISSN 8755-6839

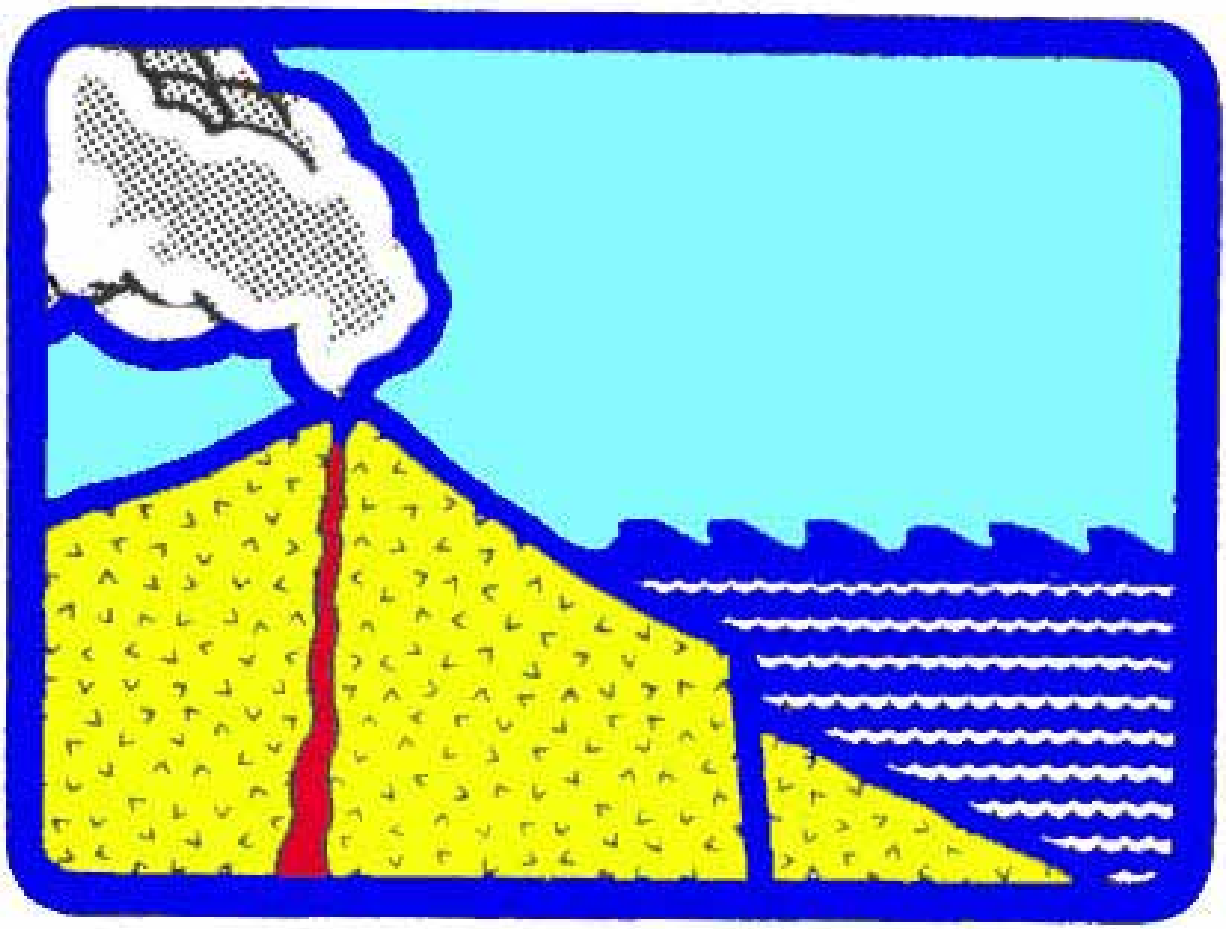

The Tsunami Society
P. O. Box 2117
Ewa Beach, HI 96706-0117, USA

WWW.STHJOURNAL.ORG